Eur. Phys. J. C (2020) 80:1063
https://doi.org/10.1140/epjc/s10052-020-08637-w

THE EUROPEAN PHYSICAL JOURNAL C

Regular Article - Theoretical Physics

The light MSSM Higgs boson mass for large tan β and complex input parameters

Henning Bahl[a], **Ivan Sobolev**[b], **Georg Weiglein**[c]

Deutsches Elektronen-Synchrotron DESY, Notkestraße 85, 22607 Hamburg, Germany

Received: 30 September 2020 / Accepted: 2 November 2020 / Published online: 18 November 2020

Abstract We discuss various improvements of the prediction for the light MSSM Higgs boson mass in the hybrid framework of the public code `FeynHiggs`, which combines fixed-order and effective field theory results. First, we discuss the resummation of logarithmic contributions proportional to the bottom-Yukawa coupling including two-loop Δ_b resummation. For large tan β, these improvements can lead to large upward shifts of the Higgs mass compared to the existing fixed-order calculations. Second, we improve the implemented EFT calculation by fully taking into account the effect of $\mathcal{CP}$-violating phases. As a third improvement, we discuss the inclusion of partial N^{3}LL resummation. The presented improvements will be implemented into `FeynHiggs`.

Contents

[a] e-mail: henning.bahl@desy.de (corresponding author)
[b] e-mail: ivan.sobolev@desy.de
[c] e-mail: georg.weiglein@desy.de

1 Introduction

The discovery of a Higgs boson at the LHC [1,2] was an important step towards the understanding of the fundamental laws of Nature. The properties of the detected particle allow a sensitive test of the predictions of the Standard Model (SM) and of theories of physics beyond the SM (BSM). In particular, in the Minimal Supersymmetric extension of the SM (MSSM) [3,4], based upon the concept of supersymmetry (SUSY), the mass of the discovered boson is not a free parameter, as in the SM, but is predicted in terms of the model parameters.

While the SM-like Higgs mass in the MSSM is smaller or equal to the mass of the Z boson at the tree-level, large quantum corrections shift it upwards towards the experimentally measured value of $M_h \sim 125$ GeV. In order to allow the use of the SM-like Higgs mass as a precision constraint on the MSSM parameter space, the precise determination of these quantum corrections is crucial [5].

The quantum corrections can be calculated in different frameworks. In the most direct approach, quantum corrections to the Higgs self-energies are calculated diagrammatically in the full theory (for recent works see [6–13]). This approach has the advantage of capturing all corrections at a specific order in perturbation theory. If the scale of SUSY

particles is, however, much larger than the electroweak scale, large logarithms emerge in the fixed-order corrections exacerbating the behaviour of the perturbative expansion. In such situations, effective field theory (EFT) techniques allow the resummation of large logarithmic corrections (for recent works see [14–21]). Without including higher-dimensional operators into the low-energy EFT, terms suppressed by the SUSY scale are, however, missed in this approach.[1] Therefore, the accuracy of the EFT approach can be diminished if one or more SUSY scales are comparable to the electroweak scale. In order to obtain a precise prediction for the SM-like Higgs boson mass for low, intermediary as well as high SUSY scales, both approaches – the fixed-order and the EFT approach – can be combined. Such hybrid approaches have been developed in [5,17,22–30].

In this paper, we focus on the hybrid approach implemented in the publicly available code `FeynHiggs` [22,23,26,31–36]. We will discuss various improvements of the incorporated EFT calculation as well as their combination with the implemented fixed-order calculation: resummation of large logarithms proportional to the bottom Yukawa coupling (including two-loop Δ_b resummation [37–39]), extension of the EFT calculation fully taking into account the effects of complex input parameters as well as an inclusion of partial N^{3}LL resummation.

This paper is structured as follows: in Sect. 2, we explain how the resummation of logarithms proportional to the bottom Yukawa coupling is incorporated into the hybrid framework. The extension of the EFT calculation for complex input parameters is discussed in Sect. 3. We explain the implementation of partial N^{3}LL resummation in Sect. 4. Numerical results are presented in Sect. 5. In Sect. 6, we give our conclusions. In the Appendices, we provide more details regarding the calculation of the two-loop threshold corrections (see Appendix A), analytic expressions for the threshold corrections to the SM-Higgs self coupling and to the couplings of the Split-SUSY model (see Appendix B), more details regarding the dependence of Δ_b on $\mathcal{CP}$-violating phases (see Appendix C), and explicit formulas for the one- and two-loop logarithmic corrections to M_h proportional to the bottom-Yukawa coupling (see Appendix D).

2 Resummation of logarithmic bottom Yukawa contributions

In this section, we describe the procedure for resumming logarithmic contributions controlled by the bottom Yukawa coupling in our hybrid framework. We first describe the employed fixed-order and EFT calculations separately. Then we discuss their combination. The resummation of the bottom Yukawa coupling for large tan β is discussed in Sect. 2.4.

2.1 Fixed-order calculation

The fixed-order part of the calculation consists of the full one-loop and $\mathcal{O}(\alpha_t\alpha_s, \alpha_t^2)$ corrections ($\alpha_s = g_3^2/(4\pi)$ with g_3^2 being the strong gauge coupling, and $\alpha_t = y_t^2/(4\pi)$ with y_t being the top Yukawa coupling) implemented into `FeynHiggs` [40–42]. In these corrections $\mathcal{CP}$-violating phases are fully taken into account.

Also, two-loop corrections proportional to the bottom-Yukawa coupling have been calculated using different renormalisation schemes for the sbottom sector. In Sect. 5, we will compare the results of two different schemes.

Renormalisation scheme 1

The present public version of `FeynHiggs` (version `2.16.1`) includes the $\mathcal{O}(\alpha_b\alpha_s, \alpha_b\alpha_t, \alpha_b^2)$ corrections derived in [43,44] ($\alpha_b = y_b^2/(4\pi)$ with y_b being the bottom Yukawa coupling). For these corrections the following renormalisation scheme is employed: The squark masses, $m^2_{\tilde{q}}$, and mixing angles $\theta_{\tilde{q}}$, and the top quark mass are renormalised in the on-shell (OS) scheme,

$$\begin{aligned}
\delta m^2_{\tilde{q}_i} &= \mathrm{Re}\,\Sigma_{\tilde{q}_i\tilde{q}_i}(m^2_{\tilde{q}_i}),\\
\delta\theta_{\tilde{q}} &= \frac{\mathrm{Re}\,\Sigma_{\tilde{q}_1\tilde{q}_2}(m^2_{\tilde{q}_1}) + \mathrm{Re}\,\Sigma_{\tilde{q}_1\tilde{q}_2}(m^2_{\tilde{q}_1})}{2(m^2_{\tilde{q}_1} - m^2_{\tilde{q}_2})},\\
\delta M_t &= \frac{M_t}{2}\,\mathrm{Re}[\Sigma_t^L(M_t^2) + \Sigma_t^R(M_t^2) + 2\Sigma_t^S(M_t^2)], \qquad (1)
\end{aligned}$$

where $\Sigma_{\tilde{q}_i\tilde{q}_i}$ is used to denote the respective scalar self-energy, Σ_t^L, Σ_t^R and Σ_t^S are the coefficients in the Lorentz decomposition of the unrenormalised top-quark self-energy,

$$\begin{aligned}
\Sigma_t(p) = {} & \not{p} P_L \Sigma_t^L(p^2) + \not{p} P_R \Sigma_t^R(p^2)\\
& + M_t \Sigma_t^S(p^2) + M_t\gamma_5\Sigma_t^P(p^2). \qquad (2)
\end{aligned}$$

Additionally, Re denotes the real part, and M_t is the OS top-quark mass.

The corrections in [43,44] have been calculated assuming vanishing $\mathcal{CP}$-violating phases. Moreover, they have been derived in the large tan β limit which implies that the bottom-quark mass m_b is put to zero if it is not multiplied with tan β. In this approach, the soft SUSY-breaking masses, the trilinear couplings of the stop and sbottom sector, as well as the top-quark mass are independent parameters. In contrast, the bottom-quark mass is treated as a dependent quantity and the expression for its counterterm is derived from the equation connecting the bottom-quark mass and the sbottom mixing

[1] An EFT study including the dominant dimension-six operators can be found in [16].

angle,[2]

$$s_{2\theta_{\tilde{b}}} = \frac{2 m_b \mu t_\beta}{m^2_{\tilde{b}_2} - m^2_{\tilde{b}_1}}, \tag{3}$$

where we introduced the abbreviations

$$s_\gamma = \sin\gamma, \quad c_\gamma = \cos\gamma, \quad t_\gamma = \tan\gamma \tag{4}$$

for a generic angle γ. Following the discussion in Refs. [43,44] we omitted terms proportional to $\sim A_b$ in Eq. (3), since they are not enhanced by factors of $\tan\beta$.

Therefore, the one-loop counterterm for the bottom-quark mass in this scheme has the following form,

$$\delta m_b = m_b \left(\frac{\delta m^2_{\tilde{b}_2} - \delta m^2_{\tilde{b}_1}}{m^2_{\tilde{b}_2} - m^2_{\tilde{b}_1}} + \frac{\delta s_{2\theta_b}}{s_{2\theta_b}} - \frac{\delta\mu}{\mu} - \delta t_\beta \right), \tag{5}$$

where $\delta\mu$ is the counterterm for the Higgsino mass parameter μ. The actual bottom quark mass, which is used in the calculation, is then given by

$$\widehat{m}_b = m_b^{\overline{\text{DR}},\text{MSSM}}(Q) \times \left(1 + \frac{\delta m^2_{\tilde{b}_2} - \delta m^2_{\tilde{b}_1}}{m^2_{\tilde{b}_2} - m^2_{\tilde{b}_1}} + \frac{\delta s_{2\theta_b}}{s_{2\theta_b}} - \frac{\delta\mu}{\mu} - \delta t_\beta \right)\Bigg|_{\text{fin}}. \tag{6}$$

It can be shown by explicit calculation that the renormalisation scale dependence of $m_b^{\overline{\text{DR}},\text{MSSM}}(Q)$ is canceled out by the scale dependence contained in the combination of the counterterms $\delta m^2_{\tilde{b}_2}$, $\delta m^2_{\tilde{b}_1}$ and $\delta s_{2\theta_b}$ in the bracket of Eq. (6). Therefore, $\widehat{m}_b$ is scale independent at the one-loop level if the Higgsino mass parameter μ and t_β are renormalised in the $\overline{\text{DR}}$[3] scheme as assumed throughout this work. In `FeynHiggs`, the associated renormalisation scale is by default set equal to M_t.

Due to the $SU(2)_L$ gauge symmetry, the bilinear soft SUSY-breaking parameters $m_{\tilde{b}_L}$ and $m_{\tilde{t}_L}$ are equal to each other at the tree level. This relation is broken at the one-loop level. The counterterms for $m_{\tilde{t}_L}$ and $m_{\tilde{b}_L}$ read

$$\begin{aligned} \delta m^2_{\tilde{t}_L} &= \cos^2\theta_{\tilde{t}}\, \delta m^2_{\tilde{t}_1} + \sin^2\theta_{\tilde{t}}\, \delta m^2_{\tilde{t}_2} \\ &\quad + (m^2_{\tilde{t}_2} - m^2_{\tilde{t}_1}) \sin 2\theta_{\tilde{t}}\, \delta\theta_{\tilde{t}} - 2\, m_t\, \delta m_t, \end{aligned} \tag{7a}$$

$$\begin{aligned} \delta m^2_{\tilde{b}_L} &= \cos^2\theta_{\tilde{b}}\, \delta m^2_{\tilde{b}_1} + \sin^2\theta_{\tilde{b}}\, \delta m^2_{\tilde{b}_2} \\ &\quad + (m^2_{\tilde{b}_2} - m^2_{\tilde{b}_1}) \sin 2\theta_{\tilde{b}}\, \delta\theta_{\tilde{b}} - 2\, m_b\, \delta m_b, \end{aligned} \tag{7b}$$

and are in general not equal to each other. In the following, we will assume that $m^2_{\tilde{t}_L}$ is given as an input parameter. Then the renormalised soft sbottom mass $m^2_{\tilde{b}_L}$ is given by

$$m^2_{\tilde{b}_L} = m^2_{\tilde{t}_L} + \delta m^2_{\tilde{t}_L} - \delta m^2_{\tilde{b}_L}. \tag{8}$$

The trilinear soft SUSY-breaking parameter A_b is fixed via the sbottom–sbottom–A-boson vertex function (see [43,44] for more details).

Renormalisation scheme 2

For our present study, we, however, do not make use of the $\mathcal{O}(\alpha_b\alpha_s, \alpha_b\alpha_t, \alpha_b^2)$ corrections already implemented in `FeynHiggs`. Instead, we employ the $\mathcal{O}(\alpha_b\alpha_s, \alpha_b\alpha_t, \alpha_b^2)$ corrections presented in [8,10] (see also [46,47]). These also include terms subleading in $\tan\beta$, allow for easier control of the renormalisation scheme and take $\mathcal{CP}$-violating phases fully into account. They will be part of an upcoming `FeynHiggs` release. For the present work, we evaluate them, however, externally and feed the numerical result back to `FeynHiggs`.[4] In this scheme the soft SUSY-breaking mass $m_{\tilde{b}_L}$ is not treated as an independent parameter and set equal to $m_{\tilde{t}_L}$. This implies

$$\delta m^2_{\tilde{b}_L} = \delta m^2_{\tilde{t}_L}, \tag{9}$$

where $\delta m^2_{\tilde{t}_L}$ is given by Eq. (7a). The consequence of this relation is that only one of the sbottom masses can be set on-shell. As a matter of convention, the mass of the second sbottom is defined in the on-shell scheme,

$$\delta m^2_{\tilde{b}_2} = \text{Re}\, \Sigma_{\tilde{b}_2\tilde{b}_2}(m^2_{\tilde{b}_2}). \tag{10}$$

We treat the mass of the bottom quark as an independent parameter which is renormalised in the $\overline{\text{DR}}$ scheme,

$$\delta m_b = \frac{m_b}{2}\, \text{Re}\, [\Sigma_b^L(m_b^2) + \Sigma_b^R(m_b^2) + 2\Sigma_b^S(m_b^2)]\Big|_{\text{div}}, \tag{11}$$

where Σ_b^L, Σ_b^R and Σ_b^S are defined in analogy to Eq. (2). The trilinear soft SUSY-breaking parameter A_b is also defined in the $\overline{\text{DR}}$ scheme,

$$\begin{aligned} \delta A_b^{\overline{\text{DR}}} &= \frac{1}{m_b} \Big[\left(\delta m^{2,\,\overline{\text{DR}}}_{\tilde{b}_1} - \delta m^{2,\,\overline{\text{DR}}}_{\tilde{b}_2} \right) \mathbf{U}_{\tilde{b}_{11}} \mathbf{U}^*_{\tilde{b}_{12}} \\ &\quad + \delta m^{2,\,\overline{\text{DR}}}_{\tilde{b}_{12}} \mathbf{U}_{\tilde{b}_{21}} \mathbf{U}^*_{\tilde{b}_{12}} + \delta m^{2,\,\overline{\text{DR}}}_{\tilde{b}_{21}} \mathbf{U}_{\tilde{b}_{11}} \mathbf{U}^*_{\tilde{b}_{22}} \Big] \\ &\quad - \left(A_b - \mu^*\, t_\beta \right) \frac{\delta m_b^{\overline{\text{DR}}}}{m_b} + t_\beta\, \delta\mu^{*,\,\overline{\text{DR}}} + \mu^*\, t_\beta\, \delta t_\beta^{\overline{\text{DR}}}, \end{aligned} \tag{12}$$

where $\mathbf{U}_{\tilde{b}}$ is the mixing matrix of the sbottom sector, and

$$\delta m^{2,\,\overline{\text{DR}}}_{\tilde{b}_{12}} = \frac{1}{2} \left(\Sigma^{(1)}_{\tilde{b}_1\tilde{b}_2}(m^2_{\tilde{b}_1})\Big|_{\text{div}} + \Sigma^{(1)}_{\tilde{b}_1\tilde{b}_2}(m^2_{\tilde{b}_2})\Big|_{\text{div}} \right)$$

[2] We use a different sign convention for μ in comparison to [43,44].

[3] To be more precise, these parameters are defined in the $\overline{\text{DR}}'$ scheme [45]. We will, however, not make any distinction between $\overline{\text{DR}}$ and $\overline{\text{DR}}'$ schemes throughout this paper except of Sect. 4.

[4] In practice, we use the `FHAddSelf` functionality (see `feynhiggs.de`).

$$= (m^2_{\tilde{b}_1} - m^2_{\tilde{b}_2})\delta\theta^{\overline{\rm DR}}_{\tilde{b}}, \tag{13a}$$

$$\delta m^{2,\,\overline{\rm DR}}_{\tilde{b}_{21}} = \left(\delta m^{2,\,\overline{\rm DR}}_{\tilde{b}_{12}}\right)^*. \tag{13b}$$

Equations (9)–(13) fix the renormalisation conditions for all parameters of the sector.

In both schemes described above it is assumed that the stop sector is renormalised using the OS scheme. We furthermore implemented a pure $\overline{\rm DR}$ renormalisation of the stop and sbottom sector as an additional option.

2.2 EFT calculation

We build upon the existing EFT calculation in `FeynHiggs` [22,23,26,36]. At the sfermion mass scale, $M_{\rm SUSY}$, all sfermions as well as the non-SM-like Higgs bosons are integrated out.[5] Performing the renormalisation-group running to lower scales and passing two additional independent thresholds for electroweakinos (charginos and neutralinos) and the gluino, the SM is recovered as EFT.[6] The currently implemented EFT calculation resums leading and next-to-leading (LL and NLL) logarithms as well as next-to-next-to-leading logarithms (NNLL) in the limit of vanishing electroweak gauge couplings. So far, however, all corrections proportional to the bottom Yukawa coupling are set to zero in the EFT calculation.

For the incorporation of the bottom Yukawa contributions, our aim was to reach the same level of accuracy as for the other corrections. For implementing LL and NLL resummation, we include the bottom Yukawa contributions to the one-loop matching condition of the SM Higgs self-coupling, λ [14,16]. Also the one- and two-loop RGEs are extended by the RGE of the bottom-Yukawa coupling and by bottom-Yukawa contributions to the RGEs of the other couplings (see e.g. [48]).

To achieve resummation at the NNLL level, we derive the $\mathcal{O}(\alpha_b\alpha_s, \alpha_b\alpha_t, \alpha_b^2)$ threshold corrections for λ making use of the two-loop Higgs self-energy corrections obtained in [8,10,42]. Details are given in Appendix A. In the limit of vanishing $\mathcal{CP}$-violating phases, we find agreement with the expressions derived in [16] using the effective-potential approach. We also add the bottom Yukawa contributions to the three-loop SM RGEs in the limit of vanishing electroweak gauge couplings [49–53] and to the calculation of the SM $\overline{\rm MS}$ vev at the electroweak scale.

[5] In this paper, we do not consider the `FeynHiggs` implementation incorporating a Two-Higgs-Doublet-Model as EFT below the sfermion scale [17].

[6] The case of the gluino being much heavier than the rest of the MSSM spectrum requires special care. This case was considered in [21].

For the EFT calculation, all sbottom input parameters are defined in the $\overline{\rm DR}$ scheme at the scale $M_{\rm SUSY}$. We choose to define $\tan\beta$ in the $\overline{\rm DR}$ scheme at the scale $M_{\rm SUSY}$.

2.3 Combination in the hybrid approach

For the combination of the fixed-order and the EFT calculation, we follow the procedure described in [22,23,26,28]. For the self-energy of the SM-like Higgs boson, the result of the fixed-order calculation, $\widehat{\Sigma}^{\rm FO}_{hh}(p^2)$, and the EFT result, $-2\lambda(M_t)(v_{\overline{\rm MS}})^2$ (with $v_{\overline{\rm MS}}$ being the SM $\overline{\rm MS}$ vev at the scale M_t), are summed. Subtraction terms are used to ensure that contributions included in both results are not counted twice,

$$\widehat{\Sigma}^{\rm hybrid}_{hh}(p^2) = \widehat{\Sigma}^{\rm FO}_{hh}(p^2) - 2\lambda(M_t)\overline{v}^2 - (\text{subtraction terms}). \tag{14}$$

In order to ease this combination, we choose to define the sbottom input parameters in the same scheme in the fixed-order and the EFT calculations: We fix them in the $\overline{\rm DR}$ scheme at the scale $M_{\rm SUSY}$. Also $\tan\beta$ and μ are fixed in the $\overline{\rm DR}$ scheme at the scale $M_{\rm SUSY}$.

A complication arises through the use of the $\overline{\rm DR}$ bottom quark mass in the EFT as well as the fixed-order calculation. After adding both results as shown in Eq. (14), the Higgs pole masses are determined taking into account the momentum dependence of the fixed-order self-energy. As discussed in detail in [28], this momentum dependence arises only from SM-type corrections as well as contributions suppressed by the SUSY scale. In order to match the result of a pure EFT calculation, in which the Higgs pole mass is determined in the SM, we have to ensure that the SM-type corrections are evaluated using only SM quantities. The $\overline{\rm DR}$ bottom-quark mass, however, is an MSSM quantity. For this reason, we reparametrise the SM bottom-quark contributions to the Higgs self-energies in terms of the SM $\overline{\rm MS}$ bottom quark mass at the scale M_t.

In our implementation, this is achieved by subtracting the UV-finite $\mathcal{O}(\alpha_b)$ self-energy, containing only the SM contributions and parametrised in terms of the MSSM bottom quark $m_b^{\overline{\rm DR},\rm MSSM}(M_{\rm SUSY})$, and then adding back the same quantity but parametrised via $m_b^{\overline{\rm MS},\rm SM}(M_t)$. The explicit expression for the one-loop SM Higgs boson self-energy renormalised in the $\overline{\rm MS}$ scheme with the tadpoles renormalised to zero is given by

$$\widetilde{\Sigma}^{\overline{\rm MS},\rm SM}_{hh}(p^2) = \frac{3m_b^2}{16\pi^2 v^2}(p^2 - 4m_b^2)B_0^{\rm fin}(p^2, m_b^2, m_b^2), \tag{15}$$

where the superscript "fin" means that in this expression we take only the finite part of the one-loop scalar integral function $B_0(p^2, m_1^2, m_2^2)$, for which we use the definition given in [54]. Since the SM-like Higgs mass is determined via an iterative solution of the pole equation, the same procedure has

to be applied to the derivative of $\widetilde{\Sigma}_{hh}^{\overline{\rm MS},\rm SM}(p^2)$ with respect to the external momentum. The $\mathcal{O}(\alpha_b\alpha_s, \alpha_t\alpha_b, \alpha_b^2)$ SM self-energies computed in the gaugeless limit are extracted from the code `FlexibleSUSY` [24,27,55] and Refs. [56,57].

In order to allow for an OS definition of the stop input parameters, a conversion of the OS parameters, used in the fixed-order calculation, to the $\overline{\rm DR}$ scheme, used in the EFT calculation, is necessary. As argued in [5,22,23,26], for this conversion only one-loop logarithmic terms should be taken into account. Only in the conversion formula for the stop mixing parameter, X_t, large logarithms appear. For the present study, we extend the formula given in [23] by including the bottom Yukawa contributions,

$$X_t^{\overline{\rm DR}}(M_{\rm SUSY}) = X_t^{\rm OS}\left\{1 + \left[\frac{\alpha_s}{\pi} - \frac{3\alpha_t}{16\pi}\left(1 - \frac{|X_t|^2}{M_{\rm SUSY}^2}\right) + \frac{3\alpha_b}{16\pi}\left(1 + \frac{|X_b|^2}{M_{\rm SUSY}^2}\right)\right]\ln\frac{M_{\rm SUSY}^2}{M_t^2}\right\}, \tag{16}$$

where X_b is the sbottom mixing parameter ($X_b = A_b - \mu^* \tan\beta$).

2.4 Determination of the MSSM bottom quark mass and Yukawa coupling

Here, we describe how we obtain the $\overline{\rm DR}$ bottom quark mass used in the fixed-order calculation as well as the $\overline{\rm DR}$ bottom Yukawa coupling used in the EFT calculation. As input, we use the SM $\overline{\rm MS}$ bottom Yukawa coupling, $y_b^{\overline{\rm MS},\rm SM}$, and the SM $\overline{\rm MS}$ vev, $v^{\overline{\rm MS},\rm SM}$, at the scale M_t. These are evolved to the SUSY scale. At this scale we determine the MSSM $\overline{\rm DR}$ bottom Yukawa coupling, $h_b^{\overline{\rm DR},\rm MSSM}$ (with $h_b c_\beta = y_b$ at the tree level), and the MSSM $\overline{\rm DR}$ vev, $v^{\overline{\rm DR},\rm MSSM}$, by matching the SM to the MSSM,

$$\left(h_b^{\overline{\rm DR},\rm MSSM} c_\beta\right)(M_{\rm SUSY}) = y_b^{\overline{\rm MS},\rm SM}(M_{\rm SUSY})\,(1 + \Delta y_b)\,, \tag{17}$$

$$v^{\overline{\rm DR},\rm MSSM}(M_{\rm SUSY}) = v^{\overline{\rm MS},\rm SM}(M_{\rm SUSY})(1 + \Delta v), \tag{18}$$

where the one-loop expression for Δv is given in Eq. (64) below. The $\overline{\rm DR}$ bottom quark mass is then determined by

$$m_b^{\overline{\rm DR},\rm MSSM}(M_{\rm SUSY}) = \left(h_b^{\overline{\rm DR},\rm MSSM} c_\beta\right)(M_{\rm SUSY}) \times v^{\overline{\rm DR},\rm MSSM}(M_{\rm SUSY}). \tag{19}$$

It is well-known that the relation between the $\overline{\rm DR}$ bottom quark mass and the SM $\overline{\rm MS}$ bottom Yukawa coupling includes terms proportional to $\tan\beta$. For large $\tan\beta$, the leading $\tan\beta$-enhanced terms can be resummed as described in [43,44,58–63]. Typically, this resummation is written in the form

$$m_b^{\overline{\rm DR},\rm MSSM} = m_b^{\overline{\rm MS},\rm SM}\frac{1+\epsilon_b}{|1+\Delta_b|}, \tag{20}$$

where Δ_b includes $\tan\beta$-enhanced terms, which are not suppressed by powers of m_b/m_t. ϵ_b contains all other terms from the one-loop relation between $m_b^{\overline{\rm DR},\rm MSSM}$ and $m_b^{\overline{\rm MS},\rm SM}$. We employ a similar relation for the matching of the bottom Yukawa coupling,[7]

$$\left(h_b^{\overline{\rm DR},\rm MSSM} c_\beta\right)(M_{\rm SUSY}) = y_b^{\overline{\rm MS},\rm SM}(M_{\rm SUSY})\frac{1+\epsilon_b-\Delta v}{|1+\Delta_b|}. \tag{21}$$

A similar procedure for the calculation of the MSSM bottom Yukawa coupling was adopted in [16]. There, however, non-enhanced terms, ϵ_b, and the threshold correction of the vev, Δv, were included into the definition of Δ_b. In our approach, we separate them to resum only $\tan\beta$ enhanced corrections to the bottom-Yukawa coupling in the same way as in [43,64]. This results only in a small numerical difference since the main contribution to $h_b^{\overline{\rm DR},\rm MSSM}(M_{\rm SUSY})$ comes from Δ_b (see also the discussion in Sect. 5).

In our implementation, we include full one-loop corrections to Δ_b. The quantity Δv is calculated at the one-loop level in the gaugeless limit. In addition, we include the leading two-loop corrections to Δ_b. These two-loop corrections are based on the results from [37–39].[8] We, however, perform an expansion of Δ_b (at the one- and two-loop level) for large $M_{\rm SUSY}$ omitting terms of higher-order in $\mathcal{O}(v^2/M_{\rm SUSY}^2)$. In addition, we adapt the renormalisation scheme to match our scheme. More precisely, in [37,39] the soft supersymmetry breaking parameters in the stop and sbottom sectors as well as the gluino mass are renormalised on-shell. Moreover, all supersymmetric particles and the top quark are decoupled from the scale dependence of the strong coupling α_s. This decoupling of the top quark and the on-shell renormalisation of the top sector induces large logarithms, $\log(M_{\rm SUSY}^2/M_t^2)$, implying that the formulas in [37–39] are not directly applicable in our framework. Since in our case the low-energy model

[7] There are terms proportional to $m_b^2\tan^2\beta$ in the one-loop relation between $m_b^{\overline{\rm DR},\rm MSSM}$ and $m_b^{\overline{\rm MS},\rm SM}$ as well as in the relation between $v^{\overline{\rm DR},\rm MSSM}$ and $v^{\overline{\rm MS},\rm SM}$. These terms are suppressed as $\sim m_b^2\tan\beta/m_t^2$ compared to the top Yukawa contribution to Δ_b and, therefore, numerically irrelevant. Therefore, we will refer to the terms in ϵ_b as "non-enhanced" terms in this paper.

[8] Similar results have been obtained in [65,66]. Moreover, the authors of [67] derived subleading two-loop corrections, which are not taken into account in the present work.

is the SM with possibly light gluinos (and electroweakinos), we do not decouple the top quark and the gluino. Also, to be consistent with the other parts of our EFT calculation we renormalise the gluino mass and the stop/sbottom masses in the $\overline{\text{DR}}$ scheme at the matching scale Q.

In the limit of all involved non-SM masses having the same value, we obtain

$$\Delta_b^{2l} = \Delta_b^{2l,\mathcal{O}(\alpha_s^2)} + \Delta_b^{2l,\mathcal{O}(\alpha_t\alpha_s)}, \tag{22}$$

$$\Delta_b^{2l,\mathcal{O}(\alpha_s^2)} = \frac{\alpha_s(Q)^2 C_F}{12\pi^2}\frac{\mu}{M_{\text{SUSY}}} t_\beta \Bigg(2C_A - C_F + 6T_R - (3C_A - 2C_F - 9T_R)\log\frac{M_{\text{SUSY}}^2}{Q^2}\Bigg), \tag{23}$$

$$\Delta_b^{2l,\mathcal{O}(\alpha_t\alpha_s)} = -\frac{\alpha_s(Q) y_t^2(Q) C_F}{384\pi^3}\frac{A_t}{M_{\text{SUSY}}} t_\beta \times \left(7 + 10\log\frac{M_{\text{SUSY}}^2}{Q^2}\right). \tag{24}$$

Here, A_t is the stop trilinear coupling ($A_t = X_t + \mu^*/\tan\beta$), Q is the renormalisation scale, $C_A = 3, C_F = \frac{4}{3}$ and $T_R = \frac{1}{2}$. Formulas also valid for non-degenerate masses are distributed as ancillary files together with this paper.

3 EFT calculation for complex input parameters

In the fixed-order approach, the dependence on $\mathcal{CP}$-violating phases is known at the one- and two-loop level [35,40–42,68]. In the EFT framework, the phase dependence has so far only been considered in case of a low-energy Two-Higgs-Doublet-Model [20,69–72]. Here, we work out the dependence on $\mathcal{CP}$-violating phases in the case of the SM (and the SM plus electroweakinos and/or gluinos) as EFT, for which so far only an interpolation of the result in case of real input parameters has been available [36].

We first discuss the case of the SM as low-energy EFT. Since the SM includes no phases (apart from the CKM phase, whose effect is negligible for the determination of the Higgs mass), $\mathcal{CP}$-violating effects in the full MSSM enter only via threshold corrections to real parameters. At the one-loop level, the only contribution to the matching of the Higgs self-coupling with a non-vanishing phase dependence is the electroweakino contribution. It depends on the phases of the bino and wino soft-breaking masses, ϕ_{M_1} and ϕ_{M_2}, as well as of the Higgsino mass parameter, ϕ_μ (explicit expressions are listed in Appendix B). This implies that at the one-loop level, there is no dependence on the phases of the squark sector (at least if the absolute values of the squark mixing parameters, $|X_q|$, are kept constant).

The phases of the stop and sbottom sector along with the gluino phase, ϕ_{M_3}, however, enter the matching of the Higgs self-coupling at the two-loop level. Based upon the fixed-order results presented in [8,10,41,42], we extract the dependence of the two-loop threshold correction on these phases at $\mathcal{O}(\alpha_{b,t}\alpha_s, \alpha_b^2, \alpha_b\alpha_t, \alpha_t^2)$ without assumptions on the internal masses (details are given in Appendix A). In case of real input parameters, we find full agreement with the results of [14,16,73]. By analysing the obtained expressions, it becomes clear how the expressions derived in [14,16,73] can be generalised to the case of complex input parameters:

- $\mathcal{O}(\alpha_q\alpha_s)$ where $q = t, b$: The expression for zero phases is a polynomial in $\widehat{X}_q$. To get the expression for non-zero phases every odd power of $\widehat{X}_q$ has to be multiplied by $\cos(\phi_{X_q} - \phi_{M_3})$, and $\widehat{X}_q$ has to replaced by $|\widehat{X}_q|$.
- $\mathcal{O}(\alpha_q^2)$ where $q = t, b$: The expression for zero phases is a sum of monomials in the variables $\widehat{X}_q$ and $\widehat{Y}_q = \widehat{X}_q + \frac{2\widehat{\mu}^*}{\sin 2\beta}$ of one of three types: the monomials which contain only even powers of $\widehat{X}_q$, the ones which contain only even powers of $\widehat{Y}_q$ and the ones which contain both $\widehat{X}_q$ and $\widehat{Y}_q$. The latter contain only even or only odd powers of $\widehat{X}_q$ and $\widehat{Y}_q$ at the same time. To get the expression for non-zero phases, every monomial which contains odd powers of $\widehat{X}_q$ and $\widehat{Y}_q$ has to be multiplied by $\cos(\phi_{X_q} - \phi_{Y_q})$, and every $\widehat{X}_q$ and $\widehat{Y}_q$ has to be replaced by $|\widehat{X}_q|$ and $|\widehat{Y}_q|$, respectively.

The generalisation of the $\mathcal{O}(\alpha_b\alpha_t)$ expression from the $\mathcal{CP}$-conserving case to the $\mathcal{CP}$-violating case is slightly more complicated since different multiplicative factors arise.

Full explicit expressions in the limit of all sfermions having the same mass are given in Appendix B.2. Fully general expressions can be found in ancillary files distributed alongside this paper.

If the low-energy theory is the SM plus electroweakinos, effective Higgs–Higgsino–Gaugino couplings are induced. These are potentially complex-valued. An explicit matching calculation at the one-loop level, however, shows that their phase is zero even if one or more of the electroweakino phases in the MSSM are non-zero. Correspondingly, also the RGEs of the SM plus electroweakinos are not modified in the presence of non-zero phases. The phases, however, enter in the threshold corrections for the bottom and top Yukawa couplings as well as the Higgs self-coupling when integrating out the electroweakinos (full expressions are listed in Appendix B).

In addition to the phase dependencies discussed above, also the Δ_b corrections (see Sect. 2.4) depend on ϕ_μ, $\phi_{M_{1,2,3}}$ and ϕ_{A_t}. The phase dependence of the one-loop correction has been derived in [64,74,75]. The phase dependence of the two-loop correction, which we derived based upon the result of [37–39] (see Sect. 2.4), has, however, been unknown so far.

We find that this dependence is the same as for the one-loop result. Namely, Eq. (23) has to be multiplied by $\cos(\phi_\mu + \phi_{M_3})$ and Eq. (24) has to be multiplied by $\cos(\phi_\mu + \phi_{A_t})$.

This can be understood by looking at the explicit two-loop diagrams (see Appendix C). They fall into three categories: either a gluon, a gluino or a sbottom quark is added to the one-loop graph. If a gluon is added, the phase dependence of the one-loop graph is obviously not changed, since the two additionally appearing strong gauge couplings do not include a phase dependence. The same is true if a sbottom quark is coupled to the one-loop graph by a four-sfermion vertex. Working in the chiral basis, it is again obvious that this coupling does not induce an additional phase dependence. The case of adding a gluino is slightly more complicated. The two additional gluon-gluino-sbottom couplings do depend on the phase of the gluino mass parameter. Working again in the chiral basis, it is easy to see that one of these two additional couplings is a left-handed coupling and the other one is a right-handed coupling. The dependence on the gluino phase cancels between the left-handed and the right-handed coupling. More details and all relevant two-loop diagrams can be found in Appendix C.

4 N^{3}LL resummation

Up to now, the EFT calculation implemented in `FeynHiggs` was restricted to full LL and NLL resummation as well as NNLL resummation in the limit of vanishing electroweak gauge couplings. In this Section, we discuss the implementation of N^{3}LL resummation at $\mathcal{O}(\alpha_t\alpha_s^2)$ based upon the work presented in [18].

The following ingredients are needed in addition to the already implemented corrections for NNLL resummation:

- SM $\mathcal{O}(\alpha_t\alpha_s^2)$ Higgs self-energy corrections,
- leading QCD corrections to the three-loop RGEs of the Higgs self-coupling, the strong gauge coupling as well as the top Yukawa coupling,
- $\mathcal{O}(\alpha_s^3)$ extraction of the $\overline{\text{MS}}$ top Yukawa coupling at the electroweak scale,
- $\mathcal{O}(\alpha_t\alpha_s^2)$ matching condition for the Higgs self-coupling between the SM and the MSSM.

The SM $\mathcal{O}(\alpha_t\alpha_s^2)$ corrections to the Higgs self-energy have been obtained in [57,76,77]; the necessary RGEs in [77,78]. Formulas for extracting the SM $\overline{\text{MS}}$ couplings at the three-loop level can be found in [48]. The $\mathcal{O}(\alpha_t\alpha_s^2)$ matching condition of the Higgs self-coupling was computed in [18] based on the $\mathcal{O}(\alpha_t^2\alpha_s^2)$ fixed-order calculation performed in [9,79,80]. The result is implemented in the publicly available code `Himalaya` [9,18]. As discussed in [18], this calculation is based on an expansion of three-loop diagrams for certain mass hierarchies. `Himalaya` provides an uncertainty estimate for this truncation error.

We implemented all these corrections into the EFT calculation of `FeynHiggs` (the link to `Himalaya` has already been implemented for the work presented in [5]). By default, `Himalaya` uses the $\overline{\text{DR}}'$ scheme [45] for the renormalisation of the squark input parameters [18]. Correspondingly, also the input parameters of `FeynHiggs` are defined in the $\overline{\text{DR}}'$ scheme if N^{3}LL resummation is activated. In case of complex input parameters, we interpolate the `Himalaya` result.[9]

The inclusion of N^{3}LL resummation in the EFT calculation can also be used within the hybrid approach. In this case we, however, require that also in the fixed-order calculation the parameters entering the three-loop threshold correction are renormalised in the $\overline{\text{DR}}'$ scheme. The two-loop conversion, that would be necessary between OS parameters used in the fixed-order calculation and $\overline{\text{DR}}'$ parameters used in the EFT calculation, is beyond the scope of the present paper.[10]

5 Numerical results

In this section, we discuss the numerical effects of the various improvements discussed above.

5.1 Resummation of logarithmic bottom Yukawa contributions

Here, we investigate the numerical effect of resumming logarithmic contributions proportional to the bottom Yukawa coupling. First, we concentrate on a scenario presented in Ref. [16]. Namely, we assume that all soft SUSY-breaking masses are equal to $M_{\text{SUSY}} = 1.5$ TeV except the gluino mass which is fixed by $M_3 = 2.5$ TeV. The stop mixing parameter is set by $X_t = \sqrt{6}M_{\text{SUSY}}$, and the trilinear couplings of the third generation fermions are equal to each other, $A_b = A_\tau = A_t$. The Higgsino mass parameter, μ, is chosen to be equal to -1.5 TeV. Due to this choice of the signs of M_3, X_t and μ the MSSM bottom Yukawa coupling is enhanced by the one-loop threshold corrections proportional to the top Yukawa coupling and the strong coupling. As in Ref. [16] all the input parameters listed above and $\tan\beta$ are assumed to be $\overline{\text{DR}}$ parameters at the scale M_{SUSY}.[11]

[9] An interpolation in case of a complex M_3 is not possible, since the expressions implemented in `Himalaya` are not dependent on the sign of M_3.

[10] The necessary two-loop squark self-energy corrections have already been calculated in [81,82].

[11] In the considered scenario the ratio M_3/M_{SUSY} equals 5/3. According to the analysis carried out in [21], the hierarchy between the gluino and squark masses is not so large that a resummation of the M_3-enhanced contributions would be required, see e.g. Fig. 1 of [21].

In the left panel of Fig. 1 we present results for M_h in dependence on $\tan\beta$. In addition to showing results obtained with the calculation presented in this paper, we display results obtained using the most recent public version of `FeynHiggs` (version `2.16.1`). Moreover, we show the result presented in Fig. 2 of [16] for comparison. This result was obtained in a pure EFT framework using a private code written by the authors of the paper which is formally equivalent to the code `HSSUSY` [24,27] at the discussed order. In the right panel of Fig. 1 we show the bottom mass, m_b, which is used in the corresponding calculations. In the case of the red dashed curve it is the "OS" bottom mass, $\widehat{m}_b$, defined by Eq. (6) and in case of the blue, red, orange and green solid lines it is $m_b^{\overline{\rm DR},\rm MSSM}(M_{\rm SUSY})$ given by Eq. (20).

In the first step of our numerical analysis, we focus on the various EFT results in the left panel of Fig. 1: the black dot-dashed line corresponds to the result obtained in [16] (red solid line in Fig. 2 of [16]). For this curve the full LL and NLL resummation of large logarithms is performed. In addition to that, NNLL logarithms are resummed to all orders in the gaugeless limit (i.e., the electroweak gauge couplings are neglected in the two-loop threshold corrections to λ). One-loop Δ_b resummation, including $\mathcal{O}(\alpha_s,\alpha_t)$ corrections, is used in the one-loop threshold correction for the bottom Yukawa coupling. The red, blue, green and orange solid lines correspond to the results of our EFT calculation with different approximation levels used in the calculation of the bottom Yukawa threshold correction. We should note here that the results presented in [16] have been obtained using the SM $\overline{\rm MS}$ top Yukawa coupling extracted at the N^{3}LO level while we by default use the NNLO value. For a proper comparison with the results of [16], we adapted our calculation to use the same level of corrections (see also the discussion in Sects. 4 and 5.3). We use this determination of the SM $\overline{\rm MS}$ top Yukawa coupling for all curves of Fig. 1.

We observe a very good agreement between our EFT result using only $\mathcal{O}(\alpha_s,\alpha_t)$ corrections in the calculation of Δ_b (solid red curve), which is the same level of accuracy as used in [16], and the result of [16] (black dot-dashed curve). The absolute difference between the two curves equals $\sim$ 0.04 GeV for $t_\beta = 15$ and $\sim$ 0.7 GeV for $t_\beta = 42$ where the curves have a very steep behavior. This difference comes mainly from the determination of the MSSM bottom Yukawa coupling at the scale $M_{\rm SUSY}$. In [16], the threshold correction for the vacuum expectation value, Δv, and non-enhanced terms were included in the definition of Δ_b while we do not include them (see Eq. (21)). If we include them into Δ_b as in [16], the absolute difference between our calculation and the calculation presented in [16] shrinks down even further ($\sim$ 0.2 GeV for $t_\beta = 42$).

For the green solid curve in the left plot of Fig. 1, we take into account electroweak corrections in the calculation of Δ_b in addition to the $\mathcal{O}(\alpha_s,\alpha_t)$ corrections used for the solid red curve. As a consequence of Eq. (62), this choice leads to a partial cancellation in the calculation of Δ_b and hence to a suppression of the MSSM bottom mass at the scale $M_{\rm SUSY}$ as one can see on the right panel of Fig. 1 showing $m_b^{\overline{\rm DR},\rm MSSM}(M_{\rm SUSY})$ in dependence of $\tan\beta$. This in turn reduces the downward shift in the Higgs mass by the one-loop threshold corrections to the SM Higgs self-coupling, λ, that is proportional to the bottom Yukawa coupling.

The blue solid curve in the left plot of Fig. 1 shows the prediction for M_h neglecting the electroweak one-loop contributions to Δ_b but including the leading two-loop QCD corrections to Δ_b. For our parameter choice, these corrections increase the absolute value of Δ_b by approximately 5%. Correspondingly, also the MSSM bottom mass is increased as can be seen in the right plot of Fig. 1. This results in a significant change of the resulting Higgs mass for $\tan\beta \gtrsim 40$ where the dependence on $\tan\beta$ is very pronounced. The orange curves in the left plot of Fig. 1 correspond to the inclusion of all corrections to Δ_b mentioned above. For the considered parameter choice, the electroweak corrections to Δ_b are roughly three times larger by absolute value than the two-loop corrections to Δ_b. This explains why the orange and the green curves lie quite close to each other.

The orange dashed curve represents the result of the hybrid calculation of M_h. Namely, we have merged the fixed-order result with the NNLL EFT calculation (see Sect. 2). The orange solid and dashed curves differ essentially by the inclusion of terms which are suppressed by the ratio $v^2/M_{\rm SUSY}^2$ into the hybrid result. Since in our case $M_{\rm SUSY}$ is chosen above the TeV scale, the size of these terms is, as expected, quite small. Therefore, the observed good agreement between the two methods serves as a consistency check of our hybrid calculation.

Finally, the red dashed curve shows the prediction for M_h obtained by `FeynHiggs-2.16.1` which we ran using the default flags as explained in [36].[12] As only modification of this version, we have used the N^{3}LO instead of the NNLO SM $\overline{\rm MS}$ top Yukawa coupling to allow for a direct comparison to the result of [16]. We see that the agreement between all the seven curves is quite good for small values of $\tan\beta$, but for $\tan\beta \gtrsim 30$ the red dashed curve shows a steep fall-off, while for the other curves the large downward shift from $b/\tilde{b}$-sector corrections sets in only at higher values of $\tan\beta$. The reason for this behaviour becomes clear when looking at the right panel of Fig. 1: the red dashed curve, which corresponds to $\widehat{m}_b$ defined in Eq. (6), increases much more rapidly for

[12] For reference, here we list the values of these input flags: `mssmpart` = 4, `higgsmix` = 2, `p2approx` = 4, `looplevel` = 2, `loglevel` = 3, `runningMT` = 1, `botResum` = 1, `tlCplxApprox` = 0.

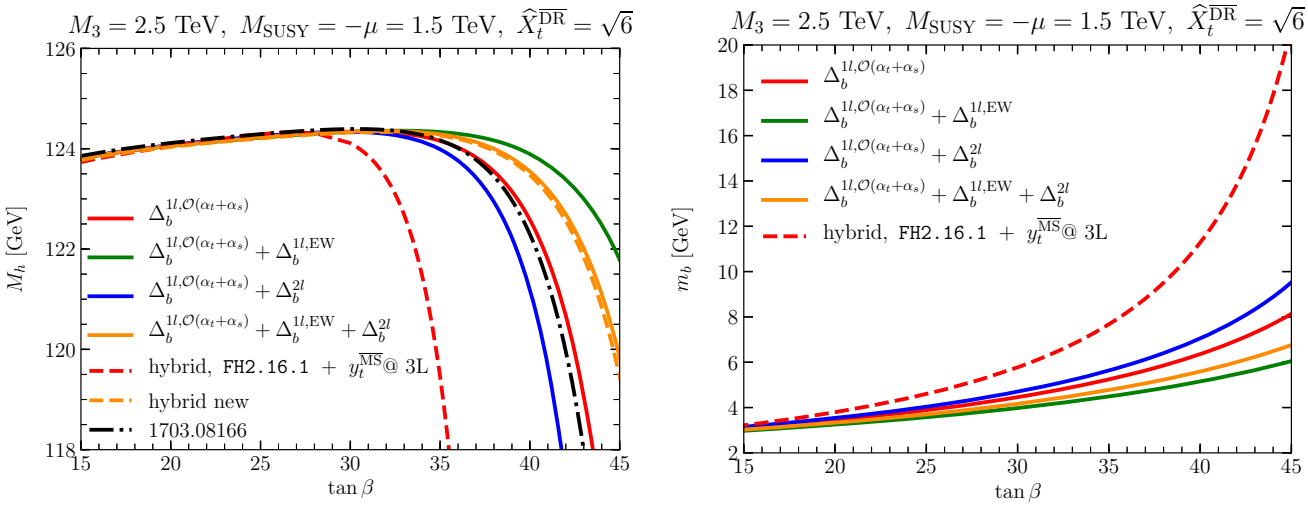

Fig. 1 Predictions for M_h (left) and m_b (right), which denotes the bottom mass used in the different calculations (see text), as a function of $\tan\beta$ for different accuracy levels in the calculation of Δ_b. For this plot we consider the same MSSM scenario as in Fig. 2 of [16]

rising $\tan\beta$ than the other four lines.[13] This expression for the bottom mass is inserted in the leading one-loop fixed order result which gives rise to a large downward shift of M_h [83–85],

$$(\Delta M_h^2)^{1-\text{loop,bottom}} \simeq -\frac{\widehat{m}_b^4 \tan^4\beta}{16\pi^2 v^2}. \tag{25}$$

This term grows rapidly in absolute value with increasing $\tan\beta$. A similar effect occurs for all other curves but there the dependence of the bottom mass on $\tan\beta$ is much milder. This is a consequence of our choice of the renormalisation scheme. Namely, the bottom mass used in our setup is the $\overline{\rm DR}$ MSSM bottom mass calculated at the scale $M_{\rm SUSY}$. All the quantities entering the calculation of Δ_b and ϵ_b are also $\overline{\rm DR}$ MSSM quantities at this scale. The most important ones are the top Yukawa coupling α_t and the strong Yukawa coupling α_s (see Eq. (62) in Appendix B). Since their values decrease with increasing scale, [14] the Δ_b correction calculated in our approach is smaller than the corresponding correction in FeynHiggs-2.16.1. In this way our approach yields more stable results for large values of $\tan\beta$ and for regions of the MSSM parameter space where the signs of the products μM_3 and μA_t are negative.

Next, we discuss the numerical effect induced by the resummation of logarithms proportional to the bottom Yukawa coupling. First of all, to have an idea how numerically important the effect is, it is instructive to have a look at the analytic one- and two-loop expressions which one can find in Appendix D. The bottom mass we use in our calculation, even though being potentially enhanced by Δ_b effects, is the smallest mass taken into account in our EFT calculation. The only way corrections containing the bottom mass may become sizeable is when these terms are additionally proportional to $\tan\beta$. This is the case when m_b is, for example, multiplied by $\widehat{X}_b$, $\widehat{Y}_t$, t_β or $1/c_\beta$. We only find such enhancements in the two-loop next-to-leading logarithmic contributions when the stop mixing parameter, $\widehat{X}_t$, is renormalised in the OS scheme (see Eqs. (83) and (84)). As a consequence, we expect the effect of the resummation to be small if we renormalise $\widehat{X}_t$ in the $\overline{\rm DR}$ scheme.

This qualitative consideration turns out to be reflected in the numerical results as one can see in the left panel of Fig. 2. The red curve corresponds to the hybrid result including the effects of the bottom Yukawa coupling only at the one-loop level in the fixed order calculation. The used MSSM $\overline{\rm DR}$ bottom mass, $m_b^{\overline{\rm DR},\rm MSSM}(M_{\rm SUSY})$, contains all the corrections discussed above (i.e. the level of accuracy corresponds to the orange curves in Fig. 1). The green curve includes additionally the $\mathcal{O}(\alpha_b\alpha_s, \alpha_b\alpha_t, \alpha_b^2)$ fixed-order corrections from [8,10]. Finally, the blue curve also contains the resummation of LL, NLL and NNLL logarithms controlled by the bottom Yukawa coupling. The same color scheme also applies to the right panel of Fig. 2 and to both plots in Fig. 3. For these plots we have picked a MSSM scenario where all soft-breaking masses and μ are equal by absolute value to the common mass scale $M_{\rm SUSY}$. Moreover, we set $A_b = 2.5 M_{\rm SUSY}$ and $t_\beta = 45$. The bino, wino and gluino masses are chosen to be positive, $M_{1,2,3} > 0$, while the Higgsino mass parameter is negative, $\mu < 0$.

For the left plot of Fig. 2 we have chosen $\widehat{X}_t^{\overline{\rm DR}}(M_{\rm SUSY}) \equiv X_t^{\overline{\rm DR}}(M_{\rm SUSY})/M_{\rm SUSY} = \sqrt{6}$. First, we note that the green and the blue curves agree very well with each other for low

[13] Note that the red dashed and the red solid line have the same accuracy level of Δ_b.

[14] Note that we have also included the leading two-loop QCD corrections to Δ_b which reduces its scale dependence.

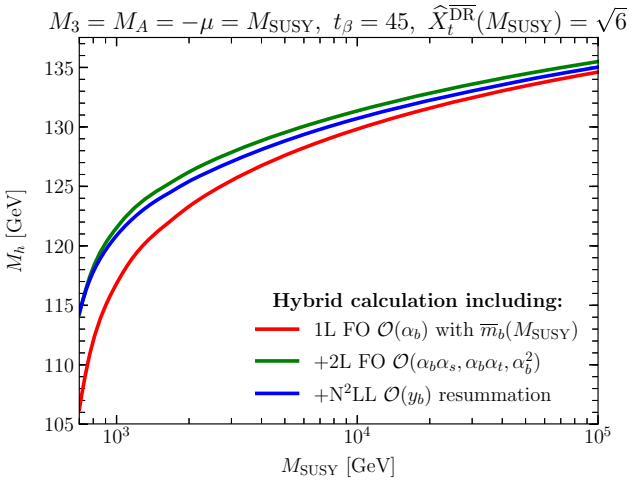

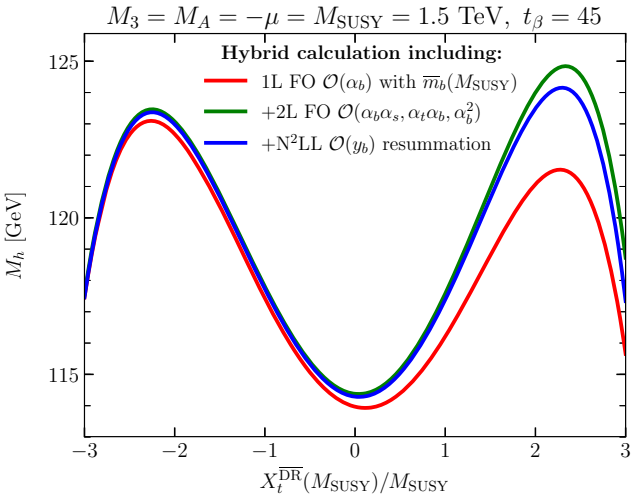

Fig. 2 M_h as a function of $M_{\rm SUSY}$ (left) and $\widehat{X}_t^{\overline{\rm DR}}(M_{\rm SUSY})$ (right). The red lines show the prediction of our hybrid calculation including only the one-loop fixed-order $\mathcal{O}(\alpha_b)$ correction. For the blue lines, we additionally included the fixed-order $\mathcal{O}(\alpha_b\alpha_s, \alpha_b\alpha_t, \alpha_b^2)$ corrections. The green lines contain additionally the resummation of logarithms proportional to the bottom Yukawa coupling up to the NNLL level

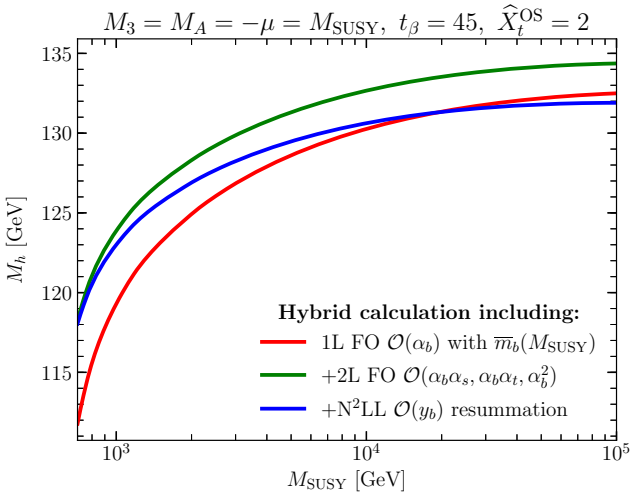

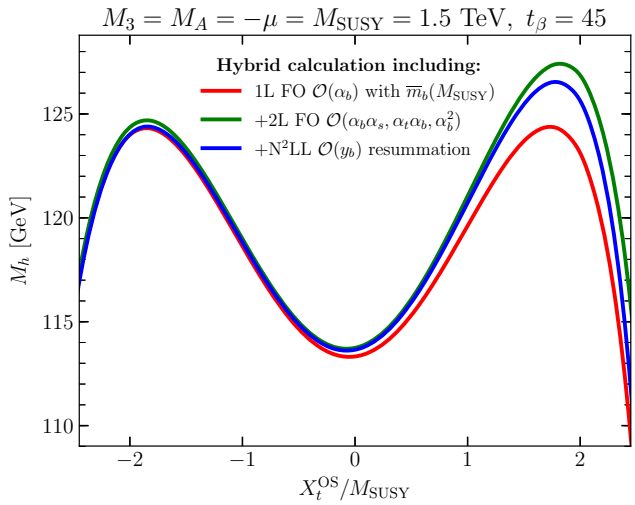

Fig. 3 Same as Fig. 2 but X_t is renormalised in the OS scheme

values of $M_{\rm SUSY}$. The difference between the two amounts to only ~ 0.3 GeV for $M_{\rm SUSY} = 700$ GeV. In this region, where the scale separation is relatively small, the resummation of higher-order logarithmic contributions is expected to be subdominant.[15] However, the two curves lie quite close to each other for the whole range of scales, even for $M_{\rm SUSY}$ as high as 10^5 GeV. This is in line with our qualitative analysis above: the logarithms containing bottom Yukawa coupling are numerically small if $\widehat{X}_t^{\overline{\rm DR}}(M_{\rm SUSY})$ is used as an input parameter.

On the other hand, a large shift of about 10 GeV between the red and the green curves in this Figure can be observed for small values of $M_{\rm SUSY}$. It decreases for rising $M_{\rm SUSY}$ and amounts to about 0.5 GeV for $M_{\rm SUSY} = 10^5$ GeV. This result indicates that for this scenario Δ_b by itself is not a good approximation for the higher-order effects controlled by the bottom Yukawa coupling in the region of small $M_{\rm SUSY}$, since

[15] It is worth noting here that the different treatment of the vacuum expectation value in the fixed-order calculation, where v_{G_F} is used, and in the EFT calculation, where $v^{\overline{\rm DR},\rm MSSM}(M_{\rm SUSY})$ is used, induces differences at order $\mathcal{O}(m_b^2\alpha(\alpha_t+\alpha_b))$ which are beyond the accuracy level of our calculation and hence may be regarded as part of the uncertainties from unknown higher-order corrections. Moreover, the different treatment of the vacuum expectation value in the two-loop threshold corrections and in the respective pieces of the fixed-order calculation, inducing a difference at the three-loop order, contributes to the small shift between the result containing the two-loop fixed order result in the $b/\tilde{b}$-sector and the one including the resummation of higher-order logarithmic contributions. A similar effect was also discussed in [26].

the MSSM bottom mass $m_b^{\overline{\rm DR},\rm MSSM}(M_{\rm SUSY})$ is large in this region due to the large and negative value of Δ_b.[16] Thus, in this scenario two-loop fixed-order corrections from the $b/\tilde{b}$-sector that go beyond the Δ_b contribution are numerically important.[17] With increasing $M_{\rm SUSY}$ the bottom mass $m_b^{\overline{\rm DR},\rm MSSM}(M_{\rm SUSY})$ decreases and the three curves get close to each other.

In the plot on the right panel of Fig. 2 we fix $M_{\rm SUSY} = 1.5$ TeV and vary $\widehat{X}_t^{\overline{\rm DR}}$. One can see that for negative $\widehat{X}_t^{\overline{\rm DR}}$ all three curves give roughly the same result. This is due to the fact that the contributions to Δ_b proportional to the strong coupling and to the top Yukawa coupling partially cancel each other. Correspondingly, the bottom mass does not acquire a significant enhancement for negative $\widehat{X}_t^{\overline{\rm DR}}$. The inclusion of the two-loop fixed-order corrections as well as the resummation of the logarithms has only a small effect in this case. On the contrary, for positive $\widehat{X}_t$ the top Yukawa and strong corrections to Δ_b add up and enhance the bottom mass.[18] In accordance with Eq. (25), this shifts the Higgs mass downwards at the one-loop level. This effect can be seen in the shape of the red curve: while for scenarios where contribution of the $b/\tilde{b}$-sector is numerically small (see e.g. Fig. 9 in [5]) the local maximum for M_h at positive values of $\widehat{X}_t^{\overline{\rm DR}}$ is typically several GeV higher than the one at negative values of $\widehat{X}_t^{\overline{\rm DR}}$, for the red curve in the right plot of Fig. 2 the maximum at positive values of $\widehat{X}_t^{\overline{\rm DR}}$ is about 2 GeV lower than the one at negative values of $\widehat{X}_t^{\overline{\rm DR}}$. Because of the large value of $m_b^{\overline{\rm DR},\rm MSSM}(M_{\rm SUSY})$ the incorporation of the two-loop corrections in the $b/\tilde{b}$-sector (green curve) has a significant effect for $\widehat{X}_t^{\overline{\rm DR}} = \sqrt{6}$, giving rise to an upward shift of more than 3 GeV. Since there is only a moderate splitting between $M_{\rm SUSY}$ and M_t, the effect of the resummation of higher-order logarithmic contributions remains relatively small (blue curve). It amounts to a downward shift of less than 1 GeV for $\widehat{X}_t^{\overline{\rm DR}} = \sqrt{6}$.

In Fig. 3, we renormalise the stop sector in the OS scheme. In the left plot $\widehat{X}_t^{\rm OS} = 2$ is chosen. This plot shares the same features at low $M_{\rm SUSY}$ as the corresponding plot in Fig. 2. However, for large $M_{\rm SUSY}$ the effect of the resummation becomes more prominent due to the presence of logarithmic terms of $\mathcal{O}(m_b^2 m_t^4)$ that are enhanced by t_β^2 (see Eq. (83) below),

$$(M_h^{\rm 2L,NLL})^2_{\rm bot,OS} \simeq 3\kappa^2 \frac{\overline{m}_b^2 \overline{m}_t^4}{v^4} t_\beta^2 \times |\widehat{A}_t|^2 (6 - |\widehat{A}_t|^2) \log \frac{M_{\rm SUSY}^2}{M_t^2}. \quad (26)$$

In the considered scenario, the resummation gives rise to a downward shift of the Higgs mass, visible as the difference between the blue curve and the green curve, by ~ 2 GeV for $M_{\rm SUSY} = 10$ TeV and by ~ 2.5 GeV for $M_{\rm SUSY} = 100$ TeV. On the right panel of this Figure we show the result of varying $\widehat{X}_t^{\rm OS}$ with fixed $M_{\rm SUSY} = 1.5$ TeV. As in the case of the $\overline{\rm DR}$ stop input parameters the three lines are very close to each other for $\widehat{X}_t^{\rm OS} < 0$. The effect of the inclusion of the two-loop $\mathcal{O}(\alpha_b\alpha_s, \alpha_b\alpha_t, \alpha_b^2)$ fixed-order corrections (green curve) and the resummation (blue curve) becomes sizeable in the region $\widehat{X}_t^{\rm OS} \gtrsim 1$. Because of the moderate value of $M_{\rm SUSY} = 1.5$ TeV the impact of the higher-order logarithmic contributions is not significantly enhanced compared to the result expressed in terms of $\widehat{X}_t^{\overline{\rm DR}}$ shown in the right plot of Fig. 2.

As a final phenomenological application of our improved calculation, we consider the $M_h^{125,\mu-}$ benchmark scenario recently defined in [86], accompanying the benchmark scenarios proposed in [87,88]. In this scenario the SUSY input parameters are fixed as

$$\begin{aligned} &M_{Q_3} = M_{U_3} = M_{D_3} = 1.5 \text{ TeV}, \quad M_{L_3} = M_{E_3} = 2 \text{ TeV}, \\ &\mu = -2 \text{ TeV}, \quad M_1 = 1 \text{ TeV}, \\ &M_2 = 1 \text{ TeV}, \quad M_3 = 2.5 \text{ TeV}, \\ &X_t = 2.8 \text{ TeV}, \quad A_b = A_\tau = A_t \,. \end{aligned}$$

For the SM parameters the ones recommended by the LHC-HXSWG [89] are used:

$$\begin{aligned} m_t^{\rm pole} &= 172.5 \text{ GeV}, \\ \alpha_s(M_Z) = 0.118, \quad G_F &= 1.16637 \cdot 10^{-5} \text{ GeV}^{-2}, \\ m_b(m_b) &= 4.18 \text{ GeV}, \\ M_Z = 91.1876 \text{ GeV}, \quad M_W &= 80.385 \text{ GeV} \,. \end{aligned}$$

The stop SUSY soft-breaking parameters are defined in the OS scheme. In [86], also the sbottom trilinear coupling is renormalised in the OS scheme. For better comparison with our previous results, we instead choose to fix A_b and the sbottom masses in the $\overline{\rm DR}$ scheme.[19] In addition, we define $\tan\beta$ at the scale $M_{\rm SUSY}$ instead of at the scale M_t, which was used in [86].

Note that for this scenario $\mu = -2$ TeV is chosen implying relatively large Δ_b corrections which enhance the cross section times branching ratio for the heavy Higgs bosons

[16] For example, for $M_{\rm SUSY} = 700$ GeV it amounts to $m_b^{\overline{\rm DR},\rm MSSM}(M_{\rm SUSY}) \simeq 7.5$ GeV.

[17] It is worth noting that due to the parameter choices, which enhance Δ_b, different levels of approximation in Δ_b yield very different results for M_h in this scenario.

[18] In particular, in the considered scenario and for $\widehat{X}_t^{\overline{\rm DR}} = \sqrt{6}$ the top-Yukawa and strong contributions to the one-loop Δ_b amount to $\Delta_b^{\mathcal{O}(\alpha_t)} \simeq -0.33$ and $\Delta_b^{\mathcal{O}(\alpha_s)} \simeq -0.41$, respectively.

[19] The difference to the corresponding result using the OS scheme for the renormalisation of the sbottom sector is very small.

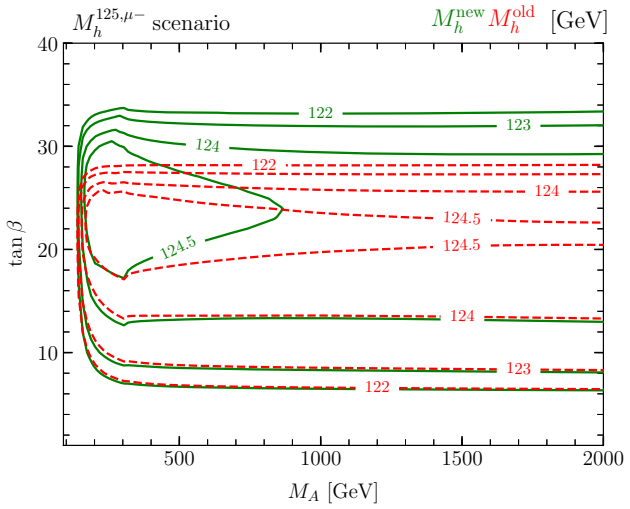

Fig. 4 Predicted contour lines for M_h in the $M_h^{125,\mu-}$ scenario using a calculation including only the leading corrections to Δ_b, corresponding to the one used in [86] (red dashed lines), and our improved calculation presented in this paper (green solid lines)

decaying to a pair of bottom quarks. In addition, the Δ_b corrections also affect the prediction for the SM-like Higgs boson, which we will investigate here.

The stop mass scale is equal to 1.5 TeV, so we do not expect the resummation of logarithms controlled by the bottom Yukawa coupling to have a major numerical impact in this case (see discussion above). On the other hand, as we have seen in Figs. 1, 2 and 3, large Δ_b corrections imply that the prediction for M_h can be sensitive to the level of accuracy in the determination of the bottom mass which is used in the fixed-order corrections at the one- and the two-loop level.

In Fig. 4 we present, in the $(M_A, \tan\beta)$ plane, the contour lines of the SM-like Higgs boson mass ranging from 122 GeV to 125 GeV.[20] We do not consider any of the experimental constraints described in detail in [86–88] and concentrate only on the prediction for the mass of the lightest Higgs boson of the MSSM. The red dashed and green solid lines correspond to two different computational setups. We calculated the red contours including only the leading one-loop corrections to Δ_b of $\mathcal{O}(\alpha_s, \alpha_t)$ and evaluated the bottom-quark mass according to Renormalisation scheme 1 as described in Sect. 2. Apart from the different definition of some of the input parameters, as mentioned above, this corresponds to the default settings of `FeynHiggs-2.16.1`, which was used in [86] for the analysis of the benchmark scenario. The green lines show the prediction based on the improved calculation described in this paper. In comparison to the red contours, we also include electroweak one-loop as well as the leading two-loop corrections to Δ_b, evaluate the bottom-quark mass at the SUSY scale according to Eq. (20) and resum logarithms proportional to the bottom-Yukawa coupling.

We notice that in the region of small $\tan\beta$ both calculations agree with each other very well since in this region the corrections from the bottom/sbottom sector are negligible. In this region the Higgs mass grows with increasing $\tan\beta$ mainly due to the growth of the tree-level mass. With a further increase of $\tan\beta$ the Higgs mass starts to decrease due to large Δ_b corrections and the rapid increase of the $\overline{\rm DR}$ bottom mass in the MSSM. This behaviour corresponds to the one that we observed in the left plot of Fig. 1. As discussed there, the mass of the SM-like Higgs computed using `FeynHiggs-2.16.1` falls faster with increasing $\tan\beta$ than the mass computed using the calculation presented in the current paper due to the lower accuracy level in the calculation of Δ_b of the previous result. Consequently, the $\tan\beta$-region in which the SM-like Higgs mass is compatible (taking into account the theoretical uncertainties) with the experimentally measured value is enlarged. The corresponding upper bound on $\tan\beta$ in this scenario is shifted from ~ 28 to ~ 33.

5.2 EFT calculation for complex input parameters

In this section, we discuss the numerical effect of including the full phase dependence into the two-loop threshold corrections to the Higgs self-coupling. First, let us briefly review the method used in `FeynHiggs` to handle non-zero phases so far. The treatment of the two-loop corrections in the presence of complex parameters is controlled by the flag `tlCplxApprox`. When it equals 3, the fixed-order $\mathcal{O}(\alpha_t\alpha_s, \alpha_t^2)$ corrections including the full phase dependence are activated and combined with the fixed-order $\mathcal{O}(\alpha_b\alpha_s, \alpha_b\alpha_t, \alpha_b^2)$ corrections. Since the implementation of the latter corrections up to now is based on the results of [43,44], that were obtained for the case of real parameters, an interpolation in the phases is invoked for this part of the two-loop corrections. Specifically, an interpolation is carried out in `FeynHiggs` when the phases of μ, M_3, X_t or X_b are non-zero. The user can choose between interpolation in A_t or X_t, and A_b or X_b. In the EFT part of the code the interpolation is always carried out in the following way. First, the RGEs are integrated numerically and the subtraction terms are calculated for all possible combinations of $+|P|$ and $-|P|$ (where $P \in \{\mu, X_t/A_t, M_3\}$).[21] After that, linear interpolation is performed on the obtained grid. In this Section, we choose to interpolate X_t in the comparison with our new results when the phase of X_t or A_t is non-zero.

The phases of the above-mentioned parameters enter the hybrid calculation via threshold corrections to the Higgs

[20] Throughout the plane, $M_h < 125$ GeV. Therefore, no 125 GeV contours appear.

[21] The threshold corrections in `FH-2.16.1` do not depend on X_b or A_b.

self-coupling and via the subtraction terms. As we mentioned in Sect. 3, both of them depend only on the absolute value $|\widehat{X}_t|$ at the one-loop level, so the interpolation would give a correct result if only LL and NLL resummation were included and the interpolation was performed in X_t. However, the two-loop threshold corrections to the Higgs self-coupling (and hence the two-loop non-logarithmic subtraction terms) do not depend just on the absolute value of X_t. For example, the $\mathcal{O}(\alpha_t\alpha_s)$ threshold correction also depends on the cosine of the phase difference, $\cos(\phi_{X_t} - \phi_{M_3})$, and the formula for the $\mathcal{O}(\alpha_t^2)$ threshold correction depends on $|\widehat{Y}_t|$ and $\cos(\phi_{X_t} - \phi_{Y_t})$. In comparison to the full formula, the application of interpolation leads to deviations at the next-to-next-to-leading logarithmic order. The phases also enter the expression for the two-loop threshold corrections of the bottom Yukawa coupling and Δ_b. First, we will, however, concentrate on MSSM scenarios in which the effect of the bottom Yukawa coupling on the Higgs mass is negligible and so we will not include any two-loop corrections of $\mathcal{O}(\alpha_b\alpha_s, \alpha_b\alpha_t, \alpha_b^2)$ for the results that are presented in Figs. 5 and 6.

In order to test our approach we first consider the same MSSM scenario as in Fig. 3 of [36]: all soft SUSY breaking masses and μ are equal to the common mass scale $M_{\rm SUSY} = 2$ TeV, $\tan\beta = 10$ and $\widehat{X}_t^{\overline{\rm DR}}(M_{\rm SUSY}) = \sqrt{6}$. We vary the phase of the gluino mass parameter M_3 in the interval $[-\pi, +\pi]$ and assume all the other input parameters to be real. In this way, we test the phase dependence of the $\mathcal{O}(\alpha_t\alpha_s)$ threshold correction.

In the left plot of Fig. 5, we show the comparison between the pure EFT prediction of `FeynHiggs-2.16.1` (red line) and our new calculation including the full phase dependence (green line). First, we notice that the two methods give the same answer for $\phi_{M_3} = 0, \pm\pi$ which is expected because in these cases M_3 is a real parameter. This serves as a cross-check for our implementation. Second, we see that the interpolation in this particular scenario is a fairly good approximation: the absolute difference between the two curves does not exceed $\sim$ 0.3 GeV. The largest deviations occur for $\phi_{M_3} \simeq \pm\frac{\pi}{4}$ and $\phi_{M_3} \simeq \pm\frac{3\pi}{4}$. Since the interpolation is only performed in one parameter, ϕ_{M_3}, the resulting curve consists of two straight lines.

In the case of the hybrid calculation (see right plot of Fig. 5), the phase dependence at the two-loop level is fully included in the fixed-order part of the calculation. However, the subtraction terms are interpolated in the same way as the EFT calculation. As a consequence of those phase-dependent contributions in the fixed-order part and the subtraction terms, the curve showing the interpolated hybrid calculation (red) has a different behaviour than the interpolated EFT calculation shown in the left plot. As in the left plot of Fig. 5, the overall difference between the full hybrid and the interpolated hybrid calculation does not exceed $\sim$ 0.3 GeV.

Next, we proceed with a scenario which is similar to the one described above, but we assume that $\widehat{X}_t$ and $\widehat{Y}_t$ are purely imaginary while keeping the same absolute value for $|\widehat{X}_t| = \sqrt{6}$ as before. As one can see in the left plot of Fig. 6, where again the result of the pure EFT calculation varying the phase of M_3 is shown, the trilinear interpolation procedure results in a straight line that does not depend on ϕ_{M_3}. In the chosen scenario, this line overestimates the result for the full expression for the Higgs mass for $\phi_{M_3}/\pi \in [-0.87, -0.13]$ and underestimates it for the other values of ϕ_{M_3}. The absolute difference between the two approaches amounts to $\sim$ 1.2 GeV for $\phi_{M_3} \simeq \frac{\pi}{2}$. The two results do not agree for $\phi_{M_3} = 0, \pm\pi$ since X_t and Y_t are chosen purely imaginary, and therefore an interpolation is also carried out with respect to those phases.

As a next step, we investigate the effects of the phase dependence in the $\mathcal{O}(\alpha_t^2)$ threshold correction. To enhance the numerical value of this correction, we choose a low value for $\tan\beta$, namely $\tan\beta = 3$. This choice, however, suppresses the tree-level Higgs mass, so to obtain a predicted value around 125 GeV we have to choose in this scenario a heavy SUSY scale of $M_{\rm SUSY} = 20$ TeV. In order to isolate the effects of the phase dependence in the considered corrections, we fix the phase of the gluino mass parameter to be equal to the phase of X_t. As a consequence of this choice, the phase dependence in the $\mathcal{O}(\alpha_t\alpha_s)$ threshold correction vanishes. We also choose the Higgsino mass parameter to be positive, $\phi_\mu = 0$.

The EFT prediction, varying the phase $\phi_{X_t} = \phi_{M_3}$, is shown in the right plot of Fig. 6. Even though we have chosen a low value of $\tan\beta = 3$ in order to enhance the impact of the $\mathcal{O}(\alpha_t^2)$ threshold correction, the overall phase dependence of the full result (green) is quite small. The difference between the Higgs mass calculated at $\phi_{X_t} = 0$ and $\phi_{X_t} = \pi$ is only $\sim$ 0.05 GeV. Lowering $\tan\beta$ even further (and pushing $M_{\rm SUSY}$ higher) does not lead to a stronger phase dependence. The behaviour of the interpolated result (red) is different. As in the case of Fig. 5, we see that the results of both methods coincide for $\phi_{X_t} = 0, \pm\pi$ since for these three points all parameters are real. For other values of ϕ_{X_t}, however, the interpolation procedure underestimates the value of M_h predicted based on the full expression by up to $\sim$ 0.5 GeV.

This large deviation can be understood by looking at Fig. 7 showing the M_h prediction of the EFT calculation including the full phase dependence. The same scenario as in the right plot of Fig. 6 is used, but ϕ_{X_t} and ϕ_{M_3} are varied independently. As visible in the plot, the contours are almost diagonal due to the small phase dependence of the $\mathcal{O}(\alpha_t^2)$ threshold corrections. The parabola-like shape of the interpolated result, as visible for the red curve in the right plot of Fig. 6, is a consequence of the bilinear interpolation in

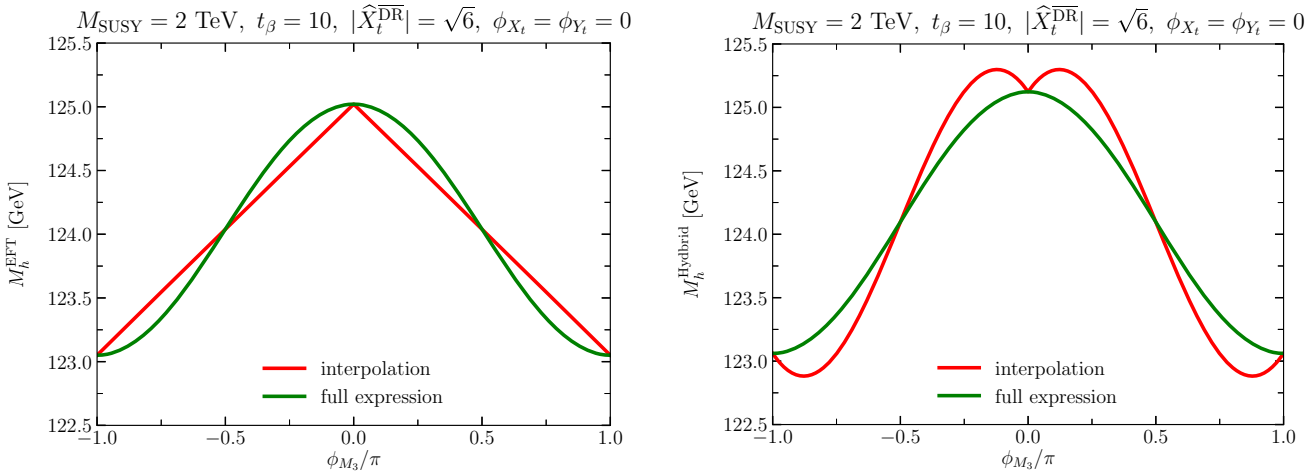

Fig. 5 Left: M_h as a function of ϕ_{M_3} setting $\phi_{X_t} = \phi_{Y_t} = 0$ calculated using the pure EFT calculation. The results obtained by using an interpolation of the phase and by including the full phase dependence are compared. Right: Same as left plot, but the results of the hybrid calculation are shown

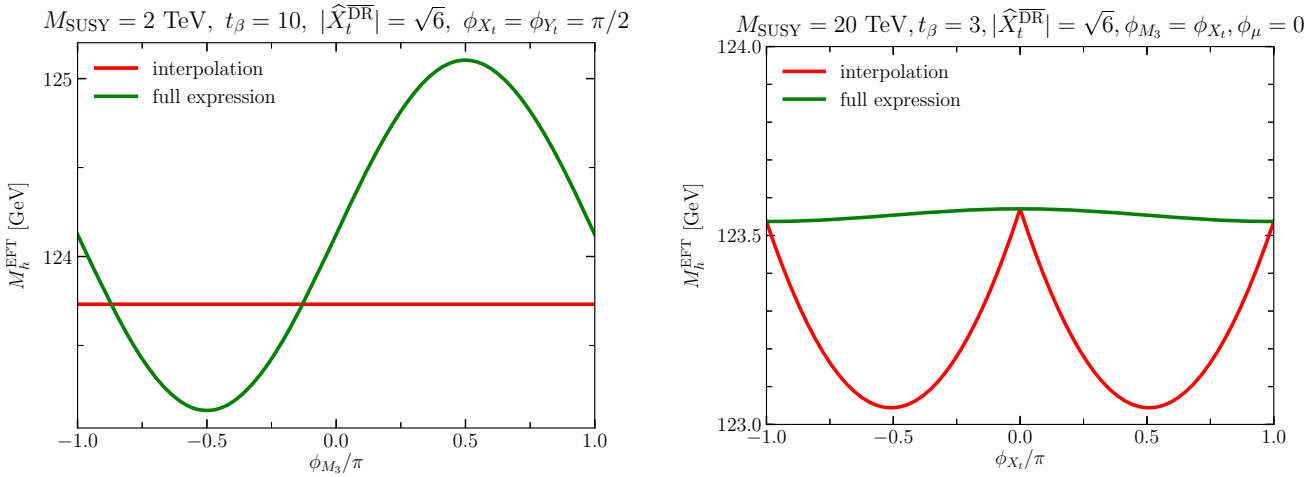

Fig. 6 Left: The same as the left plot of Fig. 5 but for $\phi_{X_t} = \phi_{Y_t} = \pi/2$. Right: M_h as a function of ϕ_{X_t} setting $\phi_{M_3} = \phi_{X_t}$ and $\phi_\mu = 0$. The results obtained by interpolating the EFT calculation and by including the full phase dependence are compared

ϕ_{X_t} and ϕ_{M_3}. For $\phi_{X_t} = \phi_{M_3} > 0$, the Higgs mass values at $(\phi_{X_t}, \phi_{M_3}) = (0,0), (0,\pi), (\pi,0), (\pi,\pi)$ enter the interpolation procedure. For the values $(\phi_{X_t}, \phi_{M_3}) = (0,\pi), (\pi,0)$ the phase dependence of the $\mathcal{O}(\alpha_t\alpha_s)$ threshold correction is picked up resulting in the large phase dependence observed for the red curve in the right plot of Fig. 6. In the considered case, an interpolation in $\phi_{M_3} = \phi_{X_t}$ rather than in ϕ_{M_3} and ϕ_{X_t} separately would improve the quality of the interpolation.

It should be noted that for the hybrid result the difference between the EFT result incorporating the full phase dependence and the one based on the interpolation, shown in the right plot of Fig. 6, is further enhanced because of the different treatment of the phase dependence in the fixed-order contribution and the subtraction terms. As a consequence, in this extreme scenario, the incomplete cancellation between the corresponding terms in the fixed-order part and the subtraction terms leads to an artificial enhancement of the deviation that can amount up to ~ 2 GeV.

As a final topic in this section, we analyse the interplay between the resummation of the logarithms proportional to the bottom Yukawa coupling and the inclusion of the full phase dependence into the EFT part of our hybrid calculation. As a starting point we go back to the scenario discussed in Sect. 5.1. Namely, we consider a single scale scenario, where all soft-breaking masses as well as the mass of the charged Higgs boson[22] are equal to 1.5 TeV, $A_b^{\overline{\rm DR}} = 2.5 M_{\rm SUSY}$, the Higgsino mass parameter is negative, $\mu = -M_{\rm SUSY}$, the bino and wino masses are chosen to be positive, $M_{1,2} > 0$, and $\widehat{X}_t^{\rm OS} = 2$. The phase of the gluino mass parameter is a

[22] Since we consider here the $\mathcal{CP}$-violating case, $M_{H^\pm}$ is chosen as an input parameter instead of M_A.

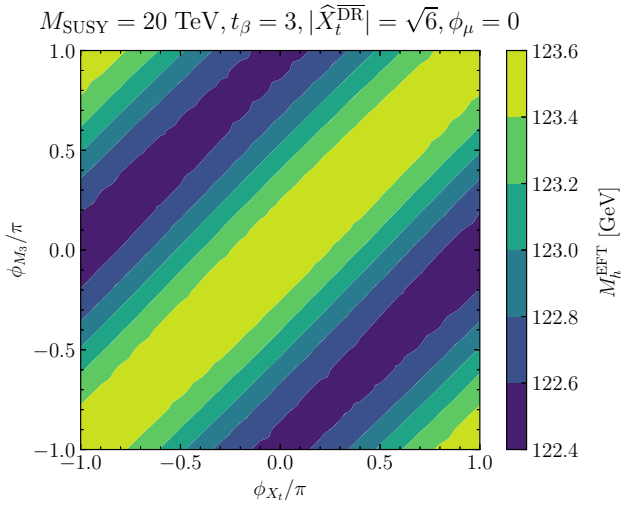

Fig. 7 Result of the EFT calculation using the full phase dependence. The same scenario as in the right plot of Fig. 6 is used, but ϕ_{X_t} and ϕ_{M_3} are varied independently

free parameter, and we vary it in the interval from $-\pi$ to $+\pi$. We examine this scenario for $\tan\beta = 30$ and $\tan\beta = 45$.

The result for M_h as a function of ϕ_{M_3} is shown in Fig. 8. The colors of the curves on the left panel correspond to the same levels of accuracy as in Fig. 2, solid lines correspond to $\tan\beta = 30$, and dashed lines correspond to $\tan\beta = 45$. For $\phi_{M_3} = \pm\pi$, the results displayed by all six lines agree with each other within ~ 0.4 GeV. Here, the strong and the top Yukawa contributions to Δ_b partially cancel each other, and the MSSM bottom mass does not acquire an enhancement. In fact, for the mentioned points the Δ_b correction is positive, so that the Δ_b corrections lead to a suppression of the bottom mass. This is visible in the right panel of Fig. 8, where the solid line (for which $|\Delta_b|$ is larger) lies below the dashed line for $\phi_{M_3} \simeq \pm\pi$.

The red dashed curve resembles the cosine-shape line shown in Fig. 5. This is due to the fact that even for $\phi_{M_3} = 0$, where the bottom mass is maximal for $\tan\beta = 30$, it is still too small to have a sizeable effect on M_h. Here, the shape of the line can be explained by the phase dependence of the two-loop fixed-order corrections of $\mathcal{O}(\alpha_t\alpha_s)$. Adding furthermore the two-loop fixed-order corrections of $\mathcal{O}(\alpha_b\alpha_s, \alpha_b\alpha_t, \alpha_b^2)$ (blue dashed line) lifts the prediction for the Higgs mass by ~ 0.2 GeV for $\phi_{M_3} = \pm\pi$ and by ~ 0.7 GeV for $\phi_{M_3} = 0$. The inclusion of the resummation of the logarithms proportional to the bottom Yukawa coupling (green dashed line) has a similar numerical effect.

The behaviour as a function of ϕ_{M_3} is significantly different for $\tan\beta = 45$. The red solid curve starts to grow when ϕ_{M_3} increases starting from $-\pi$, resembling the red dashed line in shape. However, it reaches a maximum value at $\phi_{M_3} \simeq -\frac{\pi}{3}$. This is a consequence of the fact that the Δ_b correction becomes important in this region, leading to a steep increase of the MSSM bottom mass (see right plot of Fig. 8). Thus, the one-loop corrections involving the bottom mass (see Eq. (25)) become important, giving rise to a downward shift in M_h. At $\phi_{M_3} = 0$ the bottom mass reaches ~ 5.8 GeV, and the Higgs mass prediction has a minimum at ~ 123 GeV. The point $\phi_{M_3} = 0$ in this plot corresponds to the point where $M_{\rm SUSY} = 1.5$ TeV in the left plot of Fig. 3. As in Fig. 3, we observe that the inclusion of the two-loop fixed-order corrections controlled by the bottom Yukawa coupling (the difference between the red and the green curves) has a very significant effect. The resummation of higher-order logarithmic contributions (the difference between the blue and the green curves) leads to a downward shift of ~ 1 GeV

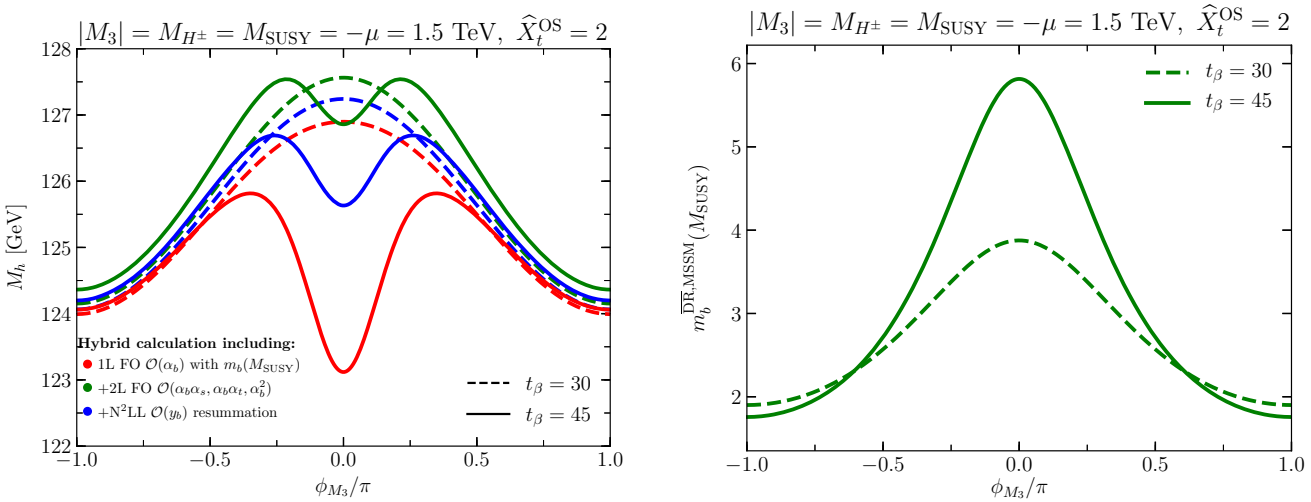

Fig. 8 Left: M_h as a function of the phase of the gluino mass ϕ_{M_3}. The red, green and blue colors on this plot mean the same as in Fig. 2. The dashed curves correspond to $\tan\beta = 30$ and the solid curves to $\tan\beta = 45$. Right: $m_b^{\overline{\rm DR},{\rm MSSM}}(M_{\rm SUSY})$ as a function of ϕ_{M_3}

for $\phi_{M_3} \simeq \pm\frac{\pi}{3}$ and of ~ 1.2 GeV for $\phi_{M_3} = 0$. The results displayed in Fig. 8 demonstrate that the (s)bottom sector contributions can have an important impact on the phase dependence. Similarly to Fig. 3, we again find that the resummation of logarithms proportional to the bottom-Yukawa coupling amount to an $\mathcal{O}(1\text{ GeV})$ effect for large $\tan\beta$ if the OS scheme is used for the renormalization of the stop sector.

5.3 N^{3}LL resummation

Here, we study the numerical effects of including N^{3}LL resummation at leading order in the strong gauge coupling (see Sect. 4) into our hybrid framework. We study a simple single-scale scenario in which all non-SM masses are set to the common scale $M_{\rm SUSY}$. Furthermore, we set all trilinear soft SUSY-breaking couplings, except for A_t, to zero. We define the stop parameters in the $\overline{\rm DR}$ scheme at the scale $M_{\rm SUSY}$. We set $\tan\beta = 10$.

In Fig. 9, we compare the results obtained using three different accuracy levels to each other: NNLL resummation with the SM top Yukawa coupling extracted at the two-loop level, NNLL resummation with the SM top Yukawa coupling extracted at the three-loop level and N^{3}LL resummation, which also involves the SM top-Yukawa coupling extracted at the three-loop level. The plots in the right part of the Figure display the difference ΔM_h between the curves in the left panel (see legends of the corresponding plots). In the upper plots, the different results are shown as a function of $M_{\rm SUSY}$. In the upper left plot, the three results (blue, red and green lines) are shown for vanishing stop mixing (solid lines) and for $\widehat{X}_t = -\sqrt{6}$ (dashed lines). For vanishing stop mixing, all three results are in good agreement with each other for low $M_{\rm SUSY}$. If $M_{\rm SUSY}$ is raised, there is, however, an increasing difference between the NNLL result (with the two-loop level SM top Yukawa coupling) and the two results involving the three-loop level SM top-Yukawa coupling of up to ~ 1 GeV for $M_{\rm SUSY} \sim 100$ TeV. This shift is almost completely caused by including the three-loop corrections to the extraction of the SM top Yukawa coupling, since the NNLL result with the SM top Yukawa coupling extracted at the three-loop level and the N^{3}LL result are in very good agreement also for $M_{\rm SUSY} \sim 100$ TeV. Also for $\widehat{X}_t = -\sqrt{6}$, the NNLL result with the SM top Yukawa coupling extracted at the three-loop level and the N^{3}LL result are in good agreement across the considered $M_{\rm SUSY}$ range (within ~ 0.3 GeV). This difference, is displayed by the red curve in the upper right plot of Fig. 9. The NNLL result with the SM top Yukawa coupling extracted at the two-loop level deviates from the other two results by ~ 0.7 GeV, as shown by the blue curve in the top right plot of Fig. 9. In this plot, furthermore the estimate of the uncertainty associated with the truncation error in the calculation of the $\mathcal{O}(\alpha_t\alpha_s^2)$ threshold correction for the Higgs self-coupling, obtained by including only partially known terms of higher-order in the hierarchy expansion (see [18] for more details), is shown as a green band. We find that this estimate is of the same size as the shift induced by including the $\mathcal{O}(\alpha_t\alpha_s^2)$ threshold correction.

In the lower plots of Fig. 9, the same quantities as in the upper plots are shown, but $M_{\rm SUSY}$ is set to 5 TeV and $\widehat{X}_t$ is varied. The shifts between the various results are only mildly dependent on $\widehat{X}_t$ (varying $\widehat{X}_t$ leads to shifts of up to 0.4 GeV). This dependence would be stronger for lower $M_{\rm SUSY}$ values. The estimate of uncertainty associated with the truncation error, however, shows a strong dependence on $\widehat{X}_t$. Whereas it is negligible for $-1 \lesssim \widehat{X}_t \lesssim 1$, it increases to up to 0.7 GeV for $|\widehat{X}_t| \sim 3.5$. As shown by the red curve in the lower right plot of Fig. 9, the difference between the NNLL result with the SM top-Yukawa coupling extracted at the three-loop level and the N^{3}LL result is rather small except for large negative values of $\widehat{X}_t$. Where this difference exceeds the level of 0.2 GeV, it is smaller than the estimated uncertainty of the truncation error.

As expected, the results for the N^{3}LL resummation are in very good agreement with the results of [18]. We observe that the main part of the shift induced by including N^{3}LL resummation is caused by taking into account the three-loop corrections to the extraction of the SM $\overline{\rm MS}$ top Yukawa coupling from the measured top mass. The shift caused by including the $\mathcal{O}(\alpha_t\alpha_s^2)$ threshold correction for the Higgs self-coupling is smaller and also associated with a rather large uncertainty for large $|\widehat{X}_t|$ values. For small $|\widehat{X}_t|$ values, the shift induced by including the $\mathcal{O}(\alpha_t\alpha_s^2)$ threshold correction for the Higgs self-coupling is found to be very small. Therefore, we choose in our implementation to use the result obtained using NNLL resummation with the SM top Yukawa coupling extracted at the three-loop level as default result until the uncertainty in the calculation of the $\mathcal{O}(\alpha_t\alpha_s^2)$ threshold correction is further reduced by incorporating additional higher-order contributions.

6 Conclusions

In this paper, we have presented an improved prediction for the lightest Higgs boson mass in the MSSM in scenarios with large $\tan\beta$, complex input parameters and large $M_{\rm SUSY}$. Our calculation builds on results that are contained in the publicly available code `FeynHiggs`.

The first improvement concerning scenarios with large $\tan\beta$ includes the change of the renormalisation scheme for the bottom mass with respect to the present implementation in `FeynHiggs`: instead of treating the bottom mass as a derived quantity, in the scheme used in our calculation it is as an independent parameter, renormalised in the $\overline{\rm DR}$ scheme in the full MSSM at scale $M_{\rm SUSY}$. The scheme that we have adopted yields numerically more stable results and turned

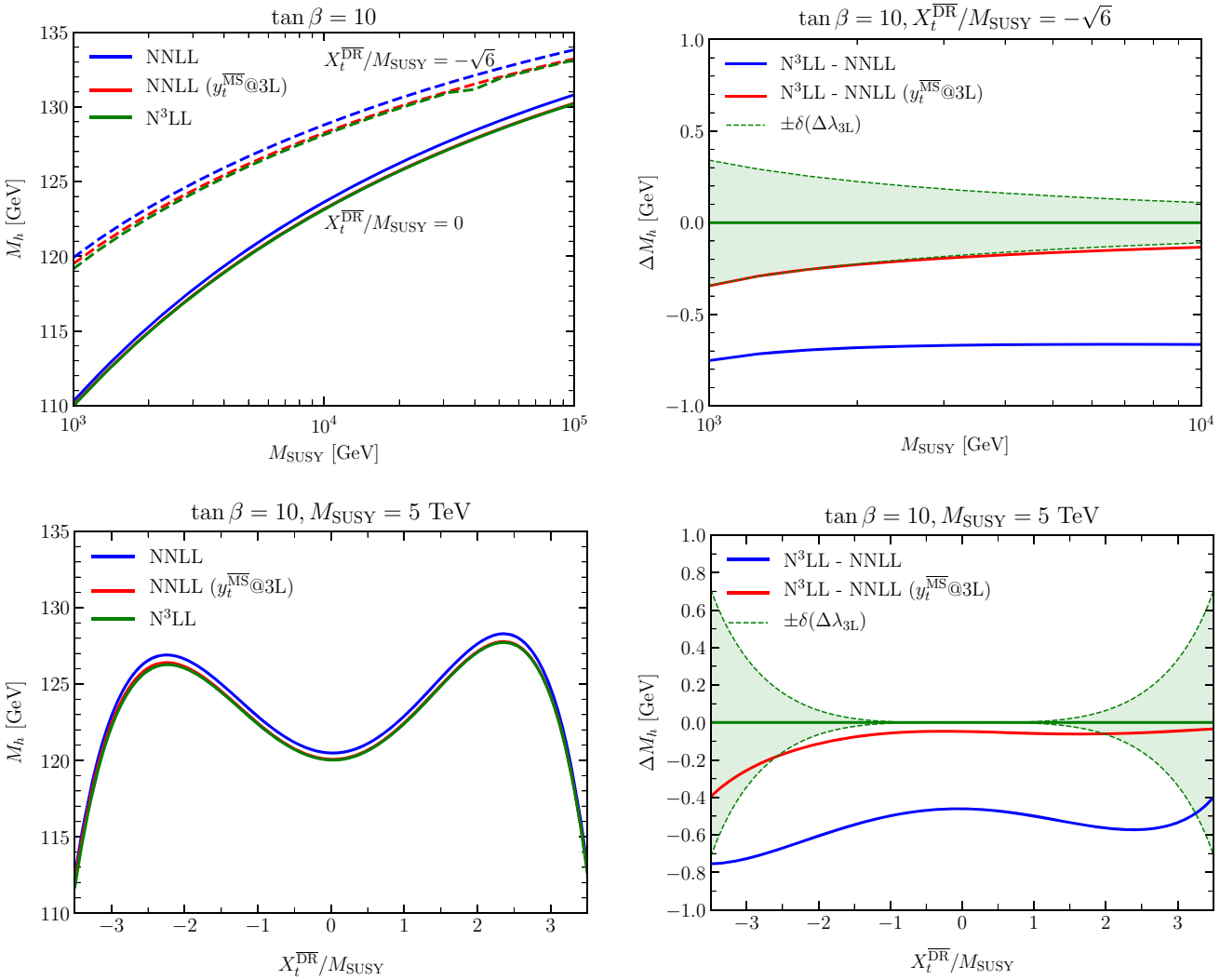

Fig. 9 Top left: prediction for M_h as a function of $M_{\rm SUSY}$ for $\widehat{X}_t = 0$ (solid lines) and $\widehat{X}_t = -\sqrt{6}$ (dashed lines). The results using NNLL resummation (blue), NNLL resummation with the SM top Yukawa coupling extracted at the three-loop level (red) and N^{3}LL resummation (green) are compared. Top right: differences of the M_h predictions using N^{3}LL and NNLL resummation (blue line) as well as using N^{3}LL and NNLL resummation with the SM top Yukawa coupling extracted at the three-loop level (red line) as a function of $M_{\rm SUSY}$ for $\widehat{X}_t = -\sqrt{6}$. In addition, the estimate for the uncertainty associated with the truncation error of the $\mathcal{O}(\alpha_t\alpha_s^2)$ Higgs self-coupling threshold correction is shown (green band). Bottom left: same as top left, but M_h is shown as a function of $\widehat{X}_t$ for $M_{\rm SUSY} = 5$ TeV. Bottom right: same as top right, but ΔM_h is shown as a function of $\widehat{X}_t$ for $M_{\rm SUSY} = 5$ TeV

out to be better suited for the combination with the EFT calculation. In the calculation of the $\overline{\rm DR}$ bottom mass, we have taken into account higher-order corrections enhanced by $\tan\beta$ by means of a resummation of the quantity Δ_b. We have incorporated full one-loop corrections to Δ_b. Moreover, we have adapted the leading two-loop QCD corrections to Δ_b obtained in [37–39] such that they are suitable for the framework of our calculation. The inclusion of this correction is formally a three-loop effect. While this correction is numerically not relevant for large parts of the parameter space, it can become sizeable for scenarios with large $\tan\beta$.

Moreover, we have included one- and two-loop threshold corrections to the SM Higgs self-coupling proportional to the bottom Yukawa coupling well as the corresponding RGE contributions up to the three-loop level. This allows resummation up to the next-to-next-to-leading-order. In contrast to the resummation of the logarithms proportional to the top Yukawa coupling or electroweak couplings, here the one- and two-loop leading logarithms are numerically negligible due to the smallness of the bottom mass. However, at the two-loop level for the case where the stop sector is renormalised in the OS scheme the next-to-leading logarithms become parametrically enhanced for large $\tan\beta$. In this case, the resummation can become numerically relevant for large $\tan\beta$ and large $M_{\rm SUSY}$.

Secondly, we used the two-loop fixed order results presented in Refs. [8,10] to derive two-loop threshold corrections to the SM Higgs self-coupling for the matching between the SM and the MSSM that are valid for the general case of complex input parameters. This enabled us to perform the EFT calculations for the case of complex parameters. We compared the results including the full phase dependence to the results obtained by the use of the interpolation routine that has been adopted in `FeynHiggs` up to now. For the pure EFT calculation, we have found the interpolation procedure to perform well in scenarios with only one non-zero phase. In scenarios with more than one non-zero phase, we observed deviations in the prediction for M_h of up to 1 GeV. For the hybrid result the incorporation of the full phase dependence of the EFT part of the calculation yields another important improvement. Up to now the corresponding contributions in the fixed-order result (containing the full phase dependence) and the subtraction terms (based on the interpolated EFT contributions) were treated differently, which could lead to an incomplete cancellation between the two types of contributions. This can lead to numerical deviations of up to 2 GeV compared to our improved result where the treatment of the phase dependence is the same in all parts of the calculation. We furthermore analysed the interplay between the resummation of the logarithms proportional to the bottom Yukawa coupling and the inclusion of the full phase dependence into the EFT part of the hybrid calculation. We have found that the impact of phase variations on the prediction for M_h can be modified very significantly through the contributions of the $b/\tilde{b}$ sector.

Finally, we combined the publicly available code `Himalaya` with `FeynHiggs` in order to obtain a prediction for M_h including N^{3}LL resummation at leading order in the strong gauge coupling. A similar analysis was performed in [29], and we find a very good agreement with the results presented in that paper. The overall effect of the N^{3}LL resummation is $\lesssim 1$ GeV, and it only weakly depends on $M_{\rm SUSY}$. We have found that employing the extraction of the SM top Yukawa coupling at the three-loop level within the existing NNLL hybrid calculation yields a result that approximates the N^{3}LL resummation well in view of the remaining theoretical uncertainties of the N^{3}LL contribution.

The improvements described in this paper will be implemented into an upcoming version of the public code `FeynHiggs`.

Acknowledgements We thank Thomas Hahn, Sven Heinemeyer, Sebastian Paßehr and Heidi Rzehak for useful discussions, Sebastian Paßehr for providing two-loop results, Emanuele Bagnaschi and Pietro Slavich for providing expressions for cross-checks as well as Alexander Voigt and Jonas Klappert for help regarding `Himalaya`. We acknowledge support by the Deutsche Forschungsgemeinschaft (DFG, German Research Foundation) under Germany's Excellence Strategy – EXC 2121 "Quantum Universe" – 390833306.

Data Availability Statement This manuscript has associated data in a data repository. [Authors' comment: All calculated two-loop threshold corrections are available in the form of `Mathematica` expressions.]

Funded by SCOAP^3.

Appendix A: Derivation of two-loop threshold corrections

In this Appendix, we derive the two-loop threshold corrections for the SM Higgs self-coupling for the matching between the SM and the MSSM based on the fixed-order calculations presented in [8,10,42]. We fully take into account the dependence on $\mathcal{CP}$-violating phases.

The threshold corrections to the quartic coupling λ can be obtained via the matching of the four-point vertex function involving the SM Higgs boson as external particle. Here, however, we follow a different approach. Since in the SM the running mass of the lightest Higgs boson is related to its quartic coupling via

$$\overline{m}_h^2 = 2\lambda v^2, \tag{27}$$

the threshold corrections to λ can be obtained via the threshold correction to the running Higgs mass $\overline{m}_h$.[23] Below we outline the method and derive the general formulas for the one- and two-loop threshold corrections to λ in the gaugeless limit. Similar methods can be found in [14,30].

In the limit $M_A \gg M_t$, the SM-like Higgs pole mass in the MSSM up to the two-loop level is given by[24]

$$(M_h)^2_{\rm MSSM} = m_h^2 - \widehat{\Sigma}^{\rm MSSM,(1)}_{hh}(m_h^2) - \widehat{\Sigma}^{\rm MSSM,(2)}_{hh}(m_h^2) + \widehat{\Sigma}^{\rm MSSM,(1)}_{hh}(m_h^2)\, \widehat{\Sigma}^{\rm MSSM,(1)\,\prime}_{hh}(m_h^2), \tag{28}$$

[23] This method is not sufficient to obtain the threshold corrections for all quartic couplings if the EFT below $M_{\rm SUSY}$ is the Two-Higgs-Doublet-Model [90].

[24] In general, only the real part of each term in the sum on the right hand side of Eq. (28) should be considered, since the Higgs self-energies have imaginary parts arising from the contributions of the particles which are lighter than the SM-like Higgs. Since in the MSSM the mass of the SM-like Higgs is close to the electroweak scale, in the usually considered scenarios these imaginary parts arise only from SM particles and, therefore, cancel out in the matching procedure.

where m_h is the MSSM tree-level mass, and the prime indicates the derivative with respect to the external momentum squared. In the gaugeless limit and the decoupling limit ($M_A \gg M_t$), $m_h = 0$ can be inserted. All parameters entering the self-energies $\widehat{\Sigma}^{\rm MSSM,(1)}_{hh}$ and $\widehat{\Sigma}^{\rm MSSM,(2)}_{hh}$ are renormalised in the $\overline{\rm DR}$ scheme while the tadpoles are renormalised to zero. The self-energies entering Eq. (28) are assumed to be expanded in the limit $v/M_{\rm SUSY} \to 0$.

Below the matching scale Q, the effective field theory is the SM. We write the matching condition for the SM running Higgs mass $\overline{m}^2_h$ as a loop expansion,

$$\overline{m}^2_h = \overline{m}^2_{h,\rm tree} + (\Delta\overline{m}^{1l}_h)^2 + (\Delta\overline{m}^{2l}_h)^2 + \cdots, \tag{29}$$

where the ellipsis denotes three-loop terms and higher. Since m_h in Eq. (28) equals zero in the considered approximation, we have $\overline{m}_{h,\rm tree} = 0$. The pole mass in the SM can then be obtained via the solution of the pole equation

$$M^2_h = \overline{m}^2_h - \widetilde{\Sigma}^{\overline{\rm MS},\rm SM}_{hh}(M^2_h), \tag{30}$$

where $\widetilde{\Sigma}^{\overline{\rm MS},\rm SM}_{hh}$ is the SM Higgs boson self-energy renormalised in the $\overline{\rm MS}$ scheme with the tadpoles renormalised to zero. Since the SM is treated as an effective field theory, its parameters are related to the corresponding parameters in the MSSM. This relation can be schematically written as follows,

$$P^{\rm SM} = P^{\rm MSSM} + \Delta P, \tag{31}$$

where P is a coupling constant, a running quark mass, or the vacuum expectation value. Inserting this relation into the self-energy $\widetilde{\Sigma}^{\overline{\rm MS},\rm SM}_{hh}(M^2_h)$ induces a shift at one order higher in the loop expansion,

$$\widetilde{\Sigma}^{\overline{\rm MS},\rm SM}_{hh} = \widetilde{\Sigma}^{\rm SM}_{hh}\Big|_{P^{\rm SM}\to P^{\rm MSSM}} + \widehat{\Sigma}^{\rm SM,shifts}_{hh}. \tag{32}$$

The first term on the right-hand side of this equation represents the self-energy which has the same analytic form as $\widetilde{\Sigma}^{\overline{\rm MS},\rm SM}_{hh}$ but with all $\overline{\rm MS}$ SM coupling constants and masses being replaced with their $\overline{\rm DR}$ MSSM counterparts. Therefore, the two self-energies are equal at the one-loop level (since in the present discussion we neglect electroweak corrections the different regularisation does not lead to a different result). The difference between the two self-energies is encoded in the quantity $\widehat{\Sigma}^{\rm SM,shifts}_{hh}$ which is of two-loop order and higher.

The renormalised self-energy of the SM-like Higgs boson in the full MSSM can be split into parts,

$$\widehat{\Sigma}^{\rm MSSM}_{hh} = \widehat{\Sigma}^{\rm SM}_{hh} + \widehat{\Sigma}^{\rm n/SM}_{hh}, \tag{33}$$

where the SM part contains contributions from the diagrams with only SM particles and the non-SM part (indicated as "n/SM") originates from the diagrams with at least one non-SM particle.

At the one-loop level, the following identity holds,

$$\widehat{\Sigma}^{\rm SM,(1)}_{hh} = \widetilde{\Sigma}^{\rm SM,(1)}_{hh}\Big|_{P^{\rm SM}\to P^{\rm MSSM}}. \tag{34}$$

where in this equation the symbols "$\widehat{\ }$" and "$\widetilde{\ }$" are used to denote the SM part of the MSSM Higgs self-energy renormalised in the $\overline{\rm DR}$ scheme and the SM Higgs self-energy renormalised in the $\overline{\rm MS}$ scheme, respectively. This equation means that the SM contributions in the full MSSM self-energy computed in the $\overline{\rm DR}$ scheme, $\widehat{\Sigma}^{\rm SM}_{hh}$, have the same analytic form as the self-energy computed in the SM in the $\overline{\rm MS}$ scheme, $\widetilde{\Sigma}^{\rm SM}_{hh}$. In Eq. (34) the replacement rule on the right-hand side, $P^{\rm SM} \to P^{\rm MSSM}$, implies that all $\overline{\rm MS}$ SM parameters in the SM self-energy have to be replaced by their $\overline{\rm DR}$ MSSM counterparts without additional shifts.[25] At the two-loop level, a relation analogous to Eq. (34) holds for the SM-type corrections to the Higgs mass proportional to the Yukawa couplings, i.e. the corrections of $\mathcal{O}(\alpha_t^2, \alpha_t\alpha_b, \alpha_b^2)$ without including any parameter shifts in the one-loop self-energy. For the mixed Yukawa-QCD corrections of $\mathcal{O}(\alpha_t\alpha_s, \alpha_b\alpha_s)$, the two different choices of the regularisation scheme (dimensional regularisation in the case of the SM and dimensional reduction in the case of the MSSM) lead to different expressions for the SM part of the self-energy. This can already be anticipated since the running $\overline{\rm MS}$ and $\overline{\rm DR}$ quark masses are not equal to each other at the one-loop level (see e.g. [84]). By using `TwoCalc` [91,92] and the scripts described in [68] we explicitly checked the following relation,[26]

$$\widetilde{\Sigma}^{\overline{\rm MS},\rm SM,\mathcal{O}(\alpha_t\alpha_s)}_{hh} + \frac{\partial}{\partial m_t}\widetilde{\Sigma}^{\overline{\rm MS},\rm SM,(1)}_{hh} \times \Delta m_t^{\overline{\rm MS}\to\overline{\rm DR}} = \widetilde{\Sigma}^{\overline{\rm DR},\rm SM,\mathcal{O}(\alpha_t\alpha_s)}_{hh}, \tag{35}$$

and the analogous relation for the $\mathcal{O}(\alpha_b\alpha_s)$ self-energies. In Eq. (35),[27]

$$\Delta m_t^{\overline{\rm MS}\to\overline{\rm DR}} = \frac{\alpha_s}{3\pi} m_t. \tag{36}$$

As explained above, the one-loop reparametrisation of the couplings and masses in the one-loop SM self-energy induces shifts at the two-loop order,

$$\widehat{\Sigma}^{\rm SM,shifts}_{hh} = \sum_P \frac{\partial}{\partial P}\widetilde{\Sigma}^{\overline{\rm MS},\rm SM,(1)}_{hh}\Delta^{(1)}P, \tag{37}$$

[25] We assume that the self-energies on the left- and the right-hand sides of Eq. (34) are expressed in terms of quark masses and vacuum expectation values of the SM-like Higgs. In this parametrisation, the SM self-energy in the full MSSM does not depend on non-SM parameters.

[26] Eq. (35) holds only at zero external momenta. At non-zero momenta an additional term, not related to the top-quark mass, appears (see [19] for details).

[27] Here we do not specify the renormalisation scheme for the strong coupling and for the top mass since a change of the renormalisation scheme is of three-loop order.

where P are all SM parameters which enter $\widetilde{\Sigma}_{hh}^{\overline{\rm MS},{\rm SM},(1)}$. The one-loop expression for $\widetilde{\Sigma}_{hh}^{\overline{\rm MS},{\rm SM},(1)}$ at zero external momentum of order $\mathcal{O}(\alpha_t,\alpha_b)$ reads

$$\widetilde{\Sigma}_{hh}^{\overline{\rm MS},{\rm SM},(1)} = \sum_{q=t,b} \frac{3\left(m_q^{\overline{\rm MS},{\rm SM}}(Q)\right)^4}{4\pi^2\left(v^{\overline{\rm MS},{\rm SM}}(Q)\right)^2} \log\frac{\left(m_q^{\overline{\rm MS},{\rm SM}}(Q)\right)^2}{Q^2}. \tag{38}$$

In this expression all masses and the vacuum expectation value (i.e., $m_q^{\overline{\rm MS},{\rm SM}}(Q)$ and $v^{\overline{\rm MS},{\rm SM}}(Q)$) are SM $\overline{\rm MS}$ parameters evaluated at the scale Q. They are related to the MSSM parameters in the $\overline{\rm DR}$ scheme at the scale Q in the following way

$$\begin{aligned} v^{\overline{\rm MS},{\rm SM}}(Q) &= v^{\overline{\rm DR},{\rm MSSM}}(Q)\left(1-\Delta^{(1)}v\right), \\ m_q^{\overline{\rm MS},{\rm SM}}(Q) &= m_q^{\overline{\rm DR},{\rm MSSM}}(Q) - \Delta^{(1)}m_q, \quad q=t,b, \end{aligned} \tag{39}$$

where the one-loop shift $\Delta^{(1)}m_q$ contains contributions of BSM particles as well as the transition between the $\overline{\rm DR}$ and $\overline{\rm MS}$ schemes. This quantity can be computed from the pole mass matching of the bottom and top masses at the one-loop level. The one-loop shift $\Delta^{(1)}v$ includes non-SM $\mathcal{O}(\alpha_t,\alpha_b)$ terms[28] while $\Delta^{(1)}m_q$ includes $\mathcal{O}(\alpha_t,\alpha_b,\alpha_s)$ corrections. With these definitions and Eq. (34), the two-loop terms which account for the shifts between the SM and the MSSM quantities acquire the following form,[29]

$$\begin{aligned} \widehat{\Sigma}_{hh}^{\rm SM,shifts} = &-\sum_{q=t,b}\frac{\partial}{\partial m_q}\widehat{\Sigma}_{hh}^{{\rm SM},(1)}\cdot\Delta^{(1)}m_q \\ &+2\widehat{\Sigma}_{hh}^{{\rm SM},(1)}\,\Delta^{(1)}v. \end{aligned} \tag{40}$$

Here we have exploited the fact that in the gaugeless limit $\widehat{\Sigma}_{hh}^{{\rm SM},(1)}$ scales as $\propto 1/v^2$. In [26] it was shown that in the heavy SUSY limit the non-SM part of the relative shift in the vacuum expectation value can be expressed via the non-SM part of the Higgs self-energy derivative,

$$\Delta^{(1)}v = -\frac{\widehat{\Sigma}_{hh}^{{\rm n/SM},(1)\prime}(m_h^2)}{2}. \tag{41}$$

Using this relation, Eq. (40) can be rewritten as follows,

$$\begin{aligned} \widehat{\Sigma}_{hh}^{\rm SM,shifts} = &-\sum_{q=t,b}\frac{\partial}{\partial m_q}\widehat{\Sigma}_{hh}^{{\rm SM},(1)}\cdot\Delta^{(1)}m_q \\ &-\widehat{\Sigma}_{hh}^{{\rm SM},(1)}\widehat{\Sigma}_{hh}^{{\rm n/SM},(1)\,\prime}. \end{aligned} \tag{42}$$

[28] Note that the one-loop shift $\Delta^{(1)}v$ in this equation is the same quantity as Δv in Eq. (18) in Sect. 2.4 for $Q = M_{\rm SUSY}$.

[29] For brevity, we will omit arguments of the self-energies in the rest of this section, implying that they always equal zero.

Taking into account Eqs. (32), (34) and (42), the pole equation Eq. (30) can be solved iteratively up to the two-loop level in the considered approximation,

$$\begin{aligned} (M_h)^2_{\rm SM} = &(\Delta\overline{m}_h^{1l})^2 + (\Delta\overline{m}_h^{2l})^2 - \widehat{\Sigma}_{hh}^{{\rm SM},(1)} \\ &- \widetilde{\Sigma}_{hh}^{\overline{\rm MS},{\rm SM},(2)} \\ &- \widehat{\Sigma}_{hh}^{{\rm SM},(1)\prime}\left((\Delta\overline{m}_h^{1l})^2 - \widehat{\Sigma}_{hh}^{{\rm SM},(1)}\right) \\ &+ \sum_{q=t,b}\frac{\partial}{\partial m_q}\widehat{\Sigma}_{hh}^{{\rm SM},(1)}\cdot\Delta^{(1)}m_q \\ &+ \widehat{\Sigma}_{hh}^{{\rm SM},(1)}\widehat{\Sigma}_{hh}^{{\rm n/SM},(1)\prime}. \end{aligned} \tag{43}$$

At the matching scale Q, the predictions for the physical Higgs mass, M_h, in the SM and the MSSM have to be equal order by order,

$$(M_h)^2_{\rm SM} = (M_h)^2_{\rm MSSM}. \tag{44}$$

By equating the one-loop pieces in Eq. (44) and taking into account Eqs. (28) and (43) we get,

$$(\Delta\overline{m}_h^{1l})^2 = -\widehat{\Sigma}_{hh}^{{\rm MSSM},(1)} + \widehat{\Sigma}_{hh}^{{\rm SM},(1)} = -\widehat{\Sigma}_{hh}^{{\rm n/SM},(1)}. \tag{45}$$

After inserting this one-loop solution back into Eq. (43), we arrive at

$$\begin{aligned} (M_h)^2_{\rm SM} = &(\Delta\overline{m}_h^{2l})^2 - \widehat{\Sigma}_{hh}^{{\rm MSSM},(1)} - \widetilde{\Sigma}_{hh}^{\overline{\rm MS},{\rm SM},(2)} \\ &+ \widehat{\Sigma}_{hh}^{{\rm SM},(1)\prime}\widehat{\Sigma}_{hh}^{{\rm MSSM},(1)} \\ &+ \sum_{q=t,b}\frac{\partial}{\partial m_q}\widehat{\Sigma}_{hh}^{{\rm SM},(1)}\cdot\Delta^{(1)}m_q \\ &+ \widehat{\Sigma}_{hh}^{{\rm SM},(1)}\widehat{\Sigma}_{hh}^{{\rm n/SM},(1)\prime}. \end{aligned} \tag{46}$$

By equating the two-loop pieces in Eq. (44) and expanding the one-loop self-energies of the Higgs boson in the full MSSM according to Eq. (33), we get

$$\begin{aligned} (\Delta\overline{m}_h^{2l})^2 = &-\widehat{\Sigma}_{hh}^{{\rm MSSM},(2)} + \widetilde{\Sigma}_{hh}^{\overline{\rm MS},{\rm SM},(2)} \\ &- \sum_{q=t,b}\frac{\partial}{\partial m_q}\widehat{\Sigma}_{hh}^{{\rm SM},(1)}\cdot\Delta^{(1)}m_q \\ &+ \widehat{\Sigma}_{hh}^{{\rm n/SM},(1)}\widehat{\Sigma}_{hh}^{{\rm n/SM},(1)\prime}. \end{aligned} \tag{47}$$

The running Higgs-boson mass $\overline{m}_h^2$ can be related to the threshold corrections to the quartic coupling λ via the relation

$$\overline{m}_h^2 = 2\Delta\lambda(Q)(v^{\overline{\rm MS},{\rm SM}})^2(Q). \tag{48}$$

To express the one- and two-loop corrections in terms of the MSSM coupling constants we have to perform the shift of the vacuum expectation value in Eq. (48),

$$\begin{aligned} \overline{m}_h^2 = &2\Delta\lambda(Q)(v^{\overline{\rm DR},{\rm MSSM}})^2(Q) \\ &\times(1+\widehat{\Sigma}_{hh}^{{\rm n/SM},(1)\prime}). \end{aligned} \tag{49}$$

By solving this equation at the one- and two-loop levels, we obtain the expressions for the matching coefficients for the

quartic coupling,

$$\Delta\lambda^{1l} = -\frac{\widehat{\Sigma}^{\mathrm{n/SM},(1)}_{hh}}{2(v^{\overline{\mathrm{DR}},\mathrm{MSSM}})^2(Q)}, \tag{50a}$$

$$\Delta\lambda^{2l} = -\frac{1}{2(v^{\overline{\mathrm{DR}},\mathrm{MSSM}})^2(Q)}\Bigg(\widehat{\Sigma}^{\mathrm{MSSM},(2)}_{hh} - \widetilde{\Sigma}^{\overline{\mathrm{MS}},\mathrm{SM},(2)}_{hh} - 2\,\widehat{\Sigma}^{\mathrm{n/SM},(1)}_{hh}\widehat{\Sigma}^{\mathrm{n/SM},(1)\prime}_{hh} + \sum_{q=t,b}\frac{\partial}{\partial m_q}\widehat{\Sigma}^{\mathrm{SM},(1)}_{hh}\cdot\Delta^{(1)}m_q\Bigg). \tag{50b}$$

As already mentioned, in the expressions above all couplings are $\overline{\mathrm{DR}}$ MSSM couplings at the scale Q. Another option is to parametrise these threshold corrections in terms of the $\overline{\mathrm{MS}}$ SM couplings at Q. In this work, we will use the $\overline{\mathrm{MS}}$ top-Yukawa coupling in the SM and the $\overline{\mathrm{DR}}$ MSSM bottom-Yukawa coupling to parametrise the one- and two-loop threshold corrections. To express the two-loop threshold corrections in terms of the SM $\overline{\mathrm{MS}}$ top-Yukawa coupling we have to reparametrise the top mass and the vacuum expectation value in the one-loop $\mathcal{O}(\alpha_t)$ threshold correction. This generates the following two-loop terms,

$$\Delta\lambda\Big|_{h_t^{\mathrm{MSSM}}\to y_t^{\mathrm{SM}}} = -\frac{1}{2(v^{\overline{\mathrm{MS}},\mathrm{SM}})^2}\Bigg(\frac{\partial}{\partial m_t}\widehat{\Sigma}^{\mathrm{n/SM},\mathcal{O}(\alpha_t)}_{hh}\cdot\Delta^{(1)}m_t + 2\,\widehat{\Sigma}^{\mathrm{n/SM},\mathcal{O}(\alpha_t)}_{hh}\,\widehat{\Sigma}^{\mathrm{n/SM},(1)\prime}_{hh}\Bigg), \tag{51}$$

which has to be added to Eq. (50b).

We have evaluated the non-SM part of the one-loop Higgs boson self-energy with the help of `FeynArts` [93–95] and `FormCalc` [96] and then expanded in the limit $m_{\tilde{t}_L}, m_{\tilde{t}_R}, m_{\tilde{b}_R} \gg m_t, m_b$. The explicit expressions for them (and their derivatives) in the gaugeless limit and for the case $m_{\tilde{t}_L} = m_{\tilde{t}_R} = m_{\tilde{b}_R} \gg m_t, m_b$ read

$$\widehat{\Sigma}^{\mathrm{n/SM},(1)}_{hh} = -\sum_{q=t,b}\frac{3m_q^4}{4\pi^2v^2} \times\left(\log\frac{M_{\mathrm{SUSY}}^2}{Q^2} + |\widehat{X}_q|^2 - \frac{|\widehat{X}_q|^4}{12}\right), \tag{52}$$

$$\widehat{\Sigma}^{\mathrm{n/SM},(1)\prime}_{hh} = \sum_{q=t,b}\frac{m_q^2}{32\pi^2v^2}\,|\widehat{X}_q|^2. \tag{53}$$

From these expressions and Eq. (50a) it is clear how the one-loop threshold corrections to λ computed in [16,73] can be generalised to the case of the MSSM with complex parameters. These corrections are polynomials in the squark mixing parameter $\widehat{X}_q$. To obtain the expression in the MSSM with complex parameters $\widehat{X}_q$ has to replaced by $|\widehat{X}_q|$.

The two-loop self-energies were taken from [8,10,42] and expanded in the limit

$$m_{\tilde{t}_L}, m_{\tilde{t}_R}, m_{\tilde{b}_R}, m_A, |\mu|, |M_3| \gg m_t, m_b$$

without any additional assumptions on the internal masses and the phases of X_t, X_b, μ and M_3. The two-loop SM self-energies in the $\overline{\mathrm{MS}}$ scheme were taken from [56,57] and extracted from the code `FlexibleSUSY` [24,27,55]. Finally, the one-loop shifts $\Delta^{(1)}m_t$ and $\Delta^{(1)}m_b$ have been computed using `FeynArts` and `FormCalc`. The resulting two-loop formulas for the threshold corrections are presented in Appendix B.2.

Appendix B: Threshold corrections for the case of non-vanishing $\mathcal{CP}$-violating phases

B.1: One-loop threshold corrections

If the sfermions and heavy Higgses are integrated out from the MSSM, effective Higgs–gaugino–Higgsino couplings, $\tilde{g}_{1u,1d,2u,2d}$, are generated (for their exact definition see e.g. [73]). In principle, they can be complex. An explicit calculation of their matching conditions at the SUSY scale $M_{\mathrm{SUSY}} = \sqrt{m_{\tilde{t}_L}m_{\tilde{t}_R}}$, however, shows that they remain real if the sfermions and heavy Higgses are integrated out. All other couplings of the EFT below the SUSY scale are also real-valued.[30]

The only exception are the mass parameters of the EWinos for the case of light EWinos. The phases of these parameters become relevant if the EWinos are integrated out at the EWino mass scale, $M_\chi = \sqrt{|M_2||\mu|}$, and the SM is recovered as EFT.[31]

The threshold corrections of the top and bottom Yukawa couplings originate only from the corrections to the external Higgs leg. They read

$$y_t^{\mathrm{SM}}(M_\chi) = y_t^{\mathrm{SM+EWinos}}(M_\chi)(1+\kappa\,\Delta_{\mathrm{WFR}}), \tag{54}$$

$$y_b^{\mathrm{SM}}(M_\chi) = y_b^{\mathrm{SM+EWinos}}(M_\chi)(1+\kappa\,\Delta_{\mathrm{WFR}}), \tag{55}$$

$$\Delta_{\mathrm{WFR}} = \frac{1}{12}\Bigg[2\tilde{g}_{1u}\tilde{g}_{1d}\cos(\phi_{M_1}+\phi_\mu)f(r_1) + (\tilde{g}_{1u}^2+\tilde{g}_{1d}^2)\left(g(r_1)+3\ln\frac{|\mu|^2}{M_\chi^2}\right) + 6\tilde{g}_{2u}\tilde{g}_{2d}\cos(\phi_{M_2}+\phi_\mu)f(r_2) + 3(\tilde{g}_{2u}^2+\tilde{g}_{2d}^2)\left(g(r_2)+3\ln\frac{|\mu|^2}{M_\chi^2}\right)\Bigg], \tag{56}$$

[30] The CKM phase is neglected here.

[31] Here, we assume that the absolute values of the EWino mass parameters M_1, M_2 and μ are of the same order of magnitude.

with

$$r_1 = \left|\frac{M_1}{\mu}\right|, \quad r_2 = \left|\frac{M_2}{\mu}\right|. \tag{57}$$

In the expressions above, $\kappa = 1/(4\pi)^2$ is used to indicate the loop order, and $\Delta_{\rm WFR}$ are the one-loop corrections to the external Higgs legs. Setting the phases to zero, we recover the result presented in Ref. [73]. The loop functions f and g are defined in the Appendix of Ref. [73].

Similarly, also the matching condition of the Higgs self-coupling is modified,

$$\lambda^{\rm SM}(M_\chi) = \lambda^{\rm SM+EWinos}(M_\chi) + \Delta\lambda \tag{58}$$

with

$$\begin{aligned}
(4\pi)^2\Delta\lambda = {}& \frac{1}{2}\Big[2\lambda\big(\tilde g_{1u}^2 + \tilde g_{1d}^2 + 3\tilde g_{2d}^2 + 3\tilde g_{2u}^2\big) \\
& - \tilde g_{1u}^4 - \tilde g_{1d}^4 - 5\tilde g_{2u}^2 - 5\tilde g_{2d}^2 \\
& - 4\tilde g_{1u}\tilde g_{1d}\tilde g_{2u}\tilde g_{2d} - 2(\tilde g_{1u}^2 + \tilde g_{2d}^2)(\tilde g_{1d}^2 + \tilde g_{2u}^2)\Big]\ln\frac{|\mu|^2}{M_\chi^2} \\
& - \frac{7}{12}(\tilde g_{1u}^4 + \tilde g_{1d}^4) f_1(r_1) - \frac{9}{4} f_2(r_2)(\tilde g_{2u}^4 + \tilde g_{2d}^4) \\
& + \frac{1}{6}\tilde g_{1u}^2\tilde g_{1d}^2[2\cos(2\phi_{M_1} + 2\phi_\mu)h_1(r_1) - 11h_2(r_1)] \\
& + \frac{1}{2}\tilde g_{2u}^2\tilde g_{2d}^2[2\cos(2\phi_{M_2} + 2\phi_\mu)h_1(r_2) - 9h_3(r_2)] \\
& + \frac{1}{3}\tilde g_{1u}\tilde g_{1d}\tilde g_{2u}\tilde g_{2d} \\
& \times \Big[\cos(\phi_{M_1} + \phi_{M_2} + 2\phi_\mu)h_4(r_1, r_2) \\
& - 4\cos(\phi_{M_1} - \phi_{M_2})\frac{r_1 r_2}{r_1 + r_2} f_8(r_1, r_2) - 7h_5(r_1, r_2)\Big] \\
& - \frac{1}{3}\big(\tilde g_{1u}^2\tilde g_{2u}^2 + \tilde g_{1d}^2\tilde g_{2d}^2\big) \\
& \times \Big[2\cos(\phi_{M_1} - \phi_{M_2})\frac{r_1 r_2}{r_1 + r_2} f_8(r_1, r_2) + \frac{5}{2}h_6(r_1, r_2)\Big] \\
& + \frac{1}{6}\big(\tilde g_{1u}^2\tilde g_{2d}^2 + \tilde g_{1d}^2\tilde g_{2u}^2\big) \\
& \times \Big[\cos(\phi_{M_1} + \phi_{M_2} + 2\phi_\mu)h_4(r_1, r_2) - \frac{4}{r_1 + r_2} f_8(r_1, r_2))\Big] \\
& - \frac{4}{3}\big(\tilde g_{1u}\tilde g_{2u} + \tilde g_{1d}\tilde g_{2d}\big)\big(\tilde g_{1u}\tilde g_{2d} + \tilde g_{1d}\tilde g_{2u}\big) \\
& \times \Big[\frac{r_1}{r_1 + r_2}\cos(\phi_{M_1} + \phi_\mu) \\
& + \frac{r_2}{r_1 + r_2}\cos(\phi_{M_2} + \phi_\mu)\Big] f_8(r_1, r_2) \\
& + \frac{2}{3}\tilde g_{1u}\tilde g_{1d}\cos(\phi_{M_1} + \phi_\mu) \\
& \times \Big[\lambda - 2\big(\tilde g_{1u}^2 + \tilde g_{1d}^2\big)\Big] f(r_1) \\
& + 2\tilde g_{2u}\tilde g_{2d}\cos(\phi_{M_2} + \phi_\mu)\Big[\lambda - 2\big(\tilde g_{2u}^2 + \tilde g_{2d}^2\big)\Big] f(r_2) \\
& + \frac{1}{3}\lambda\big(\tilde g_{1u}^2 + \tilde g_{1d}^2\big) g(r_1) + \lambda\big(\tilde g_{2u}^2 + \tilde g_{2d}^2\big) g(r_2).
\end{aligned} \tag{59}$$

The loop functions f_i are defined in the Appendix of Ref. [73]. The loop functions h_i are defined by

$$h_1(r) = -\frac{6r^2}{(1-r^2)^3}[2 - 2r^2 + (1+r^2)\ln r^2], \tag{60a}$$

$$h_2(r) = \frac{6}{11(1-r^2)^3}[2 + 3r^2 - 4r^4 - r^6 + r^2(4 + 5r^2 - r^4)\ln r^2], \tag{60b}$$

$$h_3(r) = \frac{2}{9(1-r^2)^3}[6 + 7r^2 - 8r^4 - 5r^6 + r^2(12 + 13r^2 - r^4)\ln r^2], \tag{60c}$$

$$\begin{aligned}
h_4(r_1, r_2) = {}& -\frac{6r_1 r_2}{(1-r_1^2)^2(1-r_2^2)^2(r_1^2 - r_2^2)} \\
& \times [r_1^2(1-r_2^2)^2\ln r_1^2 \\
& + (1-r_1^2)(1-r_2^2)(r_1^2 - r_2^2) \\
& - (1-r_1^2)^2 r_2^2\ln r_2^2],
\end{aligned} \tag{60d}$$

$$\begin{aligned}
h_5(r_1, r_2) = {}& \frac{6}{7(1-r_1^2)^2(1-r_2^2)^2(r_1^2 - r_2^2)} \\
& [-r_1^6(1-r_2^2)^2 - r_2^2(1-r_2^4) - r_1^4 r_2^2(1-r_2^4) \\
& + r_1^2(1 + r_2^4 - 2r_2^6) + r_1^4(1+r_1^2)(1-r_2^2)^2\ln r_1^2 \\
& - (1-r_1^2)^2(1+r_2^2)r_2^4\ln r_2^2],
\end{aligned} \tag{60e}$$

$$\begin{aligned}
h_6(r_1, r_2) = {}& \frac{6}{5(1-r_1^2)^2(1-r_2^2)^2(r_1^2 - r_2^2)} \\
& \times [-(1-r_1^2)(1-r_2^2)(r_2^4 - r_1^2 r_2^4 - r_1^4 + r_1^4 r_2^2) \\
& + (1-r_2^2)^2 r_1^6\ln r_1^2 - (1-r_1^2)^2 r_2^6\ln r_2^2].
\end{aligned} \tag{60f}$$

In the limit of $r, r_1, r_2 \to 1$ all of the loop functions h_i approach 1. Setting all phases to zero, we again recover the expression given in Ref. [73].

The corresponding expressions for the EWino contribution to the matching between the SM and the MSSM can be obtained by replacing the effective Higgs–Higgsino–gaugino couplings $\tilde g_{1u,1d,2u,2d}$ in Eq. (59) using their tree-level matching conditions [97,98],

$$\tilde g_{1d} = g'\cos\beta, \tag{61a}$$

$$\tilde g_{2d} = g\cos\beta, \tag{61b}$$

$$\tilde g_{1u} = g'\sin\beta, \tag{61c}$$

$$\tilde g_{2u} = g\sin\beta. \tag{61d}$$

The expressions for Δ_b, ϵ_b and Δv entering the one-loop threshold correction of the bottom Yukawa coupling (see Eq. (21)) read

$$(4\pi)^2\Delta_b = C_F g_3^2 t_\beta\cos(\phi_{M_3} + \phi_\mu)$$

$$
\begin{aligned}
&\times \left|\frac{\mu}{M_3}\right| \widetilde{F}_9\left(\frac{M_{Q_3}}{|M_3|}, \frac{M_{D_3}}{|M_3|}\right) \\
&+ \frac{1}{2} y_t^2 t_\beta \cos(\phi_{A_t} + \phi_\mu) \left|\frac{A_t}{\mu}\right| \widetilde{F}_9\left(\frac{M_{Q_3}}{|\mu|}, \frac{M_{U_3}}{|\mu|}\right) \\
&- \frac{3}{4} g^2 t_\beta \cos(\phi_{M_2} + \phi_\mu) \left|\frac{M_2}{\mu}\right| \widetilde{F}_9\left(\frac{M_{Q_3}}{|\mu|}, \left|\frac{M_2}{\mu}\right|\right) \\
&- \frac{g'^2}{6} t_\beta \cos(\phi_{M_1} + \phi_\mu) \Bigg[\frac{1}{3}\left|\frac{\mu}{M_1}\right| \widetilde{F}_9\left(\frac{M_{Q_3}}{|M_1|}, \frac{M_{D_3}}{|M_1|}\right) \\
&+ \frac{1}{2}\left|\frac{M_1}{\mu}\right| \widetilde{F}_9\left(\frac{M_{Q_3}}{|\mu|}, \left|\frac{M_1}{\mu}\right|\right) \\
&+ \left|\frac{M_1}{\mu}\right| \widetilde{F}_9\left(\frac{M_{D_3}}{|\mu|}, \left|\frac{M_1}{\mu}\right|\right)\Bigg], \qquad (62)
\end{aligned}
$$

$$
\begin{aligned}
(4\pi)^2 \epsilon_b = &- C_F g_3^2 \Bigg[1 + \log\frac{|M_3|^2}{Q^2} + \widetilde{F}_6\left(\frac{M_{Q_3}}{|M_3|}\right) \\
&+ \widetilde{F}_6\left(\frac{M_{D_3}}{|M_3|}\right) \\
&- \left|\frac{A_b}{M_3}\right| \cos(\phi_{A_b} - \phi_{M_3}) \widetilde{F}_9\left(\frac{M_{Q_3}}{|M_3|}, \frac{M_{D_3}}{|M_3|}\right)\Bigg] \\
&- \frac{y_b^2}{c_\beta^2}\Bigg[\frac{3}{4}\log\frac{|\mu|^2}{Q^2} + \frac{3}{8}s_\beta^2\left(2\log\frac{M_A^2}{Q^2} - 1\right) \\
&+ \widetilde{F}_6\left(\frac{M_{Q_3}}{|\mu|}\right) + \frac{1}{2}\widetilde{F}_6\left(\frac{M_{D_3}}{|\mu|}\right)\Bigg] \\
&- \frac{y_t^2}{s_\beta^2}\Bigg[\frac{1}{4}\log\frac{|\mu|^2}{Q^2} + \frac{1}{8}c_\beta^2\left(2\log\frac{M_A^2}{Q^2} - 1\right) + s_\beta^2\left(\log\frac{M_A^2}{Q^2} - 1\right) \\
&+ \frac{1}{2}\widetilde{F}_6\left(\frac{M_{U_3}}{|\mu|}\right) \\
&+ \frac{1}{2}\widetilde{F}_9\left(\frac{M_{Q_3}}{|\mu|}, \frac{M_{U_3}}{|\mu|}\right)\left(\left|\frac{A_t}{\mu}\right| \cos(\phi_{A_t} + \phi_\mu) s_\beta c_\beta - 1\right)\Bigg] \\
&- g^2\Bigg[\frac{3}{8}\log\frac{|M_2|^2}{Q^2} - \frac{3}{2}\log\frac{|\mu|^2}{Q^2} + \frac{3}{4}\widetilde{F}_6\left(\frac{M_{Q_3}}{|M_2|}\right) \\
&- \frac{3}{4}\widetilde{F}_8\left(\frac{M_{Q_3}}{|\mu|}, \left|\frac{M_2}{\mu}\right|\right)\Bigg] \\
&- g'^2\Bigg[\frac{5}{72}\log\frac{|M_1|^2}{Q^2} - \frac{1}{2}\log\frac{|\mu|^2}{Q^2} + \frac{1}{36}\widetilde{F}_6\left(\frac{M_{Q_3}}{|M_1|}\right) \\
&+ \frac{1}{9}\widetilde{F}_6\left(\frac{M_{D_3}}{|M_1|}\right) \\
&- \frac{1}{12}\widetilde{F}_8\left(\frac{M_{Q_3}}{|\mu|}, \left|\frac{M_1}{\mu}\right|\right) \\
&- \frac{1}{6}\widetilde{F}_8\left(\frac{M_{D_3}}{|\mu|}, \left|\frac{M_1}{\mu}\right|\right) \\
&+ \frac{1}{18}\left|\frac{A_b}{M_1}\right| \cos(\phi_{A_b} - \phi_{M_1}) \widetilde{F}_9\left(\frac{M_{Q_3}}{|M_1|}, \frac{M_{D_3}}{|M_1|}\right)\Bigg], \qquad (63)
\end{aligned}
$$

$$
\begin{aligned}
(4\pi)^2 \Delta v = &- \frac{y_t^2}{4}\frac{|X_t|^2}{M_{Q_3} M_{U_3}} \widetilde{F}_5\left(\frac{M_{Q_3}}{M_{U_3}}\right) \\
&- \frac{y_b^2}{4}\frac{|X_b|^2}{M_{Q_3} M_{D_3}} \widetilde{F}_5\left(\frac{M_{Q_3}}{M_{D_3}}\right). \qquad (64)
\end{aligned}
$$

The functions $\widetilde{F}_{5,6,8,9}(x)$ are defined in Appendix A of Ref. [73]. Q is the renormalisation scale, which we set equal to $M_{\rm SUSY}$. We neglect electroweak contributions to Δv.

In addition, we give here the result for the one-loop threshold correction for the top Yukawa coupling, which can be used to reexpress the two-loop threshold corrections of the Higgs self-coupling in terms of the MSSM top Yukawa coupling (see Appendix B.2). It is given by

$$
\begin{aligned}
y_t^{\rm SM}(Q) &= h_t^{\rm MSSM} s_\beta \,(1 + \Delta h_t)\,, \qquad (65) \\
(4\pi)^2 \Delta h_t &= \frac{4}{3} g_3^2 \Bigg[1 + \ln\frac{|M_3|^2}{Q^2} + \widetilde{F}_6\left(\frac{M_{Q_3}}{|M_3|}\right) \\
&+ \widetilde{F}_6\left(\frac{M_{U_3}}{|M_3|}\right) \\
&- \left|\frac{X_t}{M_3}\right| \cos(\phi_{M_3} - \phi_{X_t}) \widetilde{F}_9\left(\frac{M_{Q_3}}{|M_3|}, \frac{M_{U_3}}{|M_3|}\right)\Bigg] \\
&+ \frac{y_t^2}{s_\beta^2}\Bigg[\frac{3}{4}\ln\frac{|\mu|^2}{Q^2} + \frac{3}{8}c_\beta^2\left(2\ln\frac{M_A^2}{Q^2} - 1\right) \\
&- \frac{1}{4}s_\beta^2 |\widetilde{X}_t| \widetilde{F}_5\left(\frac{M_{Q_3}}{M_{U_3}}\right) \\
&+ \widetilde{F}_6\left(\frac{M_{Q_3}}{|\mu|}\right) + \frac{1}{2}\widetilde{F}_6\left(\frac{M_{U_3}}{|\mu|}\right)\Bigg] \\
&+ \frac{y_b^2}{c_\beta^2}\Bigg[\frac{1}{4}\ln\frac{|\mu|^2}{Q^2} + \frac{3}{8}s_\beta^2\left(2\ln\frac{M_A^2}{Q^2} - 1\right) \\
&- \frac{1}{4}c_\beta^2 |\widetilde{X}_b| \widetilde{F}_5\left(\frac{M_{Q_3}}{M_{D_3}}\right) \\
&+ \frac{1}{2}\widetilde{F}_6\left(\frac{M_{D_3}}{|\mu|}\right) + \frac{1}{2}\frac{|X_b|}{|\mu| t_\beta}\cos(\phi_\mu + \phi_{X_b}) \\
&\times \widetilde{F}_9\left(\frac{M_{Q_3}}{|\mu|}, \frac{M_{D_3}}{|\mu|}\right)\Bigg] \\
&+ g^2\Bigg[\frac{3}{8}\ln\frac{|M_2|^2}{Q^2} - \frac{3}{2}\ln\frac{|\mu|^2}{Q^2} + \frac{3}{4}\widetilde{F}_6\left(\frac{M_{Q_3}}{|M_2|}\right) \\
&- \frac{3}{4}\widetilde{F}_8\left(\frac{M_{Q_3}}{|\mu|}, \frac{|M_2|}{|\mu|}\right) \\
&- \frac{3}{4 t_\beta}\frac{|M_2|}{|\mu|}\cos(\phi_{M_2} + \phi_\mu) \widetilde{F}_9\left(\frac{M_{Q_3}}{|\mu|}, \frac{|M_2|}{|\mu|}\right) - \frac{3}{8}\Bigg] \\
&+ g'^2\Bigg[\frac{17}{12}\ln\frac{|M_1|^2}{Q^2} - \frac{1}{2}\ln\frac{|\mu|^2}{Q^2} + \frac{1}{36}\widetilde{F}_6\left(\frac{M_{Q_3}}{|M_1|}\right) \\
&+ \frac{4}{9}\widetilde{F}_6\left(\frac{M_{U_3}}{|M_1|}\right) \\
&+ \frac{1}{12}\widetilde{F}_8\left(\frac{M_{Q_3}}{|\mu|}, \frac{|M_1|}{|\mu|}\right) - \frac{1}{3}\widetilde{F}_8\left(\frac{M_{U_3}}{|\mu|}, \frac{|M_1|}{|\mu|}\right) \\
&- \frac{1}{9}\frac{|X_t|}{|M_1|}\cos(\phi_{M_1} - \phi_{X_t}) \widetilde{F}_9\left(\frac{M_{Q_3}}{|M_1|}, \frac{M_{U_3}}{|M_1|}\right)
\end{aligned}
$$

$$+\frac{1}{3t_\beta}\frac{|M_1|}{|\mu|}\cos(\phi_{M_1}+\phi_\mu)\left(\frac{1}{4}\widetilde{F}_9\left(\frac{M_{Q_3}}{|\mu|},\frac{|M_1|}{|\mu|}\right)-\widetilde{F}_9\left(\frac{M_{U_3}}{|\mu|},\frac{|M_1|}{|\mu|}\right)\right)-\frac{1}{72}\Bigg] \tag{66}$$

Setting all phases to zero, we again recover the expression given in Ref. [73].

B.2: Two-loop threshold corrections

Here, we list the two-loop threshold corrections to the Higgs self-coupling in the limit where all involved non-SM particles except for EWinos and gluinos have the same mass,

$$\begin{aligned}(4\pi)^4(\Delta\lambda)_{\alpha_t^2} = -y_t^6\Bigg\{&\frac{3|\widehat{X}_t|^6}{2}\\
&+\frac{1}{t_\beta^2}\Big(\cos(\phi_{X_t}-\phi_{Y_t})\big(12(3+16K)|\widehat{X}_t|\\
&-12(1+4K)|\widehat{X}_t|^3\big)|\widehat{Y}_t|+3(3+16K)|\widehat{Y}_t|^2\Big)\\
&-|\widehat{X}_t|^2\Big(2(7+36K)\frac{|\widehat{Y}_t|^2}{t_\beta^2}-\frac{3}{2s_\beta^2}\big(7+24K\\
&-3(5-8K)c_{2\beta}\\
&+(32|\widehat{\mu}|^2-12|\widehat{\mu}|^4)f_2(|\widehat{\mu}|)\big)\Big)\\
&+|\widehat{X}_t|^4\left(\frac{|\widehat{Y}_t|^2}{4t_\beta^2}(19+96K)-\frac{3}{8s_\beta^2}\big(23-25c_{2\beta}\right.\\
&\left.+(16|\widehat{\mu}|^2-8|\widehat{\mu}|^4)\widetilde{f}_2(|\widehat{\mu}|)\big)\right)\\
&+\frac{3}{4s_\beta^2}\Big(21+120K+32|\widehat{\mu}|^2+2\pi^2\\
&-(13-120K-2\pi^2)c_{2\beta}\\
&+\big(-32+36|\widehat{\mu}|^2+8|\widehat{\mu}|^4\big)\widetilde{f}_2(|\widehat{\mu}|)+16\widetilde{f}_3(|\widehat{\mu}|)\Big)\Bigg\},\end{aligned} \tag{67a}$$

$$\begin{aligned}(4\pi)^4(\Delta\lambda)_{\alpha_t\alpha_s} = g_3^2y_t^4\Bigg\{&\frac{4}{3}\Big(-12|\widehat{X}_t|^2\big(\widetilde{f}_1(|\widehat{M}_3|)\\
&-(1-7|\widehat{M}_3|^2+2|\widehat{M}_3|^4)\widetilde{f}_2(|\widehat{M}_3|)\big)\\
&+|\widehat{X}_t|^4\big(\widetilde{f}_1(|\widehat{M}_3|)-(1-9|\widehat{M}_3|^2+4|\widehat{M}_3|^4)\widetilde{f}_2(|\widehat{M}_3|)\big)\\
&-6\big(3+4|\widehat{M}_3|^4\widetilde{f}_2(|\widehat{M}_3|)\\
&-|\widehat{M}_3|^2\big(6\widetilde{f}_2(|\widehat{M}_3|)-8\widetilde{f}_4(|\widehat{M}_3|)\big)\big)\Big)\\
&+\frac{16}{3}\cos(\phi_{X_t}-\phi_{M_3})|\widehat{M}_3||\widehat{X}_t|\\
&\times\Big(\big(2(8-|\widehat{M}_3|^2)|\widehat{X}_t|^2-|\widehat{X}_t|^4\big)\widetilde{f}_2(|\widehat{M}_3|)\\
&-12\big(1-\widetilde{f}_4(|\widehat{M}_3|)-|\widehat{M}_3|^2\widetilde{f}_5(|\widehat{M}_3|)\big)\Big)\Bigg\},\end{aligned} \tag{67b}$$

$$\begin{aligned}(4\pi)^4(\Delta\lambda)_{\alpha_b\alpha_s} = -\frac{8}{3}g_3^2y_b^4\Bigg\{&9+4|\widehat{X}_b|^3|\widehat{M}_3|\cos(\phi_{X_b}-\phi_{M_3})\\
&\times(-2+|\widehat{M}_3|^2)\widetilde{f}_2(|\widehat{M}_3|)\\
&-12|\widehat{X}_b|^2\big(1+|\widehat{M}_3|^2(-2+|\widehat{M}_3|^2)\widetilde{f}_2(|\widehat{M}_3|)\big)\\
&+|\widehat{X}_b|^4\big(1+|\widehat{M}_3|^2(-3+2|\widehat{M}_3|^2)\widetilde{f}_2(|\widehat{M}_3|)\big)\\
&+24|\widehat{X}_b||\widehat{M}_3|\cos(\phi_{X_b}-\phi_{M_3})\big(1+\widetilde{f}_1(|\widehat{M}_3|)-2\widetilde{f}_4(|\widehat{M}_3|)\big)\\
&+6|\widehat{M}_3|^2\big((-3+2|\widehat{M}_3|^2)\widetilde{f}_2(|\widehat{M}_3|)+4\widetilde{f}_4(|\widehat{M}_3|)\big)\Bigg\},\end{aligned} \tag{67c}$$

$$\begin{aligned}(4\pi)^4(\Delta\lambda)_{\alpha_t\alpha_b} = y_t^4y_b^2\Bigg\{&-\frac{3}{2}+36K+3\pi^2\\
&+\frac{24K}{t_\beta^2}|\widehat{Y}_t|^2+\frac{1}{t_\beta^2}|\widehat{X}_b|^2|\widehat{Y}_t|^2+\frac{1}{t_\beta^2}|\widehat{X}_t|^2|\widehat{Y}_t|^2\\
&+\frac{2}{9}|\widehat{X}_t||\widehat{Y}_t||\widehat{X}_b||\widehat{Y}_b|\cos(\phi_{X_t}+\phi_{X_b}-\phi_{Y_t}-\phi_{Y_b})\\
&\times(18+(1+24K)|\widehat{X}_t|^2)\\
&-\frac{1}{6t_\beta^2}(11+48K)|\widehat{X}_b|^2|\widehat{X}_t|^2|\widehat{Y}_t|^2\\
&+\frac{48K}{c_\beta^2}\cos(\phi_{X_b}-\phi_{X_t})|\widehat{X}_b||\widehat{X}_t|\\
&+\frac{2}{s_\beta^2}|\widehat{Y}_t||\widehat{X}_b|\cos(\phi_{Y_t}-\phi_{X_b})(24K+|\widehat{X}_t|^2)\\
&+\frac{24}{s_\beta^2}(3K-\mathrm{Li}_2(1-|\widehat{\mu}|^2)+\widetilde{f}_1(|\widehat{\mu}|))\\
&+2\cos(\phi_{X_t}-\phi_{Y_t})|\widehat{X}_t||\widehat{Y}_t|\Big(\frac{|\widehat{X}_b|^2}{t_\beta^2}\\
&+6\Big(1+4K\Big(-3+\frac{1}{s_\beta^2}\Big)+2\widetilde{f}_1(|\widehat{\mu}|)\Big)\\
&+2|\widehat{X}_t|^2\Big(-\frac{1}{3}+4K-\widetilde{f}_1(|\widehat{\mu}|)-\widetilde{f}_2(|\widehat{\mu}|)\Big)\Big)\\
&+|\widehat{X}_b|^2|\widehat{X}_t|^4\Big(\frac{1}{2}-2\widetilde{f}_2(|\widehat{\mu}|)\Big)+\frac{3}{2}|\widehat{X}_b|^2|\widehat{X}_t|^2\\
&\times\Big(-2+\frac{1}{s_\beta^2}+16\widetilde{f}_2(|\widehat{\mu}|)\Big)\\
&+2\cos(\phi_{X_b}-\phi_{Y_b})|\widehat{X}_b||\widehat{Y}_b|(24K+|\widehat{X}_t|^2\\
&\times(1+(-12+|\widehat{X}_t|^2)\widetilde{f}_2(|\widehat{\mu}|))-24\widetilde{f}_4(|\widehat{\mu}|))\\
&+3|\widehat{X}_b|^2(5+8K-\frac{1}{s_\beta^2}(1+8K+2|\widehat{\mu}|^2\widetilde{f}_2(|\widehat{\mu}|))\\
&+16\widetilde{f}_4(|\widehat{\mu}|))\\
&+\frac{4}{3c_\beta^2}\cos(\phi_{X_t}-\phi_{Y_b})|\widehat{X}_t||\widehat{Y}_b|(-9+2|\widehat{X}_t|^2\\
&+12K(-6+|\widehat{X}_t|^2))\\
&+\frac{1}{c_\beta^2}\Big(36K+\big(-6+\pi^2-|\widehat{\mu}|^2\end{aligned}$$

$$
\begin{aligned}
&\times(-15+6|\widehat{\mu}|^2+\pi^2))\,\widetilde{f}_2(|\widehat{\mu}|)\\
&-(18+\pi^2)\,\widetilde{f}_4(|\widehat{\mu}|)+\big(12+|\widehat{\mu}|^2(-6+\pi^2)\big)\,\widetilde{f}_5(|\widehat{\mu}|)\Big)\\
&+3|\widehat{X}_t|^2\Big(-2(5+8K+4\,\widetilde{f}_1(|\widehat{\mu}|))\\
&-\frac{1}{s_\beta^2}(1+8K+2|\widehat{\mu}|^2\,\widetilde{f}_2(|\widehat{\mu}|))\\
&-\frac{2}{c_\beta^2}\big(-1+4K+|\widehat{\mu}|^2\big(1+\widetilde{f}_1(|\widehat{\mu}|)+\widetilde{f}_2(|\widehat{\mu}|)\big)\big)\Big)\\
&+|\widehat{X}_t|^4\Big(-\frac{3}{4}\Big(1+\frac{1}{c_\beta^2}\Big)\\
&+\big(1+\widetilde{f}_1(|\widehat{\mu}|)+\widetilde{f}_2(|\widehat{\mu}|)\big)\Big(4+\frac{|\widehat{\mu}|^2}{c_\beta^2}\Big)\Big)\\
&-3(1+8K)|\widehat{Y}_b|^2t_\beta^2+4(1+6K)|\widehat{X}_t|^2|\widehat{Y}_b|^2t_\beta^2\\
&-\frac{1}{36}(35+192K)|\widehat{X}_t|^4|\widehat{Y}_b|^2t_\beta^2\Big\}\\
&+y_t^2y_b^4\Big\{|\widehat{X}_b|^4|\widehat{X}_t|^2-\frac{3}{t_\beta^2}(1+8K)|\widehat{Y}_t|^2\\
&+\frac{4}{t_\beta^2}(1+6K)|\widehat{X}_b|^2|\widehat{Y}_t|^2\\
&-\frac{1}{36t_\beta^2}(35+192K)|\widehat{X}_b|^4|\widehat{Y}_t|^2\\
&+\frac{2}{9}\cos(\phi_{X_t}+\phi_{X_b}-\phi_{Y_t}-\phi_{Y_b})|\widehat{X}_b||\widehat{X}_t||\widehat{Y}_b||\widehat{Y}_t|\\
&\times(18+(1+24K)|\widehat{X}_b|^2)\\
&+\frac{4}{3s_\beta^2}\cos(\phi_{X_b}-\phi_{Y_t})|\widehat{X}_b||\widehat{Y}_t|(-9+2|\widehat{X}_b|^2\\
&+12K(-6+|\widehat{X}_b|^2))\\
&+|\widehat{X}_b|^4\Big(1-4(-2+|\widehat{\mu}|^2)\,\widetilde{f}_2(|\widehat{\mu}|)\\
&-\frac{1}{4s_\beta^2}\big(1-6|\widehat{\mu}|^2\,\widetilde{f}_2(|\widehat{\mu}|)+4|\widehat{\mu}|^4\,\widetilde{f}_2(|\widehat{\mu}|)\big)\Big)\\
&+2\cos(\phi_{X_t}-\phi_{Y_t})|\widehat{X}_t||\widehat{Y}_t|\big(24K+|\widehat{X}_b|^2-24\,\widetilde{f}_4(|\widehat{\mu}|)\big)\\
&+\frac{48K}{c_\beta^2}\cos(\phi_{X_t}-\phi_{X_b})|\widehat{X}_b||\widehat{X}_t|\\
&+\frac{2}{c_\beta^2}\cos(\phi_{X_t}-\phi_{Y_b})(24K+|\widehat{X}_b|^2)|\widehat{X}_t||\widehat{Y}_b|\\
&+\frac{3}{2}|\widehat{X}_b|^2|\widehat{X}_t|^2\Big(-6+\frac{1}{c_\beta^2}\Big)\\
&-\frac{1}{6}(11+48K)|\widehat{X}_b|^2|\widehat{X}_t|^2|\widehat{Y}_b|^2t_\beta^2\\
&+\frac{1}{2}\Big(-3+72K+6\pi^2+\frac{2}{s_\beta^2}\\
&\times\Big(36K+\pi^2-3\Big(-6+\big(8-11|\widehat{\mu}|^2+2|\widehat{\mu}|^4\big)\,\widetilde{f}_2(|\widehat{\mu}|)\\
&+(-4+8|\widehat{\mu}|^2)\,\widetilde{f}_4(|\widehat{\mu}|)\Big)\Big)\\
&+\frac{8}{c_\beta^2}\big(-1+3K-\mathrm{Li}_2(1-|\widehat{\mu}|^2)+(1-|\widehat{\mu}|^2)\,\widetilde{f}_2(|\widehat{\mu}|)\big)\Big)\\
&+3|\widehat{X}_t|^2\Big(5+8K+16\,\widetilde{f}_3(|\widehat{\mu}|)\\
&-\frac{1}{c_\beta^2}\big(1+8K+2|\widehat{\mu}|^2\,\widetilde{f}_2(|\widehat{\mu}|)\big)\Big)\\
&+3|\widehat{X}_b|^2\Big(9+16K-8(-1+|\widehat{\mu}|^2)\,\widetilde{f}_2(|\widehat{\mu}|)\\
&+\frac{1}{c_\beta^2}\Big(1+2|\widehat{\mu}|^4\,\widetilde{f}_2(|\widehat{\mu}|)\\
&+\frac{2}{s_\beta^2}\big(4K+|\widehat{\mu}|^2\,\widetilde{f}_2(|\widehat{\mu}|)-|\widehat{\mu}|^4\,\widetilde{f}_2(|\widehat{\mu}|)\big)\Big)\Big)\\
&+(24K+|\widehat{X}_b|^2+|\widehat{X}_t|^2)|\widehat{Y}_b|^2t_\beta^2\\
&+\frac{2}{3}\cos(\phi_{X_b}-\phi_{Y_b})|\widehat{X}_b||\widehat{Y}_b|\Big(2|\widehat{X}_b|^2\\
&\big(2+12K+3(-2+|\widehat{\mu}|^2)\,\widetilde{f}_2(|\widehat{\mu}|)\big)\\
&+18\Big(1+2\,\widetilde{f}_1(|\widehat{\mu}|)\\
&+4K\Big(-3+\frac{1}{c_\beta^2}\Big)\Big)+3|\widehat{X}_t|^2t_\beta^2\Big)\Big\},
\end{aligned}
\tag{67d}
$$

$$
\begin{aligned}
(4\pi)^4(\Delta\lambda)_{\alpha_b^2}=y_b^6\Big\{&12\cos(\phi_{X_b}-\phi_{Y_b})|\widehat{X}_b||\widehat{Y}_b|t_\beta^2\\
&(4K(|\widehat{X}_b|^2-4)+|\widehat{X}_b|^2-3)\\
&+\frac{1}{4}\Big(\frac{3}{c_\beta^2}\Big(48K(5-2|\widehat{X}_b|^2)\\
&+2|\widehat{\mu}|^2\Big(\widetilde{f}_2(|\widehat{\mu}|)\big((3-2|\widehat{\mu}|^2)|\widehat{X}_b|^4\\
&+4(3|\widehat{\mu}|^2-5)|\widehat{X}_b|^2+4|\widehat{\mu}|^2+18\big)+16\Big)\\
&-32\,\widetilde{f}_2(|\widehat{\mu}|)\\
&+16\,\widetilde{f}_3(|\widehat{\mu}|)+|\widehat{X}_b|^4-8|\widehat{X}_b|^2+4\pi^2+8\Big)\\
&-|\widehat{Y}_b|^2t_\beta^2(|\widehat{X}_b|^2-2)\big(96K(|\widehat{X}_b|^2-1)\\
&+19|\widehat{X}_b|^2-18\big)\\
&+2\big(72K(2|\widehat{X}_b|^2-5)-2|\widehat{X}_b|^2(|\widehat{X}_b|^2-6)^2\\
&-6\pi^2+39\big)\Big)\Big\}.
\end{aligned}
\tag{67e}
$$

The listed expressions are for the case where the one-loop $\mathcal{O}(\alpha_t,\alpha_b)$ corrections are expressed in terms of the SM $\overline{\text{MS}}$ top Yukawa coupling, y_t, and the MSSM $\overline{\text{DR}}$ bottom Yukawa coupling, y_b. Expressions to translate them to the MSSM $\overline{\text{DR}}$ top Yukawa coupling and the SM $\overline{\text{MS}}$ bottom Yukawa coupling, respectively, are provided in Appendix B.1.

In the Eqs. (67a)–(67e), $\widetilde{f}_{1,2,3,4,5}(x)$ are non-singular functions of $\widehat{\mu}=\mu/M_{\text{SUSY}}$ or $\widehat{M}_3=M_3/M_{\text{SUSY}}$. The functions $\widetilde{f}_{1,2,3}(x)$ are the same as the functions $f_{1,2,3}(x)$ from

Ref. [99],

$$\widetilde{f}_1(x) = \frac{x^2 \log x^2}{1-x^2}, \tag{68a}$$

$$\widetilde{f}_2(x) = \frac{1}{1-x^2}\left[1 + \frac{x^2}{1-x^2}\log x^2\right], \tag{68b}$$

$$\widetilde{f}_3(x) = \frac{(-1+2x^2+2x^4)}{(1-x^2)^2} \times \left[\log x^2 \log(1-x^2) + \mathrm{Li}_2(x^2) - \frac{\pi^2}{6} - x^2 \log x^2\right], \tag{68c}$$

$$\widetilde{f}_4(x) = \frac{x^2(\log x^2 + \mathrm{Li}_2(1-x^2))}{(1-x^2)^2}, \tag{68d}$$

$$\widetilde{f}_5(x) = \frac{x^2 \log x^2 + \mathrm{Li}_2(1-x^2)}{(1-x^2)^2}. \tag{68e}$$

with $\widetilde{f}_1(0) = 0$, $\widetilde{f}_2(0) = 1$, $\widetilde{f}_3(0) = \frac{\pi^2}{6}$, $\widetilde{f}_4(0) = 0$, $\widetilde{f}_5(0) = \frac{\pi^2}{6}$ and $\widetilde{f}_1(1) = -1$, $\widetilde{f}_2(1) = \frac{1}{2}$, $\widetilde{f}_3(1) = -\frac{9}{4}$, $\widetilde{f}_4(1) = -\frac{1}{4}$, $\widetilde{f}_5(1) = \frac{3}{4}$. We use a different notation for them than in Ref. [99], since we have already used the notation $f_i(x)$ for the functions in the threshold correction to the quartic coupling above in Eq. (59).[32]

The constant K is

$$K = -\frac{1}{\sqrt{3}}\int_0^{\pi/6} dx \log(2\cos x) \sim -0.1953256. \tag{69}$$

Fully general expressions for the two-loop threshold corrections to the SM Higgs self-coupling can be found in ancillary files distributed alongside this paper.

Appendix C: Dependence of Δ_b^{2l} on $\mathcal{CP}$-violating phases

Before deriving the phase dependence of the two-loop correction to Δ_b, we first consider the one-loop correction. The $\mathcal{O}(\alpha_s, \alpha_t)$ one-loop Δ_b correction in the heavy SUSY limit can be obtained by evaluating the diagrams in Fig. 10.[33]

These diagrams include the incoming and the outgoing b quarks with different chirality. The diagrams which involve quarks with the same chirality are subleading with respect to their powers of $\tan\beta$ and do not contribute to Δ_b [64]. The diagrams are drawn using the chiral basis in which the "left" and the "right" squarks propagate and the off-diagonal mass term is interpreted as an additional interaction (denoted as $\otimes$) which flips the chirality quantum number of the squark. In the limit $M_{\rm SUSY} \gg v$ only the diagrams with a single mass insertion contribute. This can be seen in the following way. The left diagram in Fig. 10 is proportional to

$$\propto \alpha_s\ m_b\ \mu\ t_\beta\ M_3\ C_0(0,0,0,m^2_{\tilde{t}_L}, m^2_{\tilde{t}_R}, |M_3|^2), \tag{70}$$

where C_0 is a Passarino–Veltman function corresponding to the scalar vertex function with three external legs. If all soft SUSY-breaking masses are equal to $M_{\rm SUSY}$, the expression in Eq. (70) reduces to

$$\propto \alpha_s\ m_b\ t_\beta \frac{\mu\ M_3}{M^2_{\rm SUSY}} = \alpha_s\ m_b\ t_\beta \frac{\mu}{M_{\rm SUSY}}. \tag{71}$$

The diagram with two mass insertions, which is only possible if the two external quarks have the same chirality, is proportional to

$$\begin{aligned}&\propto \alpha_s\ (m_b\ \mu\ t_\beta)^2\ M_3\ D_0(0,0,0,0,0,0,\\ &m^2_{\tilde{t}_L}, m^2_{\tilde{t}_R}, m^2_{\tilde{t}_L}, |M_3|^2)\\ &= \alpha_s\ (m_b\ \mu\ t_\beta)^2\ M_{\rm SUSY}\\ &\quad \times D_0(0,0,0,0,0,0, M^2_{\rm SUSY}, M^2_{\rm SUSY}, M^2_{\rm SUSY}, M^2_{\rm SUSY}),\end{aligned} \tag{72}$$

where D_0 is a Passarino–Veltman function corresponding to the scalar vertex function with four external legs. If all soft SUSY-breaking masses are equal to $M_{\rm SUSY}$ this diagrams behaves like

$$\begin{aligned}&\propto \alpha_s\ m_b\ t_\beta \frac{\mu\ M_3}{M^2_{\rm SUSY}} \times \frac{m_b\ \mu\ t_\beta}{M^2_{\rm SUSY}}\\ &= \alpha_s\ m_b\ t_\beta \frac{\mu}{M_{\rm SUSY}} \times \frac{m_b\ \mu\ t_\beta}{M^2_{\rm SUSY}}.\end{aligned} \tag{73}$$

We see that it is suppressed by an additional factor $m_b/M_{\rm SUSY}$ compared to the diagram with one insertion and is therefore subleading. This is consistent with the fact that only diagrams with external legs of different chirality contribute to Δ_b. Clearly, diagrams with more insertions will be suppressed by additional factors of $m_b/M_{\rm SUSY}$. Following similar arguments, one can show that diagrams similar to the right diagram in Fig. 10 with more than one mass insertion are suppressed by powers of $m_t/M_{\rm SUSY}$.

The same kind of argument applies to higher-order corrections to Δ_b [38] as can be proven by using the Kinoshita–Lee–Nauenberg theorem [101,102]. Namely, the diagrams contributing to the two-loop quantity Δ_b of order $\mathcal{O}(\alpha_s^2, \alpha_s\alpha_t)$ contain only one mass insertion.

The phases of the complex parameters A_t, μ and M_3 enter the diagrams of Fig. 10 through the mass insertion and through $(b_L \widetilde{b}^*_L \widetilde{g})$, and $(b_L \widetilde{t}^*_R \widetilde{H}^+_2)$ vertices. In particular, the mass insertion in the left diagram in Fig. 10 yields the phase

[32] We note that these functions are not independent from each other. For example, using the identities for the Spence function $\mathrm{Li}_2(x^2)$ one can show that $\widetilde{f}_3(x) = (1-2x^2-2x^4)\widetilde{f}_5(x)$. However, we decided to stick to the notations of Ref. [99]. So, we expressed our result in terms of $\widetilde{f}_{1,2,3}$ and added two more functions for better readability of the results.

[33] All diagrams in this Section were produced with `Axodraw` [100].

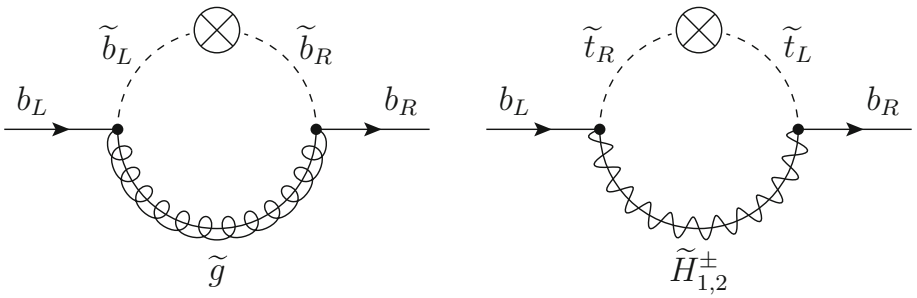

Fig. 10 Diagrams contributing to $\Delta_b^{\mathcal{O}(\alpha_s,\alpha_t)}$ at the leading order in the chiral basis

factor $\propto e^{+i\phi_\mu}$ while both vertices contain $e^{+i\frac{\phi_{M_3}}{2}}$. The overall diagram is then $\propto e^{i(\phi_{M_3}+\phi_\mu)}$. The result for the analogous diagram with incoming b_R and outgoing b_L leads to the phase factor $\propto e^{-i(\phi_{M_3}+\phi_\mu)}$. The overall phase dependence is then $\propto \cos(\phi_{M_3}+\phi_\mu)$ (see Eq. (62) in Appendix B.1). The mass insertion in the right diagram in Fig. 10 gives the phase factor $\propto e^{+i\phi_{A_t}}$, while the $(b_L\widetilde{t}_R^*\widetilde{H}_2^+)$ and $(\bar{b}_R\widetilde{t}_L\widetilde{H}_2^-)$ vertices contain the entries of the chargino mixing matrices $\mathbf{V}^*_{22}$ and $\mathbf{U}^*_{22}$. In the gaugeless limit, they are proportional to the phase factors $\propto e^{+i\frac{\phi_\mu}{2}}$. The overall diagram (together with its complex conjugated) is $\propto \cos(\phi_{A_t}+\phi_\mu)$ (see Eq. (62) in Appendix B.1).

The two-loop diagrams contributing to the quantity Δ_b at $\mathcal{O}(\alpha_s^2)$ can be split into three categories: either a gluon, a sbottom or a gluino is added to the one-loop $\mathcal{O}(\alpha_s)$ graph. Examples of the corresponding diagrams are depicted in Figs. 11, 12 and 13. The particles which are added to the one-loop graph are highlighted with red color.[34]

Following the argumentats given at the end of Sect. 3, we can conclude that in the case of the MSSM with complex parameters the two-loop Δ_b of $\mathcal{O}(\alpha_s^2)$ given in Eq. (23) has to be multiplied by $\cos(\phi_\mu+\phi_{M_3})$. The same reasoning can be applied to the $\mathcal{O}(\alpha_s\alpha_t)$ Δ_b corrections: Eq. (24) has to be multiplied by $\cos(\phi_\mu+\phi_{A_t})$.[35]

Appendix D: Leading and next-to-leading logarithms

In this part of the Appendix we present analytic expressions for the leading (LL) and next-to-leading (NLL) logarithms proportional to the bottom Yukawa coupling, which appear at the one and two-loop order in the calculation of the lightest Higgs boson mass in the MSSM. They are derived in the special case of

$$M_A = |M_3| = |\mu| = M_{Q_3} = M_{U_3} = M_{D_3} = M_{\rm SUSY}. \quad (74)$$

In the following expressions, $\kappa = 1/(4\pi)^2$, L is the logarithm of the ratio of $M_{\rm SUSY}$ and M_t,

$$L = \log\frac{M^2_{\rm SUSY}}{M_t^2}, \quad (75)$$

$\overline{m}_t$ is $\overline{\rm MS}$ SM top mass, $\overline{m}_t \equiv \overline{m}_t^{\overline{\rm MS},\rm SM}(m_t)$, $\overline{m}_b$ is the $\overline{\rm DR}$ MSSM bottom mass at the scale $M_{\rm SUSY}$ defined in Eq. (20), v is the SM Higgs vacuum expectation value $v \equiv v_{G_F} = (2\sqrt{2}G_F)^{-1/2} \simeq 174$ GeV. The ratio of the vacuum expectation values of the two Higgs doublets, $\tan\beta$, is renormalised in the $\overline{\rm DR}$ scheme at the scale $M_{\rm SUSY}$. g_3 is the strong gauge coupling, $g_3^2 = 4\pi\alpha_s$. We do not specify the renormalisation prescription for it, since it appears in the expressions for M_h starting at the two-loop level. Therefore, a change of the renormalisation scheme for g_3 is a three-loop effect. The parameter $\widehat{X}_b$ is renormalised in the $\overline{\rm DR}$ scheme at the scale $M_{\rm SUSY}$, while $\widehat{X}_t$ is fixed either in the OS scheme or in the $\overline{\rm DR}$ scheme at the scale $M_{\rm SUSY}$.

The logarithmic terms can be derived in one of the two following ways. The first method is an approximate perturbative solution of the renormalisation group equation (RGE) for the quartic coupling λ

$$\frac{d\lambda}{d\log Q^2} = \kappa\beta_\lambda^{(1)}(Q) + \kappa^2\beta_\lambda^{(2)}(Q) + \cdots, \quad (76)$$

where Q is a renormalisation scale, $\beta_\lambda^{(1)}$, $\beta_\lambda^{(2)}$ are the one- and two-loop contributions to the beta function, and the ellipsis encodes higher-order terms. Truncating the result at the second order, one obtains [85,103]

$$\lambda(M_t) = \lambda(M_{\rm SUSY}) - \beta_\lambda^{(1)}(M_{\rm SUSY})\kappa L + \frac{1}{2}\beta_\lambda^{(1,1)}(M_{\rm SUSY})\kappa L^2 - \beta_\lambda^{(2)}(M_{\rm SUSY})\kappa^2 L + \cdots, \quad (77)$$

where $\beta_\lambda^{(1,1)}(Q) = d\beta_\lambda^{(1)}/d\log Q^2$. The running Higgs mass at the scale M_t is obtained from Eq. (77) by mulitplying the result by $2v^2_{\overline{\rm MS}}$,

$$(M_h^{\overline{\rm MS},\rm SM})^2 = 2\lambda(M_t)v^2_{\overline{\rm MS}}. \quad (78)$$

The pole Higgs mass is then calculated from the pole equation [26]

$$(M_h)^2_{\rm EFT} = 2\lambda(M_t)v^2_{\overline{\rm MS}} - \widetilde{\Sigma}^{\rm SM}_{hh}(m_h^2) - \widetilde{\Sigma}^{\rm SM'}_{hh}(m_h^2)$$

[34] The rightmost diagram in Fig. 12 cannot be reduced to the left diagram in Fig. 10. This fact, however, does not change our arguments that we present here.

[35] Corresponding two-loop diagrams can be found in Appendix C of [38].

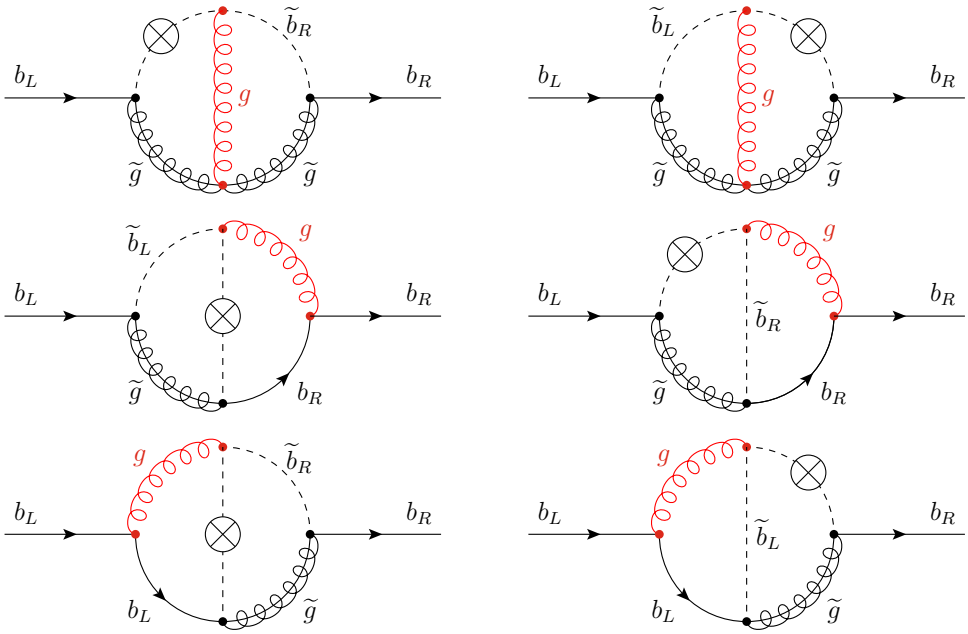

Fig. 11 The first class of two-loop diagrams contributing to $\Delta_b^{2l,\mathcal{O}(\alpha_s^2)}$: a gluon is added to the $\mathcal{O}(\alpha_s)$ one-loop graph

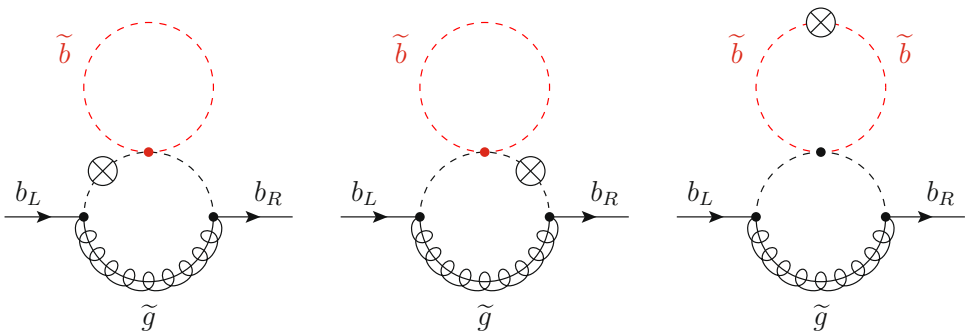

Fig. 12 The second class of two-loop diagrams contributing to $\Delta_b^{2l,\mathcal{O}(\alpha_s^2)}$: a sbottom is added to the $\mathcal{O}(\alpha_s)$ one-loop graph

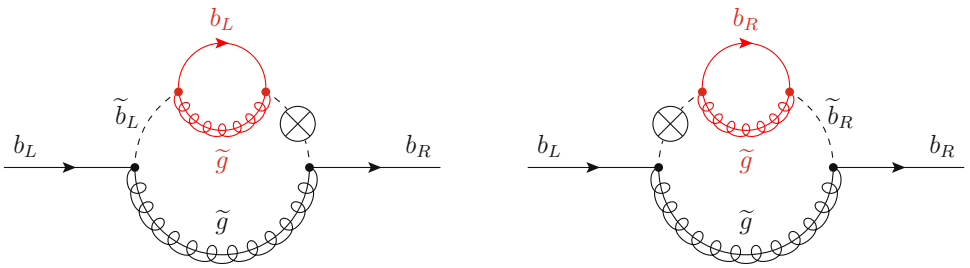

Fig. 13 The third class of two-loop diagrams contributing to $\Delta_b^{2l,\mathcal{O}(\alpha_s^2)}$: a gluino is added to the $\mathcal{O}(\alpha_s)$ one-loop graph

$$\times \left(2\lambda(M_t)v^2_{\overline{\rm MS}} - \widetilde{\Sigma}^{\rm SM}_{hh}(m_h^2) - m_h^2\right) + \cdots . \tag{79}$$

The second method is an iterative solution of the Higgs boson pole mass equation in the MSSM which in the decoupling limit $M_A \gg M_Z$ reads [26]

$$(M_h)^2_{\rm FO} = m_h^2 - \widehat{\Sigma}^{\rm MSSM}_{hh}(m_h^2) + \widehat{\Sigma}^{\rm MSSM}_{hh}(m_h^2)\widehat{\Sigma}^{\rm MSSM'}_{hh}(m_h^2) + \cdots , \tag{80}$$

where the prime stands for the derivative of the self-energy with respect to the momentum squared, and m_h^2 is the lightest Higgs boson mass at the tree level. We have checked analytically that the logarithmic terms are the same in $(M_h)^2_{\rm FO}$ and $(M_h)^2_{\rm EFT}$. This is an important cross-check of our calculation.[36]

At the one-loop level, we obtain the following contribution proportional to the bottom quark mass,

$$(M_h^{\rm 1L})^2_{\rm bot} = 6\kappa \frac{\overline{m}_b^2}{v^2}\left(2\overline{m}_b^2 - c_{2\beta}^2 m_Z^2\right) L \tag{81}$$

[36] Both methods have to give the same answer also for the non-logarithmic terms in leading order of the expansion in $v/M_{\rm SUSY}$. Imposing this condition we have derived the two-loop threshold conditions listed in Appendix B.

At the two-loop level the leading logarithmic terms read

$$(M_h^{2\text{L,LL}})^2_{\text{bot}} = -18\kappa^2 \frac{\overline{m}_b^2}{v^4}\left(\overline{m}_b^4 - \overline{m}_b^2\overline{m}_t^2 + \overline{m}_t^4\right) L^2 + 96\kappa^2 \frac{g_3^2\overline{m}_b^4}{v^2} L^2. \tag{82}$$

If $\widehat{X}_t$ is renormalised in the OS scheme, the sub-leading logarithms read

$$\begin{aligned}(M_h^{2\text{L,NLL}})^2_{\text{bot,OS}} &= -3\kappa^2 \frac{\overline{m}_b^2\overline{m}_t^4}{v^4} \\ &\times \left(-18 + 6|\widehat{X}_t|^2 - |\widehat{X}_b|^2|\widehat{X}_t|^2(6 - |\widehat{X}_t|^2) + 24\log\frac{\overline{m}_t}{\overline{m}_b}\right) L \\ &- 6\kappa^2 \frac{\overline{m}_b^4\overline{m}_t^2}{v^4}\left(1 + 4|\widehat{X}_t|^2 - 4|\widehat{X}_t||\widehat{Y}_t|\cos(\phi_{X_t} - \phi_{Y_t}) + \frac{1}{s_\beta^2}\right) L \\ &- 18\kappa^2 \frac{\overline{m}_b^6}{v^4}\left(-1 + 12\log\frac{\overline{m}_t}{\overline{m}_b} + \frac{1}{c_\beta^2}\right) L \\ &- 32\kappa^2 \frac{g_3^2\overline{m}_b^4}{v^2}\left(-1 - 12\log\frac{\overline{m}_t}{\overline{m}_b} + 2|\widehat{X}_b|\cos(\phi_{X_b} - \phi_{M_3})\right) L.\end{aligned} \tag{83}$$

If $\widehat{X}_t$ is renormalised in the $\overline{\text{DR}}$ scheme at the scale M_{SUSY}, we obtain

$$\begin{aligned}(M_h^{2\text{L,NLL}})^2_{\text{bot,}\overline{\text{DR}}} &= -3\kappa^2 \frac{\overline{m}_b^2\overline{m}_t^4}{v^4}\left(-18 + 6|\widehat{X}_t|^2 + 24\log\frac{\overline{m}_t}{\overline{m}_b}\right) L \\ &- 6\kappa^2 \frac{\overline{m}_b^4\overline{m}_t^2}{v^4}\left(1 + 4|\widehat{X}_t|^2 - 4|\widehat{X}_t||\widehat{Y}_t|\cos(\phi_{X_t} - \phi_{Y_t}) + \frac{1}{s_\beta^2}\right) L \\ &- 18\kappa^2 \frac{\overline{m}_b^6}{v^4}\left(-1 + 12\log\frac{\overline{m}_t}{\overline{m}_b} + \frac{1}{c_\beta^2}\right) L \\ &- 32\kappa^2 \frac{g_3^2\overline{m}_b^4}{v^2}\left(-1 - 12\log\frac{\overline{m}_t}{\overline{m}_b} + 2|\widehat{X}_b|\cos(\phi_{X_b} - \phi_{M_3})\right) L.\end{aligned} \tag{84}$$

We see that the choice of the renormalisation scheme for $\widehat{X}_t$ affects only the logarithmic terms proportional to $\overline{m}_b^2\overline{m}_t^4$.

References

1. ATLAS Collaboration, G. Aad et al., Observation of a new particle in the search for the Standard Model Higgs boson with the ATLAS detector at the LHC. Phys. Lett. B **716**, 1–29, (2012). https://doi.org/10.1016/j.physletb.2012.08.020. arXiv:1207.7214
2. CMS Collaboration, S. Chatrchyan et al., Observation of a new boson at a mass of 125 GeV with the CMS experiment at the LHC. Phys. Lett. B **716**, 30–61. (2012). https://doi.org/10.1016/j.physletb.2012.08.021. arXiv:1207.7235
3. H.P. Nilles, Supersymmetry, supergravity and particle physics. Phys. Rep. **110**, 1–162 (1984). https://doi.org/10.1016/0370-1573(84)90008-5
4. H.E. Haber, G.L. Kane, The search for supersymmetry: probing physics beyond the Standard Model. Phys. Rep. **117**, 75–263 (1985). https://doi.org/10.1016/0370-1573(85)90051-1
5. H. Bahl, S. Heinemeyer, W. Hollik, G. Weiglein, Theoretical uncertainties in the MSSM Higgs boson mass calculation. Eur. Phys. J. C **80**, 497 (2020). https://doi.org/10.1140/epjc/s10052-020-8079-3. arXiv: 1912.04199
6. S. Borowka, T. Hahn, S. Heinemeyer, G. Heinrich, W. Hollik, Renormalization scheme dependence of the two-loop QCD corrections to the neutral Higgs-boson masses in the MSSM. Eur. Phys. J. C **75**, 424 (2015). https://doi.org/10.1140/epjc/s10052-015-3648-6. arXiv:1505.03133
7. M.D. Goodsell, F. Staub, The Higgs mass in the CP violating MSSM, NMSSM, and beyond. Eur. Phys. J. C **77**, 46 (2017). https://doi.org/10.1140/epjc/s10052-016-4495-9. arXiv:1604.05335
8. S. Paßehr, G. Weiglein, Two-loop top and bottom Yukawa corrections to the Higgs-boson masses in the complex MSSM. Eur. Phys. J. C **78**, 222 (2018). https://doi.org/10.1140/epjc/s10052-018-5665-8. arXiv:1705.07909
9. R.V. Harlander, J. Klappert, A. Voigt, Higgs mass prediction in the MSSM at three-loop level in a pure $\overline{\text{DR}}$ context. Eur. Phys. J. C **77**, 814 (2017). https://doi.org/10.1140/epjc/s10052-017-5368-6. arXiv:1708.05720
10. S. Borowka, S. Paßehr, G. Weiglein, Complete two-loop QCD contributions to the lightest Higgs-boson mass in the MSSM with complex parameters. Eur. Phys. J. C **78**, 576 (2018). https://doi.org/10.1140/epjc/s10052-018-6055-y. arXiv:1802.09886
11. A.R. Fazio, E.A.R. Reyes, The lightest Higgs boson mass of the MSSM at three-loop accuracy. Nucl. Phys. B **942**, 164–183 (2019). https://doi.org/10.1016/j.nuclphysb.2019.03.008. arXiv:1901.03651
12. M.D. Goodsell, S. Paßehr, All two-loop scalar self-energies and tadpoles in general renormalisable field theories. Eur. Phys. J. C **80**, 417 (2020). https://doi.org/10.1140/epjc/s10052-020-7657-8. arXiv:1910.02094
13. F. Domingo, S. Paßehr, Towards Higgs masses and decay widths satisfying the symmetries in the (N)MSSM. arXiv:2007.11010
14. J.P. Vega, G. Villadoro, SusyHD: Higgs mass determination in supersymmetry. JHEP **07**, 159 (2015). https://doi.org/10.1007/JHEP07(2015)159. arXiv:1504.05200
15. G. Lee, C.E.M. Wagner, Higgs bosons in heavy supersymmetry with an intermediate m_A. Phys. Rev. D **92**, 075032 (2015). https://doi.org/10.1103/PhysRevD.92.075032. arXiv:1508.00576
16. E. Bagnaschi, J. Pardo Vega, P. Slavich, Improved determination of the Higgs mass in the MSSM with heavy superpartners. Eur. Phys. J. C **77**, 334 (2017). https://doi.org/10.1140/epjc/s10052-017-4885-7. arXiv:1703.08166
17. H. Bahl, W. Hollik, Precise prediction of the MSSM Higgs boson masses for low M_A. JHEP **07**, 182 (2018). https://doi.org/10.1007/JHEP07(2018)182. arXiv:1805.00867
18. R.V. Harlander, J. Klappert, A.D. Ochoa Franco, A. Voigt, The light CP-even MSSM Higgs mass resummed to fourth logarithmic order. Eur. Phys. J. C **78**, 874 (2018). https://doi.org/10.1140/epjc/s10052-018-6351-6. arXiv:1807.03509
19. E. Bagnaschi, G. Degrassi, S. Paßehr, P. Slavich, Full two-loop QCD corrections to the Higgs mass in the MSSM with heavy superpartners. Eur. Phys. J. C **79**, 910 (2019). https://doi.org/10.1140/epjc/s10052-019-7417-9. arXiv:1908.01670
20. N. Murphy, H. Rzehak, Higgs-boson masses and mixings in the MSSM with CP violation and heavy SUSY particles. arXiv:1909.00726
21. H. Bahl, I. Sobolev, G. Weiglein, Precise prediction for the mass of the light MSSM Higgs boson for the case of a heavy gluino. Phys. Lett. B **808**, 135644 (2020). https://doi.org/10.1016/j.physletb.2020.135644. arXiv:1912.10002
22. T. Hahn, S. Heinemeyer, W. Hollik, H. Rzehak, G. Weiglein, High-precision predictions for the light CP-even Higgs boson mass of the Minimal Supersymmetric Standard Model. Phys. Rev. Lett. **112**, 141801 (2014). https://doi.org/10.1103/PhysRevLett.112.141801. arXiv:1312.4937

23. H. Bahl, W. Hollik, Precise prediction for the light MSSM Higgs boson mass combining effective field theory and fixed-order calculations. Eur. Phys. J. C **76**, 499 (2016). https://doi.org/10.1140/epjc/s10052-016-4354-8. arXiv:1608.01880
24. P. Athron, J. Park, T. Steudtner, D. Stöckinger, A. Voigt, Precise Higgs mass calculations in (non-)minimal supersymmetry at both high and low scales. JHEP **01**, 079 (2017). https://doi.org/10.1007/JHEP01(2017)079. arXiv:1609.00371
25. F. Staub, W. Porod, Improved predictions for intermediate and heavy supersymmetry in the MSSM and beyond. Eur. Phys. J. C **77**, 338 (2017). https://doi.org/10.1140/epjc/s10052-017-4893-7. arXiv:1703.03267
26. H. Bahl, S. Heinemeyer, W. Hollik, G. Weiglein, Reconciling EFT and hybrid calculations of the light MSSM Higgs-boson mass. Eur. Phys. J. C **78**, 57 (2018). https://doi.org/10.1140/epjc/s10052-018-5544-3. arXiv:1706.00346
27. P. Athron, M. Bach, D. Harries, T. Kwasnitza, J. Park, D. Stöckinger et al., FlexibleSUSY 2.0: extensions to investigate the phenomenology of SUSY and non-SUSY models. Comput. Phys. Commun. **230**, 145–217 (2018). https://doi.org/10.1016/j.cpc.2018.04.016. arXiv:1710.03760
28. H. Bahl, Pole mass determination in presence of heavy particles. JHEP **02**, 121 (2019). https://doi.org/10.1007/JHEP02(2019)121. arXiv:1812.06452
29. R. Harlander, J. Klappert, A. Voigt, The light CP-even MSSM Higgs mass including $N^3LO + N^3$ LL QCD corrections. Eur. Phys. J. C **80**, 186 (2020). https://doi.org/10.1140/epjc/s10052-020-7747-7. arXiv:1910.03595
30. T. Kwasnitza, D. Stöckinger, A. Voigt, Improved MSSM Higgs mass calculation using the 3-loop FlexibleEFTHiggs approach including x_t-resummation. JHEP **07**, 197 (2020). https://doi.org/10.1007/JHEP07(2020)197. arXiv:2003.04639
31. S. Heinemeyer, W. Hollik, G. Weiglein, FeynHiggs: a program for the calculation of the masses of the neutral CP even Higgs bosons in the MSSM. Comput. Phys. Commun. **124**, 76–89 (2000). https://doi.org/10.1016/S0010-4655(99)00364-1. arXiv:hep-ph/9812320
32. S. Heinemeyer, W. Hollik, G. Weiglein, The masses of the neutral CP-even Higgs bosons in the MSSM: Accurate analysis at the two loop level. Eur. Phys. J. C **9**, 343–366 (1999). https://doi.org/10.1007/s100529900006, https://doi.org/10.1007/s100520050537. arXiv:hep-ph/9812472
33. T. Hahn, S. Heinemeyer, W. Hollik, H. Rzehak, G. Weiglein, FeynHiggs: a program for the calculation of MSSM Higgs-boson observables—Version 2.6.5. Comput. Phys. Commun. **180**, 1426–1427 (2009). https://doi.org/10.1016/j.cpc.2009.02.014
34. G. Degrassi, S. Heinemeyer, W. Hollik, P. Slavich, G. Weiglein, Towards high precision predictions for the MSSM Higgs sector. Eur. Phys. J. C **28**, 133–143 (2003). https://doi.org/10.1140/epjc/s2003-01152-2. arXiv:hep-ph/0212020
35. M. Frank, T. Hahn, S. Heinemeyer, W. Hollik, H. Rzehak, G. Weiglein, The Higgs boson masses and mixings of the complex MSSM in the Feynman-diagrammatic approach. JHEP **02**, 047 (2007). https://doi.org/10.1088/1126-6708/2007/02/047. arXiv:hep-ph/0611326
36. H. Bahl, T. Hahn, S. Heinemeyer, W. Hollik, S. Paßehr, H. Rzehak et al., Precision calculations in the MSSM Higgs-boson sector with FeynHiggs 2.14. Comput. Phys. Commun. **249**, 107099 (2020). https://doi.org/10.1016/j.cpc.2019.107099. arXiv:1811.09073
37. D. Noth, M. Spira, Higgs Boson couplings to bottom quarks: two-loop supersymmetry-QCD corrections. Phys. Rev. Lett. **101**, 181801 (2008). https://doi.org/10.1103/PhysRevLett.101.181801. arXiv:0808.0087
38. D. Noth, Supersymmetric precision calculations of Bottom Yukawa couplings. Ph.D. thesis, University of Zürich (2008)
39. D. Noth, M. Spira, Supersymmetric Higgs Yukawa couplings to bottom quarks at next-to-next-to-leading order. JHEP **06**, 084 (2011). https://doi.org/10.1007/JHEP06(2011)084. arXiv:1001.1935
40. S. Heinemeyer, W. Hollik, H. Rzehak, G. Weiglein, The Higgs sector of the complex MSSM at two-loop order: QCD contributions. Phys. Lett. B **652**, 300–309 (2007). https://doi.org/10.1016/j.physletb.2007.07.030. arXiv:0705.0746
41. W. Hollik, S. Paßehr, Higgs boson masses and mixings in the complex MSSM with two-loop top-Yukawa-coupling corrections. JHEP **10**, 171 (2014). https://doi.org/10.1007/JHEP10(2014)171. arXiv:1409.1687
42. W. Hollik, S. Paßehr, Two-loop top-Yukawa-coupling corrections to the Higgs boson masses in the complex MSSM. Phys. Lett. B **733**, 144–150 (2014). https://doi.org/10.1016/j.physletb.2014.04.026. arXiv:1401.8275
43. A. Brignole, G. Degrassi, P. Slavich, F. Zwirner, On the two loop sbottom corrections to the neutral Higgs boson masses in the MSSM. Nucl. Phys. B **643**, 79–92 (2002). https://doi.org/10.1016/S0550-3213(02)00748-4. arXiv:hep-ph/0206101
44. A. Dedes, G. Degrassi, P. Slavich, On the two loop Yukawa corrections to the MSSM Higgs boson masses at large $\tan\beta$. Nucl. Phys. B **672**, 144–162 (2003). https://doi.org/10.1016/j.nuclphysb.2003.08.033. arXiv:hep-ph/0305127
45. I. Jack, D. Jones, S.P. Martin, M.T. Vaughn, Y. Yamada, Decoupling of the epsilon scalar mass in softly broken supersymmetry. Phys. Rev. D **50**, 5481–5483 (1994). https://doi.org/10.1103/PhysRevD.50.R5481. arXiv:hep-ph/9407291
46. T. Fritzsche, T. Hahn, S. Heinemeyer, F. von der Pahlen, H. Rzehak, C. Schappacher, The implementation of the renormalized complex MSSM in FeynArts and FormCalc. Comput. Phys. Commun. **185**, 1529–1545 (2014). https://doi.org/10.1016/j.cpc.2014.02.005. arXiv:1309.1692
47. S. Heinemeyer, H. Rzehak, C. Schappacher, Proposals for bottom quark/squark renormalization in the complex MSSM. Phys. Rev. D **82**, 075010 (2010). https://doi.org/10.1103/PhysRevD.82.075010. arXiv:1007.0689
48. D. Buttazzo, G. Degrassi, P.P. Giardino, G.F. Giudice, F. Sala, A. Salvio et al., Investigating the near-criticality of the Higgs boson. JHEP **12**, 089 (2013). https://doi.org/10.1007/JHEP12(2013)089. arXiv:1307.3536
49. L.N. Mihaila, J. Salomon, M. Steinhauser, Renormalization constants and beta functions for the gauge couplings of the Standard Model to three-loop order. Phys. Rev. D **86**, 096008 (2012). https://doi.org/10.1103/PhysRevD.86.096008. arXiv:1208.3357
50. A.V. Bednyakov, A.F. Pikelner, V.N. Velizhanin, Anomalous dimensions of gauge fields and gauge coupling beta-functions in the Standard Model at three loops. JHEP **01**, 017 (2013). https://doi.org/10.1007/JHEP01(2013)017. arXiv:1210.6873
51. A.V. Bednyakov, A.F. Pikelner, V.N. Velizhanin, Yukawa coupling beta-functions in the Standard Model at three loops. Phys. Lett. B **722**, 336–340 (2013). https://doi.org/10.1016/j.physletb.2013.04.038. arXiv:1212.6829
52. K.G. Chetyrkin, M.F. Zoller, β-function for the Higgs self-interaction in the Standard Model at three-loop level. JHEP **04**, 091 (2013). https://doi.org/10.1007/JHEP04(2013)091, https://doi.org/10.1007/JHEP09(2013)155. arXiv:1303.2890
53. A.V. Bednyakov, A.F. Pikelner, V.N. Velizhanin, Higgs self-coupling beta-function in the Standard Model at three loops. Nucl. Phys. B **875**, 552–565 (2013). https://doi.org/10.1016/j.nuclphysb.2013.07.015. arXiv:1303.4364
54. A. Denner, Techniques for calculation of electroweak radiative corrections at the one loop level and results for W physics at LEP-200. Fortsch. Phys. **41**, 307–420 (1993). https://doi.org/10.1002/prop.2190410402. arXiv:0709.1075

55. P. Athron, J. Park, D. Stöckinger, A. Voigt, FlexibleSUSY—a spectrum generator generator for supersymmetric models. Comput. Phys. Commun. **190**, 139–172 (2015). https://doi.org/10.1016/j.cpc.2014.12.020. arXiv:1406.2319
56. G. Degrassi, S. Di Vita, J. Elias-Miro, J.R. Espinosa, G.F. Giudice, G. Isidori et al., Higgs mass and vacuum stability in the Standard Model at NNLO. JHEP **08**, 098 (2012). https://doi.org/10.1007/JHEP08(2012)098. arXiv:1205.6497
57. S.P. Martin, D.G. Robertson, Higgs boson mass in the Standard Model at two-loop order and beyond. Phys. Rev. D **90**, 073010 (2014). https://doi.org/10.1103/PhysRevD.90.073010. arXiv:1407.4336
58. R. Hempfling, Yukawa coupling unification with supersymmetric threshold corrections. Phys. Rev. D **49**, 6168–6172 (1994). https://doi.org/10.1103/PhysRevD.49.6168
59. L.J. Hall, R. Rattazzi, U. Sarid, The top quark mass in supersymmetric SO(10) unification. Phys. Rev. D **50**, 7048–7065 (1994). https://doi.org/10.1103/PhysRevD.50.7048. arXiv:hep-ph/9306309
60. M. Carena, M. Olechowski, S. Pokorski, C.E.M. Wagner, Electroweak symmetry breaking and bottom - top Yukawa unification. Nucl. Phys. B **426**, 269–300 (1994). https://doi.org/10.1016/0550-3213(94)90313-1. arXiv:hep-ph/9402253
61. M. Carena, D. Garcia, U. Nierste, C.E.M. Wagner, Effective Lagrangian for the $\tilde{t}bH^+$ interaction in the MSSM and charged Higgs phenomenology. Nucl. Phys. B **577**, 88–120 (2000). https://doi.org/10.1016/S0550-3213(00)00146-2. arXiv:hep-ph/9912516
62. J. Guasch, P. Hafliger, M. Spira, MSSM Higgs decays to bottom quark pairs revisited. Phys. Rev. D **68**, 115001 (2003). https://doi.org/10.1103/PhysRevD.68.115001. arXiv:hep-ph/0305101
63. S. Heinemeyer, W. Hollik, H. Rzehak, G. Weiglein, High-precision predictions for the MSSM Higgs sector at $O(\alpha_b\alpha_s)$. Eur. Phys. J. C **39**, 465–481 (2005). https://doi.org/10.1140/epjc/s2005-02112-6. arXiv:hep-ph/0411114
64. L. Hofer, U. Nierste, D. Scherer, Resummation of tan-beta-enhanced supersymmetric loop corrections beyond the decoupling limit. JHEP **10**, 081 (2009). https://doi.org/10.1088/1126-6708/2009/10/081. arXiv:0907.5408
65. S.P. Martin, Fermion self-energies and pole masses at two-loop order in a general renormalizable theory with massless gauge bosons. Phys. Rev. D **72**, 096008 (2005). https://doi.org/10.1103/PhysRevD.72.096008. arXiv:hep-ph/0509115
66. L. Mihaila, C. Reisser, $\mathcal{O}(\alpha_s^2)$ corrections to fermionic Higgs decays in the MSSM. JHEP **08**, 021 (2010). https://doi.org/10.1007/JHEP08(2010)021. arXiv:1007.0693
67. M. Ghezzi, S. Glaus, D. Müller, T. Schmidt, M. Spira, Refinements of the bottom and strange MSSM Higgs Yukawa couplings at NNLO. arXiv: 1711.02555
68. T. Hahn, S. Paßehr, Implementation of the $\mathcal{O}(\alpha_t^2)$ MSSM Higgs-mass corrections in $\texttt{FeynHiggs}$. Comput. Phys. Commun. **214**, 91–97 (2017). https://doi.org/10.1016/j.cpc.2017.01.026. arXiv:1508.00562
69. A. Pilaftsis, C.E.M. Wagner, Higgs bosons in the minimal supersymmetric standard model with explicit CP violation. Nucl. Phys. B **553**, 3–42 (1999). https://doi.org/10.1016/S0550-3213(99)00261-8. arXiv:hep-ph/9902371
70. M. Carena, J.R. Ellis, A. Pilaftsis, C.E.M. Wagner, Renormalization group improved effective potential for the MSSM Higgs sector with explicit CP violation. Nucl. Phys. B **586**, 92–140 (2000). https://doi.org/10.1016/S0550-3213(00)00358-8. arXiv:hep-ph/0003180
71. M. Carena, J. Ellis, J.S. Lee, A. Pilaftsis, C.E.M. Wagner, CP violation in heavy MSSM Higgs scenarios. JHEP **02**, 123 (2016). https://doi.org/10.1007/JHEP02(2016)123. arXiv:1512.00437
72. H. Bahl, N. Murphy, H. Rzehak, Hybrid calculation of the MSSM Higgs boson masses using the complex THDM as EFT. arXiv:2010.04711
73. E. Bagnaschi, G.F. Giudice, P. Slavich, A. Strumia, Higgs mass and unnatural supersymmetry. JHEP **09**, 092 (2014). https://doi.org/10.1007/JHEP09(2014)092. arXiv:1407.4081
74. K. Williams, The Higgs sector of the complex minimal supersymmetric standard model. Ph.D. thesis, Durham University (2008)
75. K.E. Williams, H. Rzehak, G. Weiglein, Higher order corrections to Higgs boson decays in the MSSM with complex parameters. Eur. Phys. J. C **71**, 1669 (2011). https://doi.org/10.1140/epjc/s10052-011-1669-3. arXiv:1103.1335
76. S.P. Martin, Three-loop corrections to the lightest Higgs scalar boson mass in supersymmetry. Phys. Rev. D **75**, 055005 (2007). https://doi.org/10.1103/PhysRevD.75.055005. arXiv:hep-ph/0701051
77. S.P. Martin, Four-loop standard model effective potential at leading order in QCD. Phys. Rev. D **92**, 054029 (2015). https://doi.org/10.1103/PhysRevD.92.054029. arXiv:1508.00912
78. K.G. Chetyrkin, M.F. Zoller, Leading QCD-induced four-loop contributions to the β-function of the Higgs self-coupling in the SM and vacuum stability. JHEP **06**, 175 (2016). https://doi.org/10.1007/JHEP06(2016)175. arXiv:1604.00853
79. R.V. Harlander, P. Kant, L. Mihaila, M. Steinhauser, Higgs boson mass in supersymmetry to three loops. Phys. Rev. Lett. **100**, 191602 (2008). https://doi.org/10.1103/PhysRevLett.101.039901. https://doi.org/10.1103/PhysRevLett.100.191602. arXiv:0803.0672
80. P. Kant, R.V. Harlander, L. Mihaila, M. Steinhauser, Light MSSM Higgs boson mass to three-loop accuracy. JHEP **08**, 104 (2010). https://doi.org/10.1007/JHEP08(2010)104. arXiv:1005.5709
81. S.P. Martin, Two-loop scalar self-energies and pole masses in a general renormalizable theory with massless gauge bosons. Phys. Rev. D **71**, 116004 (2005). https://doi.org/10.1103/PhysRevD.71.116004. arXiv:hep-ph/0502168
82. S.P. Martin, Refined gluino and squark pole masses beyond leading order. Phys. Rev. D **74**, 075009 (2006). https://doi.org/10.1103/PhysRevD.98.119901. https://doi.org/10.1103/PhysRevD.74.075009. arXiv:hep-ph/0608026
83. M. Carena, J.R. Espinosa, M. Quiros, C.E.M. Wagner, Analytical expressions for radiatively corrected Higgs masses and couplings in the MSSM. Phys. Lett. B **355**, 209–221 (1995). https://doi.org/10.1016/0370-2693(95)00694-G. arXiv:hep-ph/9504316
84. M. Carena, H.E. Haber, S. Heinemeyer, W. Hollik, C.E.M. Wagner, G. Weiglein, Reconciling the two loop diagrammatic and effective field theory computations of the mass of the lightest CP—even Higgs boson in the MSSM. Nucl. Phys. B **580**, 29–57 (2000). https://doi.org/10.1016/S0550-3213(00)00212-1. arXiv:hep-ph/0001002
85. P. Draper, G. Lee, C.E.M. Wagner, Precise estimates of the Higgs mass in heavy supersymmetry. Phys. Rev. D **89**, 055023 (2014). https://doi.org/10.1103/PhysRevD.89.055023. arXiv:1312.5743
86. H. Bahl, P. Bechtle, S. Heinemeyer, S. Liebler, T. Stefaniak, G. Weiglein, HL-LHC and ILC sensitivities in the hunt for heavy Higgs bosons. arXiv:2005.14536
87. E. Bagnaschi et al., MSSM Higgs boson searches at the LHC: benchmark scenarios for run 2 and beyond. Eur. Phys. J. C **79**, 617 (2019). https://doi.org/10.1140/epjc/s10052-019-7114-8. arXiv:1808.07542
88. H. Bahl, S. Liebler, T. Stefaniak, MSSM Higgs benchmark scenarios for Run 2 and beyond: the low $\tan\beta$ region. Eur. Phys. J. C **79**, 279 (2019). https://doi.org/10.1140/epjc/s10052-019-6770-z. arXiv:1901.05933
89. LHC Higgs Cross Section Working Group Collaboration, D. de Florian et al., Handbook of LHC Higgs cross sections: 4. Deciphering the nature of the Higgs sector. arXiv:1610.07922

90. H. Bahl, I. Sobolev, Two-loop matching of renormalizable operators: general considerations and applications **2010** (1989)
91. G. Weiglein, R. Mertig, R. Scharf, M. Böhm, in *New Computing Techniques in Physics Research II*, ed. by D. Perret-Gallix (World Scientific, Singapore, 1992), p. 617
92. G. Weiglein, R. Scharf, M. Bohm, Reduction of general two loop selfenergies to standard scalar integrals. Nucl. Phys. B **416**, 606–644 (1994). https://doi.org/10.1016/0550-3213(94)90325-5. arXiv:hep-ph/9310358
93. J. Küblbeck, M. Böhm, A. Denner, Feyn arts: computer algebraic generation of Feynman graphs and amplitudes. Comput. Phys. Commun. **60**, 165–180 (1990). https://doi.org/10.1016/0010-4655(90)90001-H
94. H. Eck, J. Kublbeck, Computer algebraic generation of Feynman graphs and amplitudes, in *2nd International Workshop on Software Engineering, Artificial Intelligence and Expert Systems for High-energy and Nuclear Physics* (1992), pp. 677–682
95. T. Hahn, Generating Feynman diagrams and amplitudes with FeynArts 3. Comput. Phys. Commun. **140**, 418–431 (2001). https://doi.org/10.1016/S0010-4655(01)00290-9. arXiv:hep-ph/0012260
96. T. Hahn, M. Perez-Victoria, Automatized one loop calculations in four-dimensions and D-dimensions. Comput. Phys. Commun. **118**, 153–165 (1999). https://doi.org/10.1016/S0010-4655(98)00173-8. arXiv:hep-ph/9807565
97. G. Giudice, A. Romanino, Split supersymmetry. Nucl. Phys. B **699**, 65–89 (2004). https://doi.org/10.1016/j.nuclphysb.2004.08.001. arXiv:hep-ph/0406088
98. G.F. Giudice, A. Strumia, Probing high-scale and split supersymmetry with Higgs mass measurements. Nucl. Phys. B **858**, 63–83 (2012). https://doi.org/10.1016/j.nuclphysb.2012.01.001. arXiv:1108.6077
99. J.R. Espinosa, R.-J. Zhang, Complete two loop dominant corrections to the mass of the lightest CP even Higgs boson in the minimal supersymmetric standard model. Nucl. Phys. B **586**, 3–38 (2000). https://doi.org/10.1016/S0550-3213(00)00421-1. arXiv:hep-ph/0003246
100. J.C. Collins, J. Vermaseren, Axodraw Version 2. arXiv:1606.01177
101. T. Kinoshita, Mass singularities of Feynman amplitudes. J. Math. Phys. **3**, 650–677 (1962). https://doi.org/10.1063/1.1724268
102. T. Lee, M. Nauenberg, Degenerate systems and mass singularities. Phys. Rev. **133**, B1549–B1562 (1964). https://doi.org/10.1103/PhysRev.133.B1549
103. P. Draper, H. Rzehak, A review of Higgs mass calculations in supersymmetric models. Phys. Rep. **619**, 1–24 (2016). https://doi.org/10.1016/j.physrep.2016.01.001. arXiv:1601.01890